Domestic Slurry Hydraulics in Transport

Thota Radhakrishnan, Adithya Krishnan

DOI
10.4233/uuid:ef44e517-ca14-46a8-93e4-43c38b265b30

Publication date
2019

Document Version
Final published version

Citation (APA)
Thota Radhakrishnan, A. K. (2019). *Domestic Slurry Hydraulics in Transport*. [Dissertation (TU Delft), Delft University of Technology]. https://doi.org/10.4233/uuid:ef44e517-ca14-46a8-93e4-43c38b265b30

Important note
To cite this publication, please use the final published version (if applicable).
Please check the document version above.

Domestic Slurry Hydraulics in Transport

Adithya Krishnan Thota Radhakrishnan

Going
beyond
the toilet ...

Understanding the flow of
non-Newtonian slurries in relation
to concentrated domestic slurries.

Domestic Slurry Hydraulics in Transport

Going beyond the toilet...

Domestic Slurry Hydraulics in Transport

Dissertation

for the purpose of obtaining the degree of doctor
at Delft University of Technology,
by the authority of the Rector Magnificus, prof. dr. ir. T.H.J.J. van der Hagen
chair of the Board for Doctorates,
to be defended publicly on
Thursday 3 October 2019 at 12:30 o'clock

by

Adithya Krishnan THOTA RADHAKRISHNAN

Master of Science in Chemical Engineering, TU Eindhoven, the Netherlands
born in Chennai, India

This dissertation has been approved by the promotors.

Composition of the doctoral committee:

Rector Magnificus	chairperson
Prof. dr. ir. F.H.L.R. Clemens	Delft University of Technology, promotor
Prof. dr. ir. J.B. van Lier	Delft University of Technology, promotor

Independent members:

Prof. dr. ir. Z. Kapelan	Delft University of Technology
Prof. dr. ing. D. Muschalla	Graz University of Technology, Austria
Prof. dr. S.J. Tait	University of Sheffield, United Kingdom
Prof. dr. ir. G. Zeeman	Wageningen University & Research
Prof. dr. ir. W.S.J. Uijttewaal,	Delft University of Technology, reserve member

Other member:

Prof. dr. ir. C. Poelma	Delft University of Technology

This research was funded by Technology Foundation STW, the Netherlands under grant number 13347.

ISBN: 978-94-6366-208-6
Printed by: Gildeprint, Enschede
Cover design by Adi (Vectors from Vecteezy.com)

An electronic version of this document is available free of charge in the TU Delft Repository at `http://repository.tudelft.nl/`.

to amma, appa, akka

Preface

What a journey this has been. A journey of excitement and dullness, of triumphs and failures, of motivation and discouragement. Surviving this journey of intense emotions wouldn't have been possible without the many people I have shared these four years with. I want to thank:

Francois Clemens, without whom this journey wouldn't have least been successful. Who, at every obstacle had an answer. Thank you, for giving me this opportunity.

Jules van Lier for the support and guidance in writing all the papers and in particular my thesis.

My colleagues the sewer horses, Johan and Wouter for those particular closed door discussions, Nikola for all his drama, Alex for the beers and making my first year enjoyable, Mathieu, Matthijs, Bram, Job, Eva, Kostas, Danai, for all those shared office experiences. And Dhruv for all the climbing we did and the CFD work.

Antonio, without whom surviving this PhD would have been impossible. I still remember those days, starting the PhD together, talking about how the years would go by, arguing about everything and sometimes forgetting what we were arguing about. A lot has changed and yet somethings remain. Thanks for motivating me to finish the PhD. Sophie, the little french who made me addicted to sweets, cakes and chocolates. Thank you both for making Delft feel like home.

Armand Middeldorp, for helping with setting up the experiment at the water lab. Mohammed Jafar, for all the help in the lab and all the fun during lunch. I want to also thank the thesis students Phongsatorn Srisuttisaard and Laurenzo Middel who worked with me in this project.

Building and working on the big slurry loop in Deltares was an arduous task with frustration at every point along the way. I tried my best to get whatever data I could out of it. I want to thank the slurry loop for not giving up on me. I want to thank Frenk Boekhout and, the interns Around Dom and Bob Kerssens for helping me build the loop.

Climbing became a big part of my life, and undoubtedly changed my life, my

physical and mental well-being, which also helped me to cope with the PhD. Climbing wouldn't have been the same fun without Dhruv, Nina, Jun and Nathali, thanks for trying to be funny.

A special thanks to the DDD group, David, Michal, JJ and Kawang for all the food and 40+ life lessons. JJ, thank you for the friend and a great climbing partner you've been. I want to also thank the "mocha in moha" group for all those great climbing experiences.

Manochitra, with whom I started climbing and with whom I found a family far away from home. And Sofia, thanks for being my barrio friend and for listening to me whenever I needed.

Lucia, for showing me a world I had never known before, for giving me a new sense to life and love.

I wasn't a particularly easy child to handle growing up, and whatever I have achieved in my life wouldn't have been possible without my family, amma, appa and akka. And, I want to dedicate this book to them.

And the PhD, for teaching me patience and persistence.

Wageningen, September 2019

Contents

Nomenclature

Acronyms

CDS	Concentrated Domestic Slurry
CHB	Combined Herschel-Bulkley
FSF	Fully Sheared Flow
FWD	Food Waste Disposers
GKW	Ground Kitchen Waste
GSS	Golden Section Search
GTR	Genetic + Trust Region algorithm
HB	Herschel-Bulkley
NS	New Sanitation
PSF	Partially Sheared Flow
RMSE	Root Mean Square Error
RMSNR	Root Mean Square of Normalised Residual
RPM	Rotation Per Minute
SSR	Squared Sum of Residual
SU	Structural Unit
TSS	Total Suspended Solids
UIV	Ultrasound Imaging Velocimetry

Symbols

$\dot{\gamma}$	Shear-rate	$1/\mathrm{s}$
λ	Regularisation parameter	$-$
μ	Viscosity	$\mathrm{Pa} \cdot \mathrm{s}$

ρ	Density	$\mathrm{Kg/m^3}$
τ	Shear-stress	Pa
τ_y	Yield stress	Pa
A	Cross-sectional area	$\mathrm{m^2}$
C	Total Suspended Concentration in % (wt./wt.)	–
D	Diameter	m
E	Rheological temperature constant	°C
f	Fanning friction factor	–
h	Height of cylinder	m
I	Turbulence intensity	–
K	Consistency index	$\mathrm{Pa \cdot s^n}$
L	Length (of pipe)	m
M	Torque on cylinder	$\mathrm{N \cdot m}$
N	Number of data points	–
n	Behaviour index	–
P	Pressure	Pa
Q	Volumetric flow rate	$\mathrm{m^3/s}$
R	Radius	m
r	Radial distance from the axis	m
Re	Reynolds number	Pa
V	Average flow velocity	m/s
v	Local velocity	m/s
v'	Root mean square of the turbulent velocity fluctuations	m/s
y	Distance from pipe wall, normal to axis	m
Z	Stability parameter	–

Subscripts

ann	of the annular zone
B	of Bingham rheological model

CHB	of Combined Herschel-Bulkley rheological model
e	entry or exit
H	of Hanks
HB	of Herschel-Bulkley rheological model
i	Inner cylinder
MR	of Metzner-Reed
o	Outer cylinder
PL	of Power law rheological model
plug	of the plug zone
r	radial component
RJ	of Ryan and Johnson
S	of Slatter
shear	of the sheared zone
trans	at which transition occurs
w	at the wall
z	axial component

List of Figures

List of Tables

CHAPTER 1

Motivation

Sanitation systems have for many years provided means for safe conveyance of human waste. They are one of the greatest innovations in general public health (Ferriman, 2007). The present day sewer based systems stemmed out as a solution to the health crisis of the 18^{th} and 19^{th} century (Brewer and Pringle, 2015) and, has since then been continuously improved upon. Sanitation in general, has evolved from being simple collection-conveyance systems in getting rid of wastewater from urban areas to elsewhere downstream (water streams; i.e. rivers, canals, seas). The increase in scale of population in urban areas lead to the emergence of complex sewer based centralised systems. The constructed treatment plants were initially to remove organic matter from wastewater before their disposal downstream. Without treatment plants, a non-controlled discharge of nutrients into water bodies will lead to eutrophication and species diversity loss. At present and in the near likely future, wastewater treatment plants will be extended to also address micro-pollutants. Although the centralised sewer-based conveyance and treatment systems solve acute problems of health, hygiene and the environment from pollutants, they are reaching their limits with respect to their sustainability. With consuming extensive amounts of water for conveyance and exhausting substantial energy for treatment, their shortcomings seem apparent. Having potential to recover resources from wastewater; the opportunity has not been realised (Larsen et al., 2013). These systems are predominantly restricted to industrialised countries which demand huge investments in infrastructure. Thus far, the conventional centralised systems act as a mere conveyance system with treatment just for the safe disposal of wastewater and the removal of polluting constituents such as the nutrients. However, the nutrients such as nitrogen, phosphorous, potassium and sulphur are essential for the growth of plants. For reaching a sustainable balance in the nutrient cycle, these nutrients should be recovered from the wastewater (Larsen et al., 2013). The search for sustainable alternatives have lead to the development of **N**ew **S**anitation (**NS**) systems. Concepts of source separation, decentralisation and resource recovery form the core of NS systems. The shift in the sanitation paradigm towards NS systems is based on efficient resource management towards the pursuit

for sustainability.

1.1 New Sanitation

Before proceeding to describe NS concepts, it is instructive to first characterise the different product streams that they handle. From a resource management perspective, this would, therefore, be indicative of the value of the product streams. As opposed to conventional sewer-based systems which are considered to handle the mixed wastewater, NS systems handle the constituents of wastewater including the waste itself as exclusive products (Figure 1.1). These product streams are brown water (contains faeces and flush water), black water (contains urine and brown water), grey water (which entails all the other streams arising from cleaning, washing and bathing activities) and food waste (if food waste disposers are installed in the kitchen).

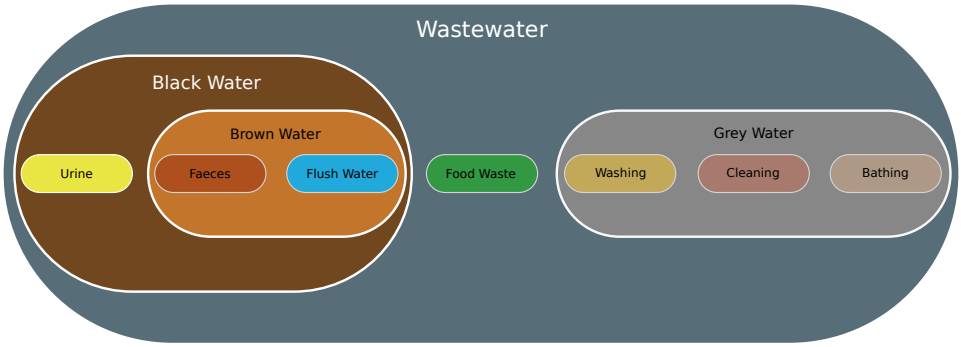

Figure 1.1: Product streams arising from New Sanitation systems

The product streams present opportunities for resources to be recovered from them. The potential resources are mentioned in Table 1.1. An in-depth assessment of the chemical compounds present in the product streams and their resource opportunities can be found in Freidler et al. (2013).

With resource management and resource recovery making up the core of NS systems, there are various different sub-concepts. These concepts aid in realising the potential resource opportunities from the product streams and belong to three key elements of the system: collection, transport and treatment. In its entirety, NS concepts incorporate source separation, decentralisation and resource recovery. A schematic representation of such a system is presented in Figure 1.2. These concepts are further explained under the key elements in the following sections.

Table 1.1: Resources from product streams

Product stream	Resource opportunity
Brown water	Nutrient (Phosphorous) recovery and energy production from the organic mater present
Yellow water	Urine being the constituent, holds a high nutrient (Nitrogen and Phosphorous) content which presents an opportunity for its recovery and removal of micro-pollutants (e.g. medicines)
Black water	Mix of brown and yellow water, giving opportunity for the recovery of nutrients (Nitrogen and Phosphorous) and energy
Grey water	Heat for local use can be recovered and water can be reused
Food waste	Introducing food waste disposers in kitchens gives the potential to recover nutrients (Nitrogen and Phosphorous) from food waste and energy from the organic matter

1.1.1 Collection

Collection concepts are fundamentally based on efficient resource management. The commonly recognised approaches for implementing this are source separation, food waste disposer and vacuum toilets.

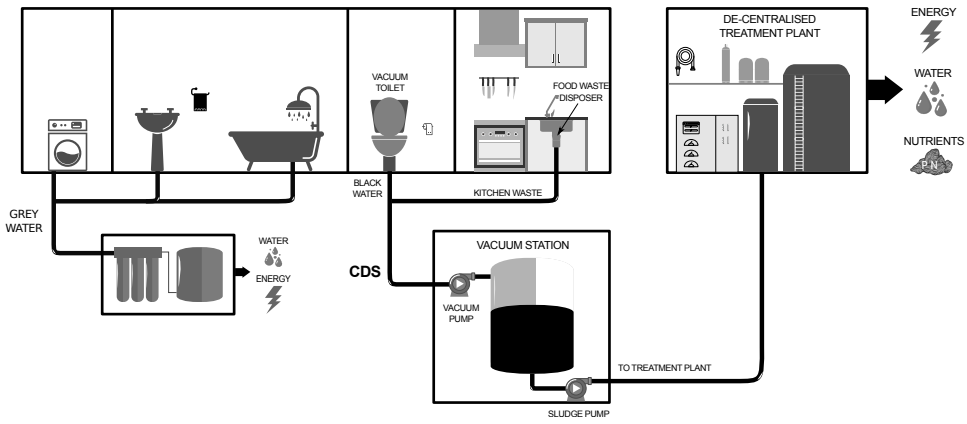

Figure 1.2: Schematic drawing of a New Sanitation system according to source separated decentralised sanitation and resource recovery concept

Source separation

Source separation is an integral part of the novel collection concepts in NS. The purposed is separate collection of wastewater streams with respect to their source, to be treated separately. As mentioned in the earlier sections, the constituents of wastewater are seen as exclusive products with potential resource opportunities. The justification for this is that each product stream can be separately treated and resources extracted efficiently, if dilution is prevented for the concentrated streams (Kujawa-Roeleveld and Zeeman, 2006; Larsen and Gujer, 1997; Tervahauta et al., 2013).

Vacuum toilets

Conventional sewer-based sanitation systems predominantly act as a conveyance system, to provide a safe disposal of the human excreta. To necessitate conveyance, large quantities of potable water are used. Adding to this, the resulting waste water is highly diluted. This hinders resource recovery, as concentrated product streams result in cost-effective resource recovery techniques (Kujawa-Roeleveld and Zeeman, 2006; Larsen and Gujer, 1997; Larsen et al., 2009). Many investigators of sustainable sanitation concepts have claimed that a low dilution is beneficial for the efficiency of resource recovery and essential to the success of NS systems (Larsen et al., 2009; Otterpohl et al., 2002). As an alternative to gravity based collection, vacuum collection systems are added to source separation. The vacuum toilets are employed to reduce water consumption to < 1 L per flush and will keep the slurry concentrated.

Food waste disposers

In general, organic wastes form more than 40% (by weight) of the municipal solid waste (Hoornweg and Bhada-Tata, 2012), of which around 30% make up for food scraps. These are 'misplaced' resources, from which nutrients and energy could be recovered (Braun and Wellinger, 2003; Iacovidou et al., 2012b). To realise this, **F**ood **W**aste **D**isposers (FWD) have been identified as an effective food waste management strategy (Iacovidou et al., 2012a; Lundie and Peters, 2005; Nakakubo et al., 2012).

FWDs or kitchen grinders, as they are commonly referred to, are used to dispose household organic waste into the sewer system by macerating the food waste. In the Netherlands, FWDs connected to the conventionl collection systems are not allowed owing to an increased energy demand in the aeration tanks of the activated sludge system. However, additional waste load is known to increase biogas production through anaerobic digestion (Bolzonella et al., 2003; Braun and Wellinger, 2003; Iacovidou et al., 2012b). In addition, it also reduces the amount of waste that needs to be collected by municipal waste transport using vehicles. FWDs form an essential part of NS systems in which the concentrated waste is treated with anaerobic digestion, incorporating additional means for nutrient recovery.

1.1.2 Transport

Product streams from NS systems are very much concentrated, containing high concentrations of organic solids. These slurries which are essentially a mixture of water and organic particulate which are likely to composed of cohesive solids (faeces), fibres (toiletpaper, hair, etc.), non-cohesive solids with a wide particle size distribution & relatively low density and liquids (water, urine) (Ashley et al., 2005). Domestic slurries that originate from households that employ NS are likely to contain a significant fraction of kitchen waste with low dilution. Thus, making them highly viscous when compared to water.

Sewer based systems use gravity to transport the wastewater, which are highly diluted. On the other hand, on employing NS systems, they require an alternative and flexible means of transportation in order to handle the different ranges of product streams that may be very viscous. The common modes mentioned for transport inside and outside the house are gravity, vacuum, pressurised, pneumatic and non-piped systems (Harder, 2012).

1.1.3 Treatment

The goals for treatment of the product streams that arise from NS systems is to eliminate possible human and environmental health hazards (pathogens) and recover the resources from them. Whereas, resources in conventional sewer based systems are misplaced, as they are mere conveyance systems that treat the wastewater for its safe disposal. New sanitation aims at recovering these resources. Decentralisation plays a key role in this. It aims at treating the product streams closer to its generation, thereby resulting in smaller conveyance networks. This concept is synonymous with on-site treatment, which refers to treatment at the source. There are many technologies that support that efficient recovery of resources from NS streams (Larsen et al., 2013). Greywater, generally treated on-site gives the potential to reuse the generated water locally (Larsen et al., 2013). Energy and nutrients from black water or brown water are recovered at decentralised treatment units (Kujawa-Roeleveld and Zeeman, 2006; Otterpohl et al., 2002; Larsen et al., 2013).

1.2 Missing link

During the last few decades, NS concepts have been pioneered at a small scale. A large number of these pilots have been described in literature and in case studies (Larsen et al., 2013). The available literature focuses on source separation concepts, decentralisation and feasibility of small-scale treatment concepts. Although these concepts are efficient, they are very sensitive towards specific technology choices (Larsen et al., 2009). A repeated emphasis has been placed on the boundary conditions within which these systems are successful (Larsen et al., 2013). These treatment and collection concepts need a certain scale to render the entire sanitation system economically feasible. But transportability issues have been neglected, despite the fact that an integrated approach to the feasibility of new sanitation concepts should address all

the key elements of a sanitation concept: collection, transport and treatment. Even though, treatment and collection concepts have been researched intensively, transportation issues have been largely overlooked. The Dutch Foundation for Applied Research on Water Management and Wastewater Treatment (STOWA) has recommended to further investigate black water transport concepts (Palsma et al., 2010). An unreliable transportation system is a show-stopper for these sanitation systems. Sustainable sanitation systems will not be introduced widely until transportability issues have been investigated in sufficient detail.

Efficient transport of domestic slurries being the missing link in NS concepts, it has to be investigated to avoid failure of future sanitation systems and will be the focus of this study. Assessing the transportability of the slurries from NS systems will render a fit-for-purpose technical feasibility of large-scale application of new sanitation systems, including all known benefits that are associated with these systems: improved nutrient recovery, effective resource management, and improved energy production. Furthermore, the need for renovation of existing sewer-based systems may accelerate the large-scale introduction of NS concepts (Larsen et al., 2013).

1.3 Challenge of transport

Conventional sewer systems transport wastewater using large sewer networks (based on gravity) that must operate under both dry and wet weather conditions. The design rules for these networks must accommodate peak dry weather flows, storm water (surface run off) and control over sediments (specifying minimum wall shear stress from flow). With the paradigm shift to NS systems, transport technologies must necessitate the handling of a wide range of liquids and slurries (product streams). The implementation of source-separation, vacuum toilets and kitchen grinders result in slurries that originate from this system to have a high suspended solids concentration (low dilution and additional organics load). This source-separated **C**oncentrated **D**omestic **S**lurry (**CDS**) consisting of black water (human faecal waste, urine, and flushed water) and **G**round **K**itchen **W**aste (**GKW**; from food waste disposers) must be efficiently managed. At the core of management of these slurries lies its transportation from collection to treatment. For this purpose, design guidelines for the systems to transport these slurries are necessary, which has been identified to be non-existent. It is therefore important to fill this knowledge gap.

The current status of transporting CDS in existing systems is by pressurised pipelines (Larsen et al., 2013), and will remain so in the foreseeable future. Before design guidelines are established it is pertinent to understand the behaviour of these slurries that are being transported. An improved understanding of the behaviour of concentrated domestic slurries is required for the design of an efficient pipeline transport for CDS. The latter is required for a holistic evaluation of NS systems. Two aspects of transport behaviour, i.e. rheological properties and flow characterisation have been identified to be key in establishing these guidelines which will be discussed in the following sections.

1.3.1 Rheological characterisation

In order to design and operate a pipeline transport system for source-separated CDS, detailed knowledge about the physical and flow properties of the transported fluid, particularly rheology, is essential (Chilton et al., 1996; Heywood, 1991; Wasp et al., 1977; Slatter, 1995). It has been shown that even the basic aspects of a pipeline design, for example the expected flow regime (laminar or turbulent) and pressure drop, can be misjudged without a rigorous understanding of the rheology (Eshtiaghi et al., 2012; Slatter, 1995; Chilton et al., 1996).

Numerous studies have investigated the rheology of similar slurries such as primary sludge as well as secondary sludge, in treatment plants as recently summarized by Eshtiaghi et al. (2013b) and Ratkovich et al. (2013). The rheology studies describe the slurries in general as non-Newtonian in its flow behaviour and highly viscous. However, the obtained rheology specific results are not directly applicable to CDS as they do not represent the contents of CDS in its untreated form as opposed to that of primary or secondary sludge. Currently, there is a lack of information about the rheological properties of CDS, which must be determined. It is also known that concentration of the suspended solids and temperature of the slurry greatly influence the rheological properties (Eshtiaghi et al., 2013b; Ratkovich et al., 2013). It is therefore imperative that these influences are also studied.

1.3.2 Flow characterisation

New sanitation systems are commonly implemented with pressurised pipes to transport the CDS from the collection point to the treatment facility (Example: Sneek, Leuwaarden). Although no particular litereature was found on the transportation of CDS in pressurised pipes, a report by Harder (2012) outlines the common modes of transportation and concludes that pressurised pipe transport as single-phase and two-phase (including air) slurry could be promising given its application to similar slurries encountered in food and chemical industries. With the most commonly incurred means being single phase slurry transport, it will form the core of this study. In particular, it will focus on non-Newtonian slurries as this is the fluid behaviour of CDS 1.3.1.

Basic aspects of the design guidelines for pipeline transport need to account for the pressure loss incurred (energy loss) and the flow regime present where the prediction of laminar or turbulent flow is important. To prevent sedimentation of the constituents (suspended solids) of the slurry, the flow regime must be turbulent (which provides the minimum wall shear stress against sedimentation). These aspects of design will have to encompass a wide range of configurations from horizontal flow to inclined flow and minor local losses (pipe fittings and junctions) to assess and implement optimal slurry transportation.

The state of the art in flow characterisation of non-Newtonian slurries spans across various research domains. While some focus on predicting the incurred pressure loss in transporting the slurries (Slatter, 1995; Assefa and Kaushal, 2015), others have

focussed on predicting transitions from laminar to turbulent flow (Güzel et al., 2009b). The models for pressure loss predictions are varied and have their specific use (Slatter, 1995). The usage of these models pertaining to the specific non-Newtonian behaviour of CDS is unknown. As the transportation of these slurries must occur at turbulent regime, the flow parameters for which this occurs for CDS must also be established.

1.4 Research Objective

This work aims at contributing to bridge the gap in NS systems, as outlined in the previous sections. This is done by addressing the issues related to the transport of CDS and will be focussed on the challenges of transport (Section 1.3), namely the rheological and flow characterisation of CDS. Based on this, the research objectives are formulated as follows:

- Rheological characterization of CDS.
- Determine the influence of suspended solids concentration and temperature on the rheology of CDS.
- Examine the relation between pressure loss incurred on transportation of the slurry to its rheological characterisation.
- Observe and determine the transition from laminar to turbulent flow of slurries (in general non-Newtonian fluids).

1.5 Strategy

The objectives of this thesis is centred around the flow characterisation of CDS. The strategy adopted to address this is described here. Figure 1.3 provides an outline to the thesis presenting the relation to the different chapters.

In characterising the flow of CDS, a description of the pressure drop incurred in flow in pipes through various flow parameters is provided. This is done by using a non-Newtonian flow model. The rheology of CDS is required by the non-Newtonian flow model to characterise its flow. This non-Newtonian flow model is built and calibrated using the flow characterisation of a model slurry. A model slurry is used in lieu of CDS, as the properties of CDS is not stable in time, it poses health risks and cannot be handled easily. Firstly, the rheological properties of the model slurry are examined. And later an experimental set-up is built to study the flow characteristics of the model slurry at various flow parameters. Its transition from laminar to turbulent flow is also observed. Using these results, a suitable non-Newtonian flow model is selected.

The rheological characterisation of CDS is presented in Chapter 2 and 3. A rotational Couette rheometer is used for this purpose. Chapter 2 presents in detail the rheological measurements in a narrow gap rheometer and the influence of temperature

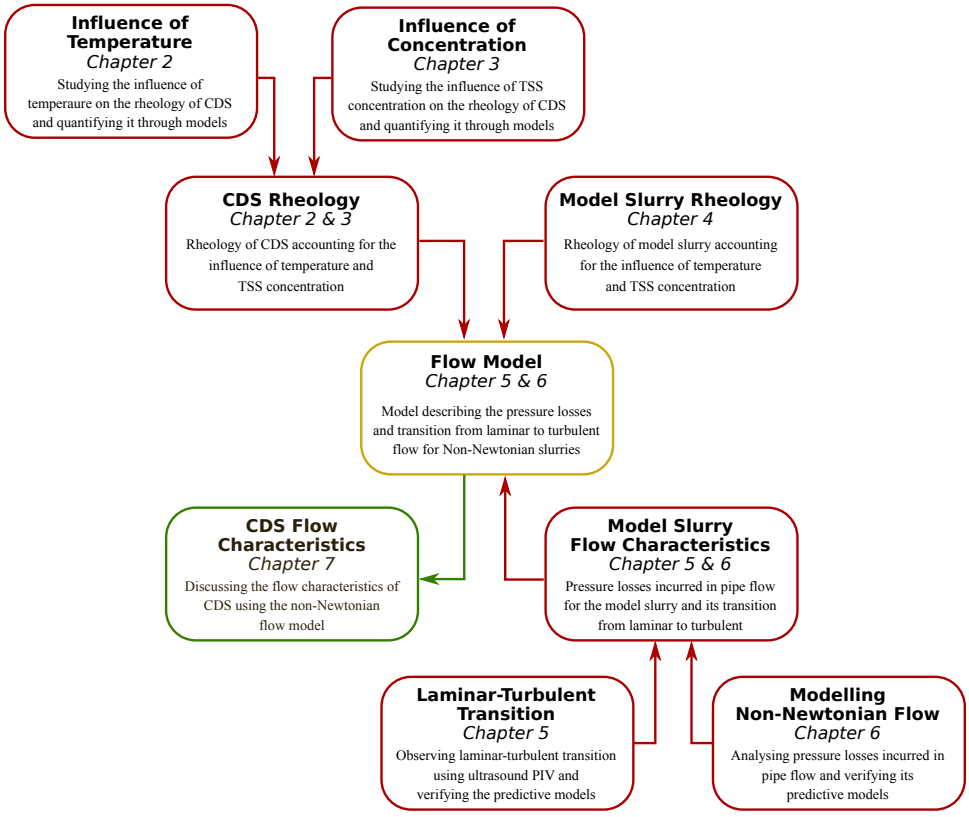

Figure 1.3: Outline of the thesis presenting the relation between the different parts of the thesis

on the rheology. Although, the influence of concentration is discussed in Chapter 2, this is done using sieved slurry. For a complete understanding of the influence of concentration, the unsieved slurry must be studied. For this a wide gap rheometer is also used, in this case to characterise the un-sieved slurry which is presented in Chapter 3. Along with this, the influence of varying the suspended solids concentration is described.

A large pipeline loop is built to study the flow characteristics of the model slurry. Details of this loop and the experimental techniques used for this study is presented in Chapter 4. The flow transition of the model slurry from laminar to turbulence is observed using Ultrasound Imaging Velocimetry (UIV) which is presented in Chapter 5. Using these observations, the models available to predict the transition are verified for non-Newtonian slurries. The pressure drop measured for the model slurry in the experimental pipe loop is analysed in Chapter 6 along with the models used to predict these pressure drops.

Chapter 7 provides a summary of the theoretical framework that is set-up for the flow characterisation from the previous chapters. It also provides a discussion on the application of this knowledge in designing CDS transport networks for NS systems. Chapter 8 draws conclusions on the work presented in this thesis along with recommendations for future work and the knowledge gap that needs to be filled.

Part I

Rheological Characterisation

Chapter 2 is based on:

Thota Radhakrishnan, A.K., van Lier, J.B., Clemens, F.H.L.R. (2018). Rheological characterisation of concentrated domestic slurry. *Water research*, 141 (2018): 235-250.

Thota Radhakrishnan, A.K., Alidai, A., Pothof, I.W.M., Clemens, F.H.L.R. (2015). Transport aspect of domestic slurry: a step ahead forward towards new sanitation systems. Presented at the *10th Urban Drainage Modelling Conference*, Mont-Saint-Anne, Qubec, Canada, 20 - 23 September 2015.

Pothof, I.W.M., Alidai, A., Thota Radhakrishnan, A.K., Clemens, F.H.L.R. (2015). The missing link in future sanitation. Presented at *Environmental Technology for Impact (ETEI2015)*, Wageningen, Netherlands, 29 - 30 April 2015.

CHAPTER 2

Rheology: Influence of Temperature

The state of the art on the solids content of wastewater in traditional sewer systems is summarised in the book Solids in Sewers (Ashley et al., 2005). Although it provides great details regarding the origin and physio-chemical properties of the wastewater, rheological properties have not been characterised. It is common that a viscosity close to pure water is considered for the design of traditional sewer systems (Hager, 2010). However, CDS is much less diluted compared to the traditional domestic waste (Tervahauta et al., 2013); therefore, it is expected to have a considerably larger (apparent) viscosity.

Many studies have investigated the rheological behaviour of the primary, secondary, and aerobic/anaerobic digested sludge in treatment plants as summarised in (Eshtiaghi et al., 2013a; Ratkovich et al., 2013). It was concluded that the sludge is a non-Newtonian fluid showing a shear-thinning thixotropic behaviour. On the existence of the yield stress, no agreement was found. However, the obtained results are not directly applicable to the CDS, because primary and secondary sludge do not represent fresh faecal sludge and they undergo different treatments that change the structure of suspended organic matter present in the slurry. A study on fresh faecal sludge by (Woolley et al., 2014), is the only available literature on this. Unfortunately, their study doesnt give much information on procedure and collection to make the study useful for analysis. The inclusion of waste from FWDs also increases the flow complexity of these slurries. Although many researchers have recommended FWDs, they have also indicated that for a large scale implementation or for higher market penetration, the implications of FWDs on environment and on the sewer system need to be examined; an overview of this can be found in Iacovidou et al. (2012a). Evidently, the rheological knowledge of sludge in treatment plants cannot be directly used to reliably estimate the rheological properties of CDS; therefore, proper measurement needs to be conducted to investigate these properties. The current work presents measurements that were carried out to characterise the rheological properties of CDS. The influence of two parameters, namely temperature and concentration is examined. Based on the outcome of the measurement, the fluid models that describe the rheological behaviour of CDS are introduced. Also, the inclusion of GKW is accessed from a rheological aspect of these slurries.

2.1 Methods and Materials

2.1.1 CDS Slurry

A sample each of two different domestic slurries were collected. ***Slurry 1***, black water consisting of human faecal waste, toilet paper and flushed water was collected from a vacuum collection experimental facility in the building of DeSaH B.V. in Sneek, the Netherlands. The vacuum collection system consists of a urine separation vacuum toilet connected to a collection tank through a vacuum pump. The vacuum pump is fitted with a cutter upstream (Figure 2.1b) to cut the incoming waste. ***Slurry 2***, BlW with GKW was collected from the housing project Noorderhoek consisting of 215 houses in Sneek, Netherlands. These houses have source separation implemented in them along with vacuum toilets and food (kitchen) waste disposers. Slurry 2 is collected from a collection tank as shown in Figure 2.1a. It has to be noted that prior to the collection, the CDS passes through a cutter pump (as shown in Figure 2.1b) which transfers it from a vacuum tank to the collection tank (as schematized in Figure 2.1a). In some vacuum stations, the waste is directly transferred from the vacuum tank to the treatment plant by sewage pumps without any intermediate collection tanks. In such configurations, there are cutters installed upstream of the tank to break down the large lumps.

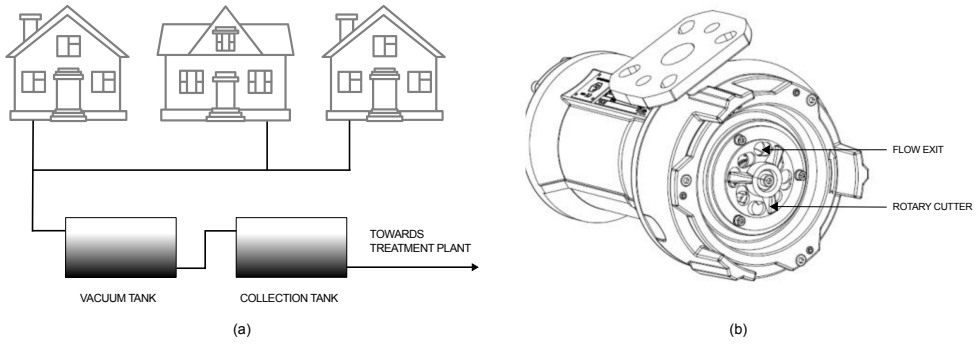

Figure 2.1: a) Schematic drawing of a vacuum collection station. b) Cutter pump (submersible dis-integrator pump manufactured by Landustrie).

The slurries thus collected were immediately transported to the laboratory in a cool box at $4°C \pm 1°C$. The procedure followed the advice for the preservation of wastewater slurry given in (APHA, 2005) in order to retard biological activity and microbiological decomposition in the samples. In order to preserve the original moisture content and avoid reactions with air, the samples were kept in sealed containers. Once in laboratory, the samples were maintained refrigerated at the same conditions, minimizing changes in the organic compounds during storage until testing.

To obtain slurry 1 as fresh as possible, the collection tank was emptied and cleaned a day before sampling and the toilets were connected to the tank at the morning of collection day. In addition, to obtain a good representative sample, slurry 2 was collected during the evening, at the peak of usage of the toilets and food waste disposers. The maximum retention time of the slurries were five hours at the room temperature. The samples were tested within 3 days of its collection.

Sample preparation

Existence of large particles in a sample puts a constraint on the geometry of the rotational rheometer. In order to ensure a continuum description of the flow, a gap size to a maximum particle size ratio should be 10 or more to guarantee a shear flow (Van Wazer, 1963). To ensure this, both slurries 1 and 2 were screened by passing through a mesh with opening size of 2 mm for removing coarse particles. THe coarse particles only comprise a negligible portion of the total solids in the wastes. Hereafter, the samples were then screened using a mesh of opening size of 0.125 mm to remove particles larger than 0.125 mm. This particular mesh size was chosen to minimise the material loss during sieving, to ensure repeatability and to maximise the particle to rheometer gap ratio. Through this procedure, the total suspended solids (TSS) that is lost from sieving is between 10% to 20%. This low percentage of loss can be attributed to the presence of a grinder pump (as shown in Figure 2.1b), which transfers the CDS from the vacuum tank to the collection tank. The cumulative particle size distribution for both slurries 1 and 2 presented in Figure 2.2 (measured using a laser diffraction particle size analyser), is used to calculate the minimum gap size. As a standard, the minimum gap size must be 10 times the D_{90} (representative particle size) of the slurry. The D_{90} for slurry 1 is 51 μm and for slurry 2 is 80 μm. Therefore, a gap size of 800 μm would be satisfactory for both slurries.

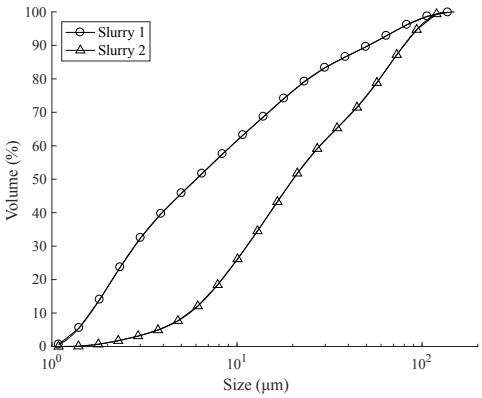

Figure 2.2: Cumulative particle size distribution of slurry 1 and slurry 2.

The TSS upon collection of slurry 1 was 2.6 % TSS (wt./wt.) and slurry 2 was 1.8 % TSS (wt./wt.). The samples were then concentrated to study its rheology at various concentrations. Using gravity settling slurry 1 was concentrated to 7.2 % TSS (wt./wt.) and slurry 2 to 3 % TSS (wt./wt.). The obtained supernatant of each sample was respectively used to dilute the sample to obtain different concentrations. Slurry 1 was further concentrated to 11.2 % TSS (wt./wt.) by centrifugation at 10 G for 1 min, and then diluted to 10 % using the supernatant. The centrifugation procedure was adapted to make sure that the settled particles were suspended upon gentle shaking. This was deemed necessary to ensure that the original flocs were maintained with minimal changes. A summary of the investigated concentration is presented in Table 2.1.

Table 2.1: Summary of investigated slurry concentrations

Slurry 1: Faecal		Slurry 2: Faecal + GKW	
Concentration	Concentrating method	Concentration	Concentrating method
(% TSS wt./wt.)		(% TSS wt./wt.)	
11.2	Centrifugation	3	Gravity
10	Centrifugation	2.6	Gravity
7.2	Gravity	2.1	Gravity
5	Gravity	1.8	Gravity
3.9	Gravity	1.2	Gravity
3.2	Gravity	1.0	Gravity
2.6	Gravity		
1.8	Gravity		
1.4	Gravity		
0.7	Gravity		
0.4	Gravity		

2.1.2 Rheometry

Commonly used rheometers, capable of measuring fundamental rheological properties of sludge, are placed into two general categories (Eshtiaghi et al., 2013a,b): rotational rheometer and capillary rheometers. Advantages and disadvantages of each category have been described in (Eshtiaghi et al., 2013a; Seyssiecq et al., 2003; Slatter, 1997). The rotational rheometer has become widely accepted in recent years as the most common class of rheometer utilised in sludge rheology (Eshtiaghi et al., 2013a), and is also used in this study.

The rheology measurements were performed with a MCR302 instrument from Anton Paar (Graz, Austria) equipped with a standard cup and bob (cup diameter: 29.29 mm, bob diameter: 27 mm, bob length: 40.5 mm). This geometry has a gap size 1145 μm, satisfying the minimum required gap size mentioned in section 2.1. A Peltier temperature control system was used to set and maintain the temperature with an accuracy of $\pm 0.1°C$. The rheology was measured at $10°C$, $20°C$, $30°C$ and $40°C$ for each concentration to determine the influence of temperature. To avoid evaporation during the measurements, a lid was installed on the cup to cover the sample. It is suggested that for slurries of this nature, a pre-shear is required to erase material memory and to have similar initial conditions for all samples (Baudez et al., 2011, 2013). Therefore, for each investigation the sample was pre-sheared for 5 min at a shear-rate of 1000 s^{-1}, and then left to rest for 5 min, these conditions were found suitably to reproduce results. The rheogram for each investigation was obtained by a step-wise shear ramp-up procedure, and recording the steady state shear-stress for every set shear-rate. Through the step-wise shear ramp-up the inertia of the equipment is avoided by waiting for steady state at each measurement point (Baroutian et al., 2013). This ensures that the inertia of the fluid and the equipment is eliminated. A ramp-down procedure is avoided as it would considerably include the inertia of the fluid; as the fluid that is rotating at a higher angular velocity is slowed down which causes a delay in reaching steady-state. The shear-rate range was so determined to avoid the occurrence of secondary flows (Thota

Radhakrishnan et al., 2015). At the end of every test, the used sample was discarded and a fresh sample was used for the next test.

Table 2.2: Rheological models

$\tau = \mu\dot{\gamma}$	the Newtonian model that represents a linear relationship between shear-stress and shear-rate
$\tau = K_{PL}\dot{\gamma}^{n_{PL}}$	the Power law model that represents a power law relationship between the shear-stress and shear-rate showing a shear thinning behaviour with $n_O < 1$
$\tau = \tau_{yB} + \mu_B\dot{\gamma}$	the Bingham model represents a fluid with a yield stress. The yield stress is the minimum shear-stress required for the fluid to start flowing
$\tau = \tau_{yHB} + K_{HB}\dot{\gamma}^{n_{HB}}$	the Herschel-Bulkley (HB) model is used to represent a shear-thinning fluid with a yield stress
$\tau = \tau_{yCHB} + \mu_{CHB}\dot{\gamma} + K_{CHB}\dot{\gamma}^{n_{CHB}}$	the combined Herschel-Bulkley (CHB) used by Baudez et al. (2011, 2013) represents well the linear shear-thinning behaviour at high shear-rates giving a constant high-shear viscosity. It is merely a HB model coupled with a Newtonian model

2.1.3 Rheological model

Rheological models are an empirical representation of the obtained rheogram (graphical representation of shear-stress vs. shear-rate). For design purposes, the rheological models are used rather than the rheograms. As rheology is the single most important representation of the hydrodynamic behaviour, any discrepancy with the rheological prediction using the model would lead to poor process design as rheology is usually extrapolated for turbulent flow predictions (Slatter, 1997). Therefore, the choice of the rheological model is critical in this aspect. The models used commonly are presented in Table 2.2. Elaborate reviews on the models available have been already provided in articles by Seyssiecq et al. (2003), Ratkovich et al. (2013) and Eshtiaghi et al. (2013a,b).

2.1.4 Statistical assessment

To access the predictive capability of the selected rheological models mentioned in section 2.1.3 the following statistical descriptors are used. The root mean square error (RMSE, Equation 2.1) measures the overall accuracy of the model. The squared sum of residual (SSR, Equation 2.2) measures the square of the absolute deviation of the model.

$$RMSE = \sqrt{\frac{\sum_{i=1}^{N}(\tau_i - \hat{\tau}_i)^2}{N}} \tag{2.1}$$

$$SSR = \sum_{i=1}^{N} (\tau_i - \hat{\tau}_i)^2 \tag{2.2}$$

2.1.5 Parameter estimation

The goal of the parameter estimation step is to determine a unique set of model parameters for the obtained rheometric data (Ratkovich et al., 2013). This is done using optimisation algorithms by minimizing the square of the residuals between the model and the experimental data. Although this step seems straightforward (by using commercially available software), implicit assumptions in the optimization algorithms, violation of boundaries of the model parameters and over parametrisation can lead to obtaining parameters that are often not unique or physically meaningless. Care must be taken in estimating these parameters and for this reason two optimization algorithms have been used in the study and shall be detailed below:

Genetic + Trust Region algorithm (GTR)

Minimization of the square of the residuals is a quadratic problem. Most gradient-based optimization algorithms are very sensitive to the initial point and thus obtain only some local minima in the proximity of the initial point. As most rheological models are non-linear, there may exist many local minima. Identifying the most optimal minima (preferably the global minimum) of these satisfying the boundary conditions in place requires the optimization procedure to run many initial points, for which the results of the Genetic Algorithm provide valuable information (i.e. it results in a global map of the location of local minima, which in turn are candidates to be investigated further using some gradient based search algorithm). A Genetic algorithm is one such tool that helps in achieving this in a systematic manner. In this algorithm, an initial population of a random set of parameters (within the boundary specified) is generated. In our case the boundaries depend on the parameters and in general are, $0 < \tau_y$, $0 < K$ and $0 < n < 1$. Using the objective function, the corresponding fitness values for each set of parameters is determined. Using this information, a new generation is produced by applying three genetic operations namely: reproduction, crossover and mutation (Chaudhuri et al., 2006). These operations ensure that a minimum that is found is investigated, and also new sets of parameters are added to avoid being stuck in a local minimum. More information on this approach can be found in (Chaudhuri et al., 2006; Rooki et al., 2012). Each population that is generated is likely to converge to the global minimum. Although a stand-alone genetic algorithm is sufficient for convergence, but to ensure this a gradient-based optimization algorithm is coupled with it. After a number of generations (termination) from the Genetic Algorithm, a part of the population with high scores of fitness value based on the RMSE (Equation 2.1) is taken and fed to a gradient-based optimization procedure. A trust region (Byrd et al., 1987) optimization which is a simple gradient based algorithm is used in this case. Hereafter, the parameter set with the lowest RMSE (Equation 2.1) is chosen as the optimal solution. This entire algorithm is schematized in Figure 2.3. In this study, this algorithm is used in general for all modelling purposes.

Golden section search (GSS)

The golden section search method was proposed by (Ohen and Blick, 1990) for determining model parameters of the Robertson-Stiff fluid model. This numerical scheme was later

modified by (Kelessidis et al., 2006) to be used for predicting the parameters for a HB fluid model. In their paper (Kelessidis et al., 2006), the authors demonstrated that the GSS method lead to meaningful and appropriate values for the model parameters. This algorithm is particularly helpful when the parameters are correlated, which is the case with the HB model and will be discussed later. The algorithm essentially de-couples the parameters and reduces the correlation in their estimation. This numerical scheme has been used in this paper and is presented in Figure 2.4. In this study, this algorithm is only used to find more accurate solutions for the HB model.

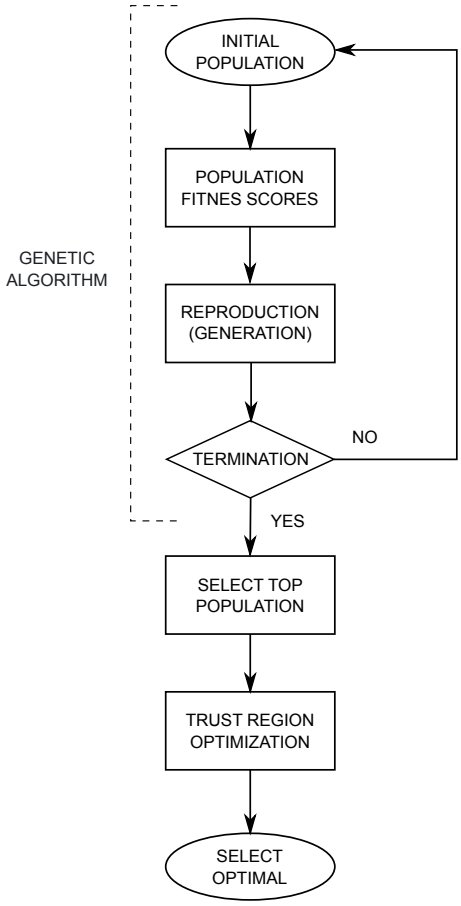

Figure 2.3: Genetic + trust region parameter estimation algorithm shown in a flow diagram.

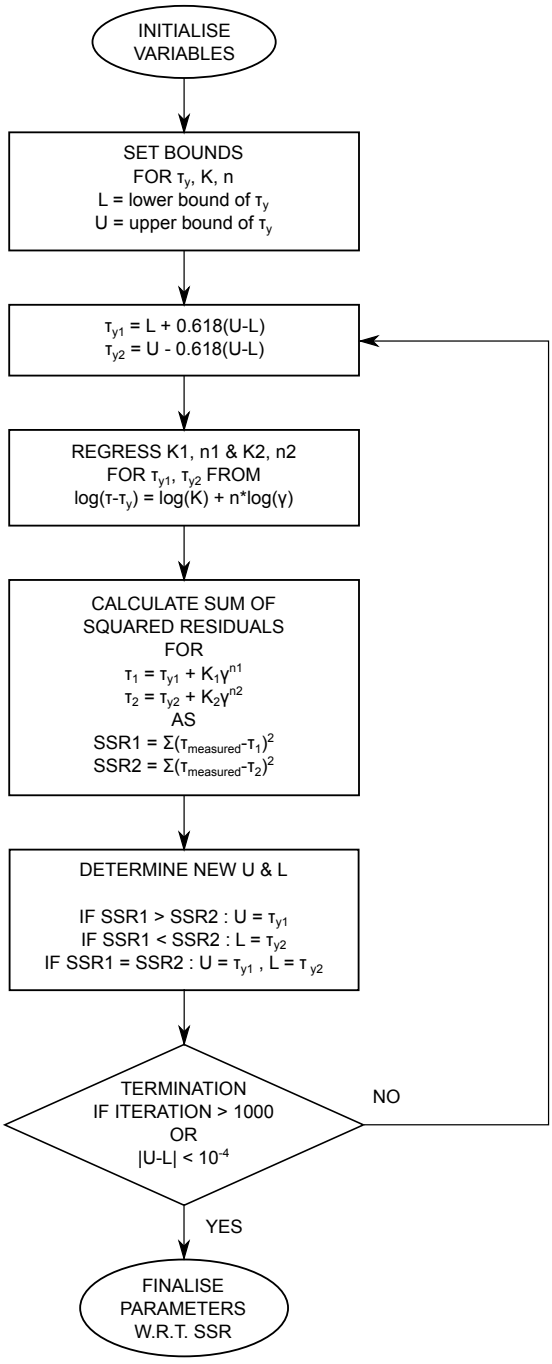

Figure 2.4: Golden section search parameter estimation algorithm shown in a flow diagram.

2.2 Results and discussion

2.2.1 Rheology

The rheograms for slurry 1 as shown in Figure 2.5 (a few representative rheograms) and slurry 2 as shown in Figure 2.6 (a few representative rheograms) at various concentrations and temperatures were obtained using the shear-rate ramp up procedure mentioned in section 2.1.2. For slurry 1 the concentrations ranged between 0.4 % and 11.2 % TSS (wt./wt.) and for slurry 2 the concentration ranged between 0.8 % and 3.0 % TSS (wt./wt.). For each sample the influence of temperature was evaluated at $10°C$, $20°C$, $30°C$ and $40°C$. The steady-state laminar data was used in creating these rheograms. This was ensured by identifying the onset of secondary flows (Thota Radhakrishnan et al., 2015), and removing it from the obtained data. More details on identifying laminar flow and secondary flow along with the range of shear-rates can be found here (Thota Radhakrishnan et al., 2015). This therefore influenced the maximum applicable shear-rate for each concentration and temperature depending on the onset of secondary flows.

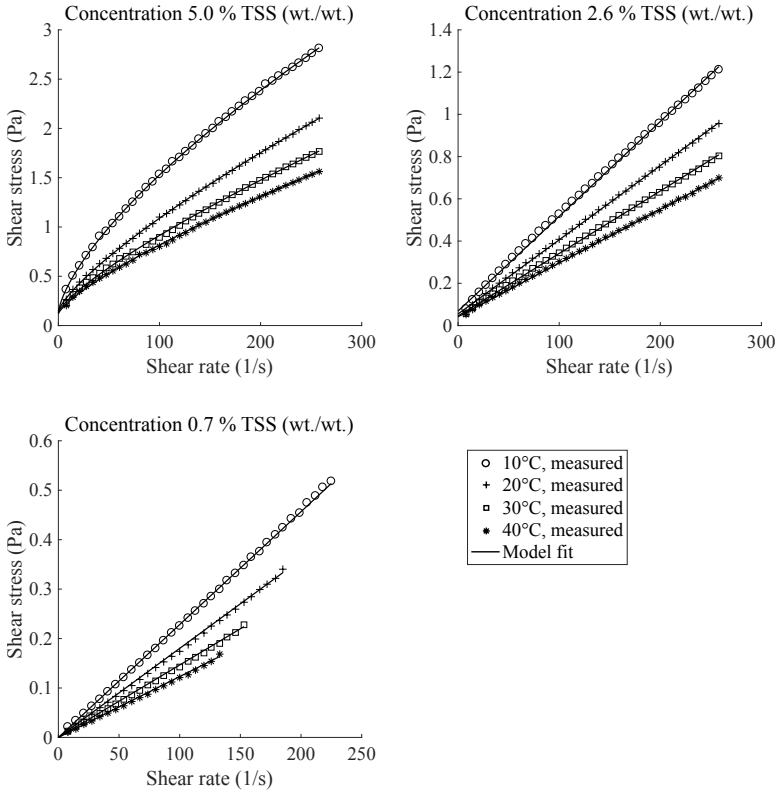

Figure 2.5: Representative rheograms for Slurry 1 at various concentrations and temperatures; the respective model used for fitting is indicated in table 2.

From the rheograms, it can be observed that the shear-stress increases non-linearly with

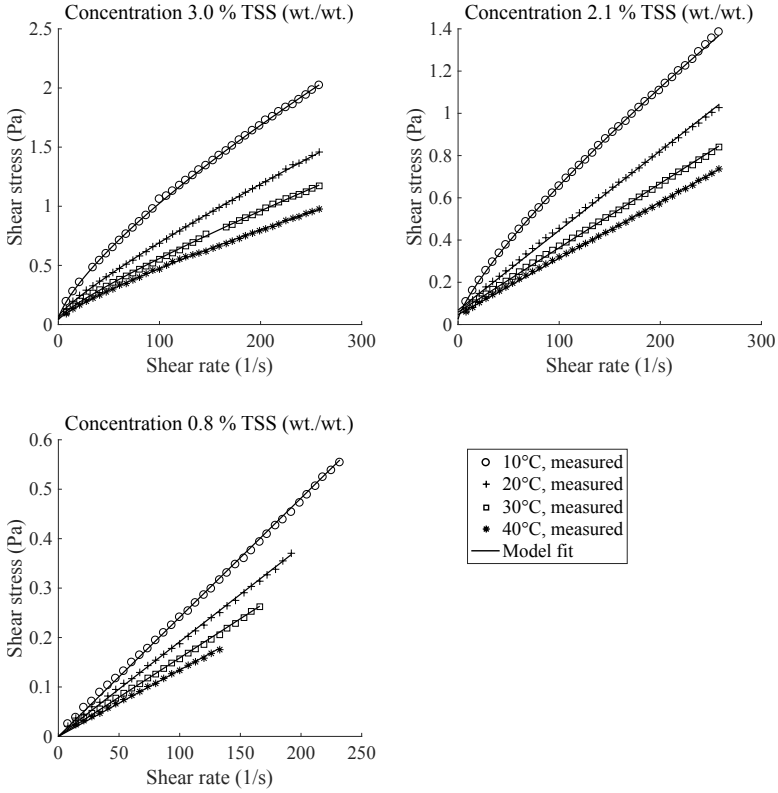

Figure 2.6: Representative rheograms for Slurry 2 at various concentrations and temperatures; the respective model used for fitting is indicated in table 3.

respect to the shear-rate at high TSS concentrations in slurry 1. At low TSS concentration, the shear-stress is a linear function of shear-rate for both slurry 1 and 2. As for the influence of temperature, it is observed that the increase in temperature reduces the shear-stress. This can be attributed to the increase in thermal motion of the molecules and thereby reducing the forces between the molecules resulting in an ease of the flow of the slurry, thus lowering the viscosity.

The influence of increasing the solid content in the slurry can be seen in Figure 2.7, which is slurry 1 at various concentrations but at a fixed temperature of $20°C$. The illustration shows an increase in shear-stress with the increase in shear-rate. This observation has also been reported in many other studies (Baroutian et al., 2013). This increase is due to the increase in interactions between the constituent particles present in the slurry. The increase in interactions results in increase in the energy loss, thereby requiring more energy i.e. high shear-stress to keep the slurry in a prescribed motion. As mentioned in (Baroutian et al., 2013), polysaccharides and proteins are likely the determining constituents for the rheological properties of these slurries.

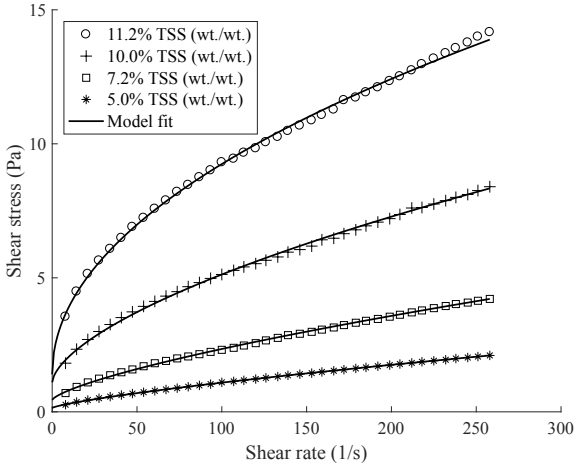

Figure 2.7: Rheogram of slurry 1 at various concentration and a fixed temperature of 20°C; the respective model used for fitting is indicated in table 2.

2.2.2 Rheological modelling

The rheological models described in section 2.1.3 were used to describe the obtained rheology data. It must be noted that this process of fitting the experimental data to a rheological model is tedious; it requires a priori information and a structured methodology. This is due to the empirical nature of the models that are used to fit the data. In practice a single model is used to fit an entire data set, but this fails due to the correlation between the parameters (Ratkovich et al., 2013). This can be seen from the errors (Figures 2.8 and 2.9, Appendix Tables A.1 and A.2) from the model fitting using the GTR algorithm to the different models. The model comparison is done using the residuals from the same optimisation algorithm so as to not bias the results. Therefore, based on the RMSE errors from the parameter estimation, the best model is chosen to represent the rheology data. At low concentrations, there is a linear relationship between the shear-stress and shear-rate, but at concentrations > 3 % TSS it is observed there exists a non-linear/non-Newtonian relationship.

The yield stress isn't a measured quantity. It is one that is derived as a parameter from the model, essentially extrapolating the obtained rheology data. It is therefore difficult to estimate the true yield stress, and a minimum threshold yield stress of 0.01 Pa is taken for considering its existence. This value is used to determine the appropriate model at low % TSS. From Figures 2.8 and 2.9, although the Bingham model fits better at lower % TSS, a linear model is chosen as the yield stress from the Bingham model is < 0.01 Pa. The power law model was the least suitable for all the cases. At higher % TSS, the CHB model used by (Baroutian et al., 2013) is a better fit than that of the HB model. This can entirely be attributed to the increase in the degree of freedom of the optimisation by adding another parameter. But, to further investigate the applicability of the HB and CHB models, the identifiability of their parameters is to be accessed.

To assess the identifiability of the parameters, principal component analysis (PCA) is

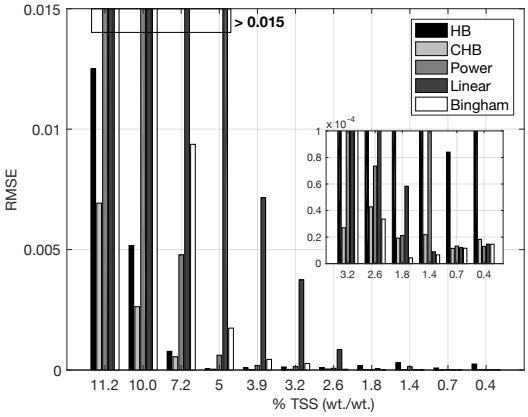

Figure 2.8: RMSE for the model fit of slurry 1 rheograms at 20°C

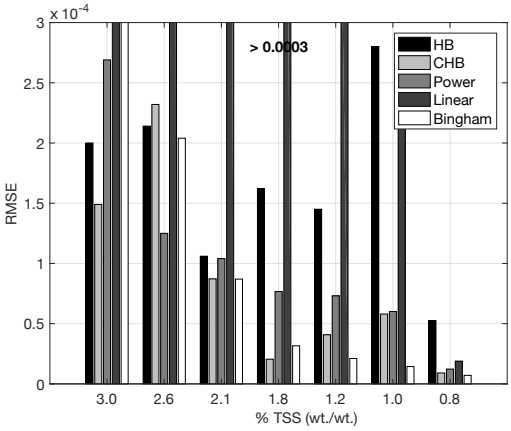

Figure 2.9: RMSE for the model fit of slurry 2 rheograms at 20°C

used. This is done using the Jacobian of the rheological models from Equation 2.3 (for HB model) and Equation 2.7 (for CHB model). Singular value decomposition of the matrix $\underline{J}^T\underline{J}$ (Equation 2.12) gives information about the identifiability of the parameters. The diagonal terms of the matrix is the variance of the parameter combination and the matrix $\underline{V}$ gives the singular values. Figure 2.10 illustrate the singular values of the parameter combination. It can be seen that the CHB model performs poorly as the parameter combinations are co-dependent. This implies that there cannot be a meaningful parameter estimation using this model. But, when accessing the Eigen vectors of the HB model (Figure 2.10), it can be seen that the parameter combinations are less co-dependent. Therefore, the HB model is a more relevant model to be used.

$$\underline{J}_{HB} = \begin{bmatrix} \frac{\partial \tau_1}{\partial \tau_{yHB}} & \frac{\partial \tau_1}{\partial K_{HB}} & \frac{\partial \tau_1}{\partial n_{HB}} \\ \vdots & \vdots & \vdots \\ \frac{\partial \tau_N}{\partial \tau_{yHB}} & \frac{\partial \tau_N}{\partial K_{HB}} & \frac{\partial \tau_N}{\partial n_{HB}} \end{bmatrix} \tag{2.3}$$

$$\frac{\partial \tau_1}{\partial \tau_{yHB}} = 1 \tag{2.4}$$

$$\frac{\partial \tau_1}{\partial K_{HB}} = \dot{\gamma}^{n_{HB}} \tag{2.5}$$

$$\frac{\partial \tau_1}{\partial n_{HB}} = K_{HB} n_{HB} \dot{\gamma}^{n_{HB}-1} \tag{2.6}$$

$$\underline{J}_{CHB} = \begin{bmatrix} \frac{\partial \tau_1}{\partial \tau_{yCHB}} & \frac{\partial \tau_1}{\partial \mu_{CHB}} & \frac{\partial \tau_1}{\partial K_{CHB}} & \frac{\partial \tau_1}{\partial n_{CHB}} \\ \vdots & \vdots & \vdots & \vdots \\ \frac{\partial \tau_N}{\partial \tau_{yCHB}} & \frac{\partial \tau_N}{\partial \mu_{CHB}} & \frac{\partial \tau_N}{\partial K_{CHB}} & \frac{\partial \tau_N}{\partial n_{CHB}} \end{bmatrix} \tag{2.7}$$

$$\frac{\partial \tau_1}{\partial \tau_{yCHB}} = 1 \tag{2.8}$$

$$\frac{\partial \tau_1}{\partial \mu_{CHB}} = \dot{\gamma} \tag{2.9}$$

$$\frac{\partial \tau_1}{\partial K_{CHB}} = \dot{\gamma}^{n_{CHB}} \tag{2.10}$$

$$\frac{\partial \tau_1}{\partial n_{CHB}} = K_{CHB} n_{CHB} \dot{\gamma}^{n_{CHB}-1} \tag{2.11}$$

$$\underline{J}^T \underline{J} = \underline{U} \Sigma \underline{V} \tag{2.12}$$

To increase the identifiability of a unique parameter set of the HB model, in this study a method of Golden Section search (section 2.1.5) is used. This is a better algorithm in estimating the parameters for the HB model as can be seen from the RMSE ratios in Figure 2.11. As this method is only applicable to the HB model, it is not applied to the entire dataset. For this, the GTR algorithm is used to identify for which of the dataset a HB model applies and then the GSS algorithm is used on these datasets.

The final estimated parameters for the models are shown in the Tables A.3 and A.4 in the Appendix. For the sake of representation, the HB model is used, because the HB model is a generalised model for including both the Bingham (with $n = 1$) and the Newtonian model (with $\tau_y = 0$ and $n = 1$).

2.2.3 Effect of concentration and temperature

Many studies have already concluded that changes in concentrations and temperature influence the rheology of the slurries to a great extent (Baroutian et al., 2013; Eshtiaghi et al., 2013a; Mori et al., 2006; Ratkovich et al., 2013; Sanin, 2002; Seyssiecq et al., 2003). Studying the influence of temperature and concentration to the flow of the fluid i.e. rheology, is

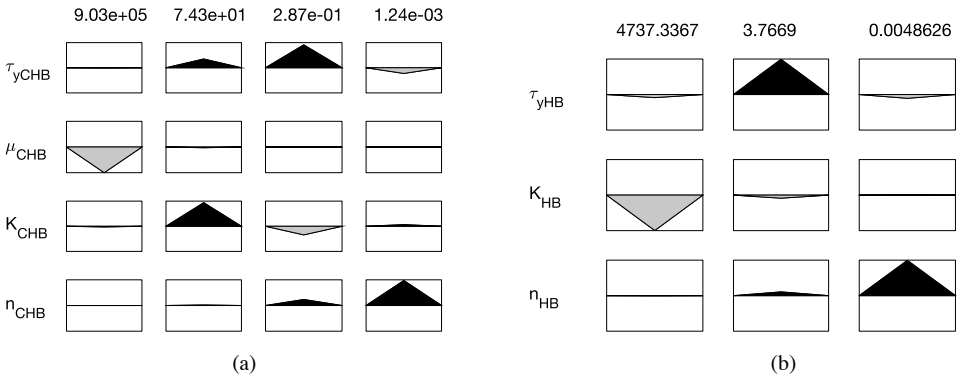

Figure 2.10: Singular values and eigen vectors of the parameters for (a) CHB model and (b) HB model using rheometric data of slurry 1 at 20°C with 11.2 % TSS.

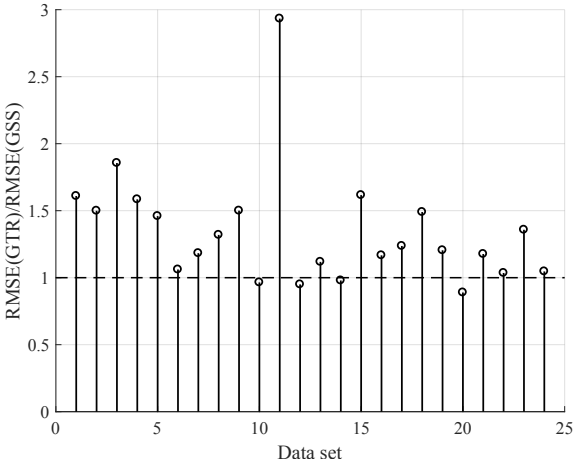

Figure 2.11: Plotting the ratio of the RMSE from the algorithm GTR to the one from GSS of the for the data set of Slurry 1 concentration ranging 11.2 till 3.2 % TSS of temperatures 10°C, 20°C, 30°C, 40°C.

considered important, because many transportation applications and slurry handling equipment such as mixers, aerators and heat exchangers encounter gradients of temperature and concentration. These gradients may occur due to the design of such equipment or the hydrodynamic flow in them (centrifugation, settling, mixing). An interesting outcome of the rheological modelling is to breakdown the influence of concentration and temperature on the rheology to the different parameters in the model. As each parameter represents a particular phenomenon in the behaviour of the fluid flow, it is easier to understand its contribution to the flow behaviour when studied separately. The HB model will be used as a general non-Newtonian model to represent the entire range of slurry rheology.

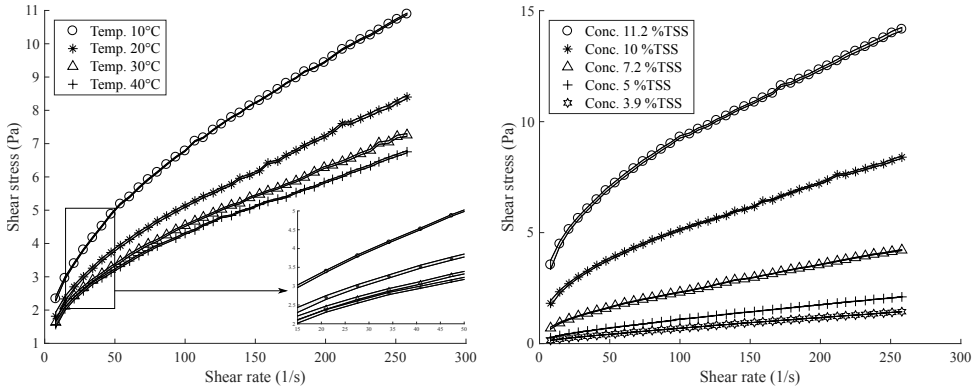

Figure 2.12: Plot of the uncertainty band of the predicted values of the regressed rheological model as compared to the measure data. Plot (a) is for various temperatures of slurry 1 at 10 % TSS. Plot (b) is of various concentrations of slurry 1 at 20°C.

Studying the influence of temperature and concentration through the rheological parameters imposes an extra step of caution, and this is to quantify the uncertainty in the prediction of the rheology using the parameters that have been estimated using the algorithms. What this means is that there is an inherent error presented in the models prediction with the parameters estimated. This error represents an uncertainty band of the prediction. For the models/parameters to represent the behaviour of the slurry to the influence of temperature and concentration, the error/uncertainty bands from the model prediction must not overlap with one another. Implying that, for example investigating the influence of temperature on 10% slurry as shown in Figure 2.12a, the uncertainty band of the model prediction of 10% slurry at different temperatures must not overlap. If they do, then the model parameters regressed do not represent the influence of temperature as is seen from experimental observation. Therefore, before evaluating the influence of temperature and concentration on the rheological parameters, an assessment of the uncertainty of the prediction of the models must be performed. This is to remove the uncertainty of incorrectly identifying the influence of conditions of the variables. This is done through Gausss law of error propagation. The uncertainty in the prediction is found using Equation 2.14, which is for a HB model where the covariance is obtained using Equation 2.13. From this, it can be observed that the uncertainty band for evaluating the effect of temperature (Figure 2.12a) and concentration (Figure 2.12b) do not overlap, thereby emphasizing its influence.

$$
\begin{aligned}
cov_{HB} &= \sigma^2_{residues}[\underline{J}^T\underline{J}]^{-1} \\
&= \begin{bmatrix} \sigma^2_{\tau_{yHB}} & \sigma_{\tau_{yHB}}\sigma_{K_{HB}} & \sigma_{\tau_{yHB}}\sigma_{n_{HB}} \\ \sigma_{\tau_{yHB}}\sigma_{K_{HB}} & \sigma^2_{K_{HB}} & \sigma_{K_{HB}}\sigma_{n_{HB}} \\ \sigma_{\tau_{yHB}}\sigma_{n_{HB}} & \sigma_{n_{HB}}\sigma_{K_{HB}} & \sigma^2_{n_{HB}} \end{bmatrix}
\end{aligned} \tag{2.13}
$$

$$
\begin{aligned}
\sigma^2_\tau =& (\frac{\partial\tau}{\partial\tau_{yHB}})^2\sigma^2_{\tau_{yHB}} + (\frac{\partial\tau}{\partial K_{HB}})^2\sigma^2_{K_{HB}} + (\frac{\partial\tau}{\partial n_{HB}})^2\sigma^2_{n_{HB}} \\
&+ 2(\frac{\partial\tau}{\partial\tau_{yHB}})(\frac{\partial\tau}{\partial K_{HB}})\sigma_{\tau_{yHB}}\sigma_{K_{HB}} \\
&+ 2(\frac{\partial\tau}{\partial\tau_{yHB}})(\frac{\partial\tau}{\partial n_{HB}})\sigma_{\tau_{yHB}}\sigma_{n_{HB}} \\
&+ 2(\frac{\partial\tau}{\partial K_{HB}})(\frac{\partial\tau}{\partial n_{HB}})\sigma_{K_{HB}}\sigma_{n_{HB}}
\end{aligned} \tag{2.14}
$$

Influence of temperature

On accessing the influence of temperature on the rheological parameters (Figure 2.13), no particular trend can be derived. Although from Figure 2.5 and 2.6, it can clearly be seen that the shear stress decreases for a given shear rate with temperature. Implying that the viscosity decreases with temperature; the same does not reflect on the individual parameters. For this reason, the influence of the temperature on the rheology is resolved through its effect on the apparent viscosity. An Arrhenius type equation (Abu-Jdayil et al., 2010; Battistoni et al., 1993; Pevere et al., 2009; Yang et al., 2009) is used for this purpose. The apparent viscosity (Ratio of shear-stress by shear-rate at a shear-rate) can be described using Equation 2.15 as a function of temperature, where a and E are constants.

$$\mu_{app} = a\epsilon^{E/T} \tag{2.15}$$

On taking the ratio of the apparent viscosities at two different temperatures, we get Equation 2.16, which is independent of the constant a. Implying, if the apparent viscosity at a particular temperature is known, with the knowledge of E (rheological temperature constant, $^\circ C$), the apparent viscosity at another temperature can be calculated.

$$\frac{\mu_{app,T_1}}{\mu_{app,T_2}} = \epsilon^{E(\frac{1}{T_1}-\frac{1}{T_2})} \tag{2.16}$$

Accessing the value of E for apparent viscosity ratios at various concentrations and shear rates, an average value of $7.5^\circ C$ was obtained (Figure 2.14), and this holds good for slurry 1 and slurry 2. Knowing the value of E is useful, as in the following sections parameter models are introduced for the slurry at $20^\circ C$, and to obtain the rheology at other temperatures, this rheological temperature constant can be used.

Yield stress τ_y

The yield stress specifies the minimum stress that is required for the slurry to start deforming at a constant strain rate, below which it does not deform. Over the range of concentrations, the yield stress increases exponentially as illustrated in Figure 2.15. There is a pronounced exponential behaviour in slurry 1. Whereas in slurry 2 an underlying behaviour is not identified, this could be that the sample size is small and at low concentrations. An exponential

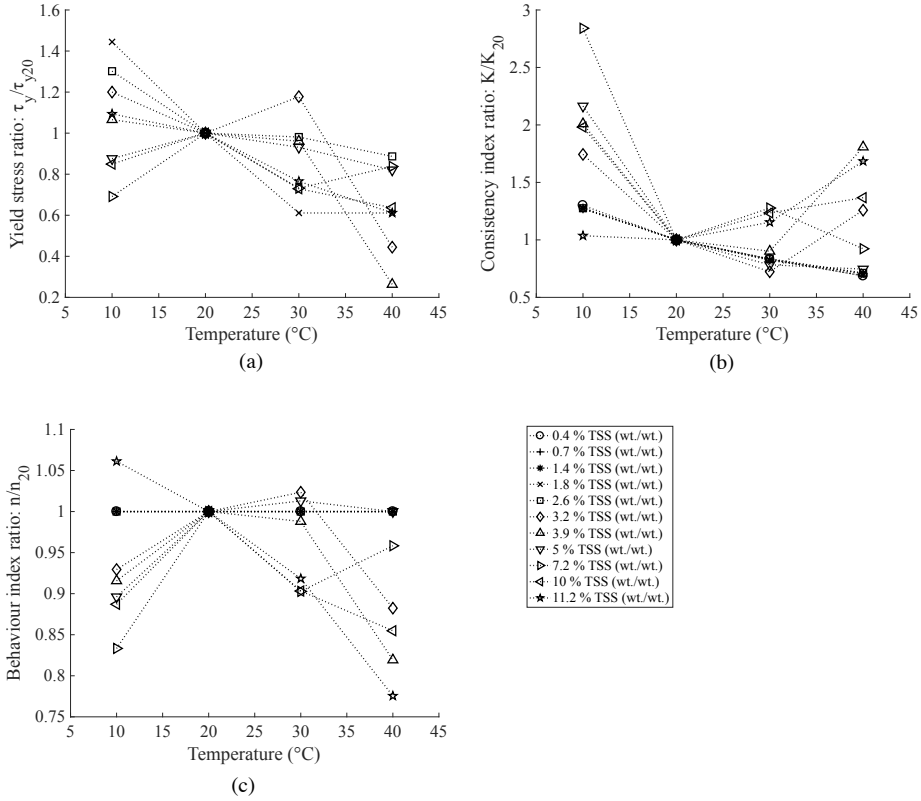

Figure 2.13: Plotting the influence of temperature to the rheological parameters (a) Ratio of yield stress to the yield stress at 20°C (b) Ratio of consistency index to the consistency index at 20°C (c) Ratio of behaviour index to the behaviour index at 20°C.

model (figure 2.16a, Equation 2.17, < 5 % deviation from the measurements) is used describe the influence of concentration on yield stress of slurry 1 at 20°C (chosen as a representative), this model type has been reportedly used in other works (Eshtiaghi et al., 2013a; Seyssiecq et al., 2003). It can be seen that the yield stress is effectively 0 below a threshold concentration and then increases above this concentration. The exponential behaviour in slurry 1 can be explained through the increase in particle interactions as the concentration increases. These interactions are weak physical forces between particles and molecules. Although these forces are weak, with the increase in concentrations the number of neighbouring particles in interaction increase and thus creating a structure. The yield stress tends to zero at low concentrations and is physically meaningful only after reaching a certain concentration (also observed in Equation 2.17, a threshold concentration), where its effects can be felt. For our case of slurry 1 this is 1.5 % TSS.

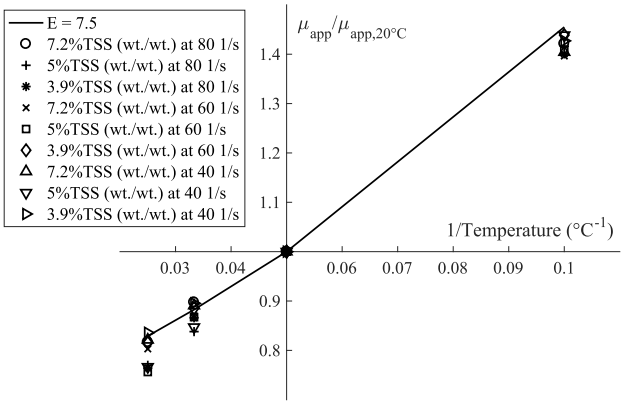

Figure 2.14: Plot of apparent viscosity ratio with the inverse of temperature for different concentrations and shear rates along with the curve representing the apparent viscosity's temperature dependence with $E = 7.5°C$ (for slurry 1).

$$\tau_y = \begin{cases} 0.0012(C - 1.5)^{2.1} & \text{for } C > 1.5 \\ 0 & \text{for } C < 1.5 \end{cases} \tag{2.17}$$

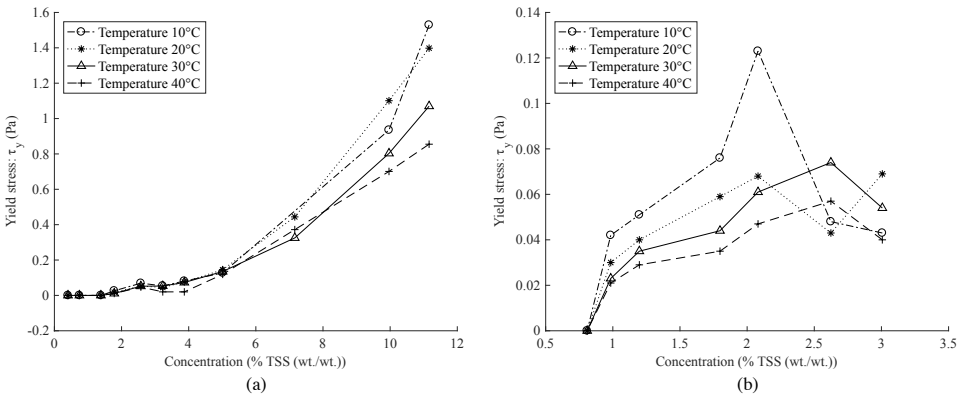

Figure 2.15: Change of yield stress τ_y with concentration and temperature in (a) slurry 1 and (b) slurry 2.

Consistency index K

The consistency index gives an idea about the viscosity of the slurry. Although, both the τ_y and n are required to compute the absolute viscosity, K can be used to perceive the viscous behaviour of the slurry. Over the range of concentrations, the consistency index

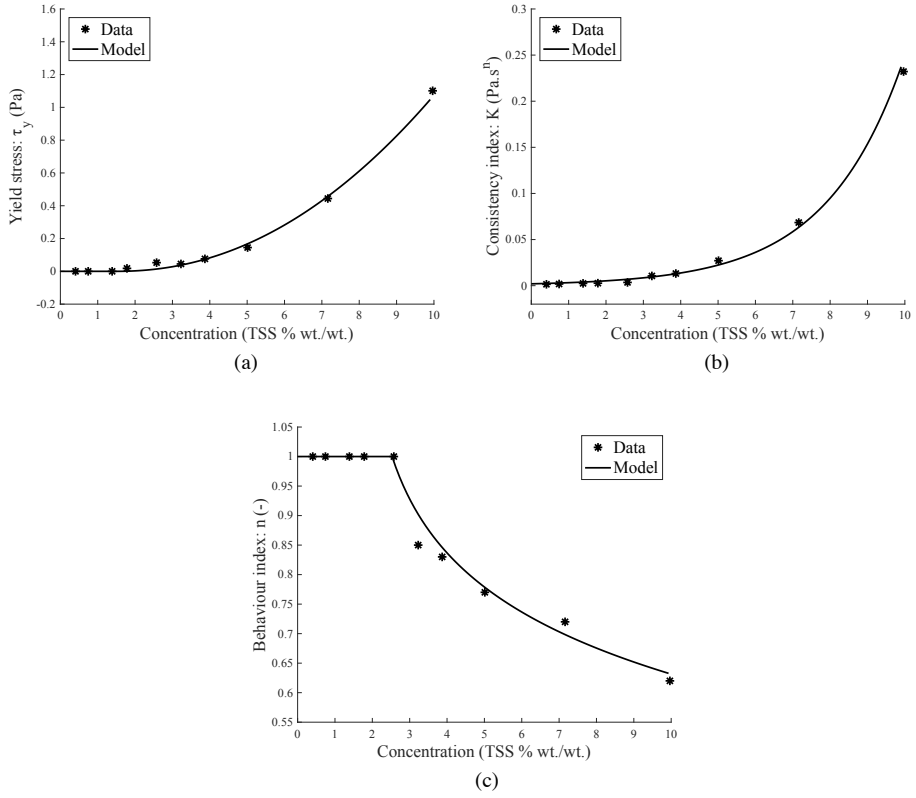

Figure 2.16: Models representing the influence of concentration on (a) yield stress (b) consistency index (c) behaviour index for slurry 1 at 20°C.

exponentially increases (Figure 2.17). As a representative, Equation 2.18 (derived with < 5 % deviation) describes the concentration dependence of the consistency index of slurry 1 at 20°C (Figure 2.16b). It takes the value of the viscosity of water at 0 % TSS of the slurry. The exponential increase of the flow index is observed in both slurry 1 and 2 clearly. The observed behaviour, which is similar to the yield stress, can also be attributed to the forces between the constituent particles.

$$K = 0.002\epsilon^{0.48C} \tag{2.18}$$

Behaviour index n

The behaviour index describes the shear thinning behaviour of the slurry. This is an important parameter as it governs the influence of the change in shear-rate on the shear-stress. Newtonian fluids have the behaviour index as 1, meaning that an increase in shear-rate increases the shear-stress proportional to the consistency index. But with non-Newtonian Fluids with the behaviour index less than 1 implies that a change in shear-rate might not

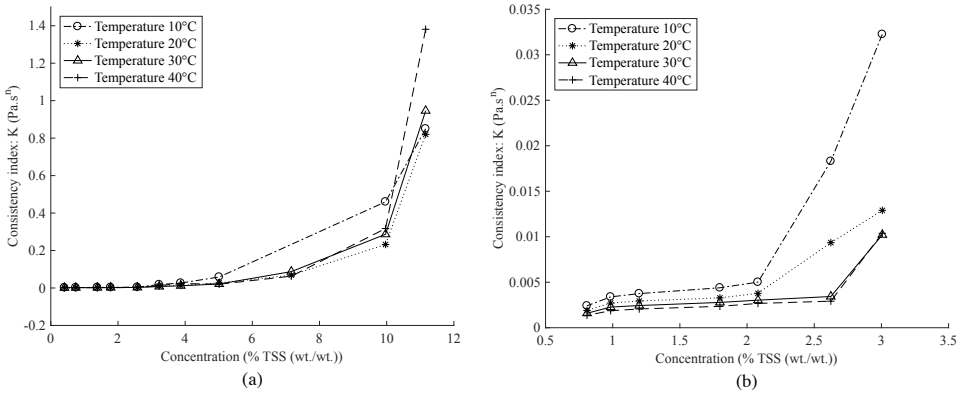

Figure 2.17: Change of consistency index K with concentration and temperature in (a) slurry 1 and (b) slurry 2.

necessarily reflect in a sizeable change in the shear-stress even though the consistency index has a high value. This is essentially the shear thinning behaviour observed in these slurries. As a representative, Equation 2.19 (derived with < 5 % deviation) describes the behaviour index as a function of concentration for slurry 1 at $20°C$ (Figure 2.16c). Over the range of concentrations, the onset of shear-thinning behaviour is at a concentration of 2.5 % TSS. Above this concentration, the behaviour index decreases gradually with the concentration of the slurry (Figure 2.18). This behaviour may be a reflection of the fluid structures, referred to by Quemada (1998) as a structural unit, SU, introducing the concept of effective volume fraction of the SUs as a basis for rheological models. The shear thinning behaviour occurs with the breakup of fluid structures and the constituent particles aligning in the direction of the flow. At low shear-rates, there isn't enough shearing to breakup these fluid structures, but as the shearing rate increases more fluid structures are broken and the constituent particles align with the flow, thereby making it easier to flow, i.e. shear thinning. The increase in concentration causes an increase in fluid structures present and by that the proportion of fluid structures broken is higher, i.e. increased shear thinning.

$$n = \begin{cases} 0.97 - 0.16\ln(C - 1.7) & \text{for } C > 2.5 \\ 1 & \text{for } C < 2.5 \end{cases} \tag{2.19}$$

Effect of adding ground kitchen waste

Comparing the viscosities of both the slurries, it is observed that the viscosity of slurry 2 is on an average (approximate averaging: over all concentration and 3 different shear-rates) 50 % more than that of slurry 1 (Figure 2.19). This could be explained by comparing the particle size distribution of both slurries (Figure 2.2). Slurry 2 has a higher D90 than that of slurry 1 (section 2.1.1). Adding to this, the proportion of larger particles is higher in slurry 2 than in slurry 1 (Figure 2.2) signifying that the particle size distribution of kitchen waste tends towards larger particles. Therefore, this affirms that the particle size distribution plays a major role in determining the viscosities of slurries of this nature. That being said, the sample collected here is small to put forth a strong conclusion about the addition of kitchen waste. Further research could shed light on these aspects.

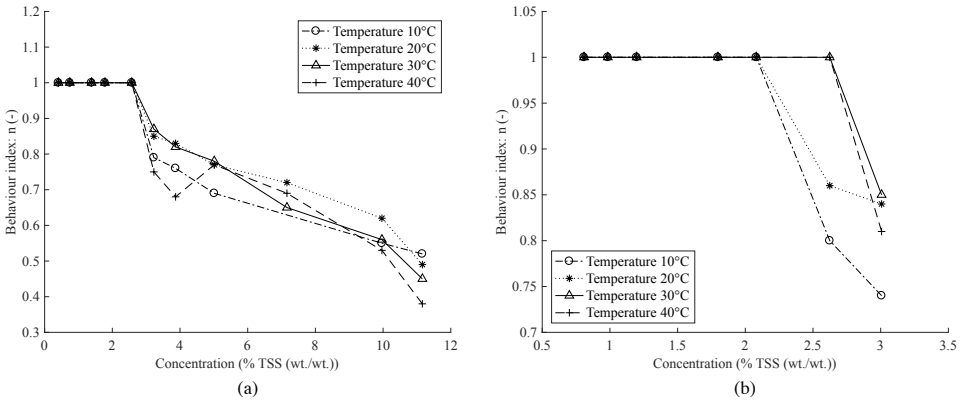

Figure 2.18: Change of behaviour index n with concentration and temperature in (a) slurry 1 and (b) slurry 2.

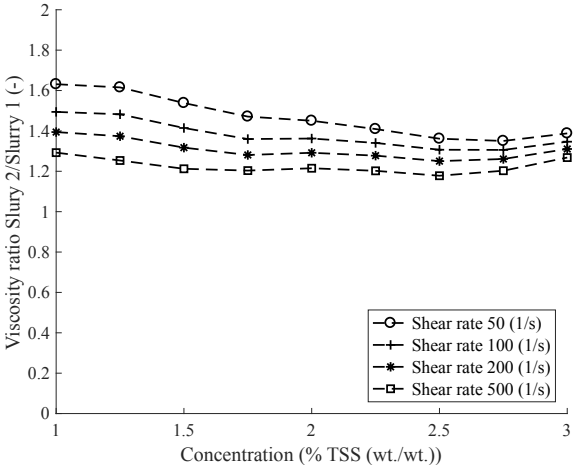

Figure 2.19: Plot of viscosity ratio between Slurry 1 and 2 against TSS concentration at different shear rates.

2.3 Conclusion

To study the hydrodynamic behaviour of concentrated domestic slurries, 2 sample slurries from a pilot project involving novel sanitations systems were collected. Slurry 1 contained black water and slurry 2 black water with ground kitchen waste. These samples were later processed and studied for their rheology using a narrow gap couette rheometer chosen appropriately for their particle size distribution. Rheograms were obtained for various TSS concentration and temperatures of slurries. Among the rheological models explored, the Herschel-Bulkley (HB) model fits best the purpose of describing the obtained rheograms. In general, the viscosity increases with increase in TSS concentration and decreases with

increase in temperature; and this reflects on the parameters. To describe the effect of temperature on the rheology of the slurry, an Arrhenius type equation is used. The influence of concentration on the rheology is described using the changes in these parameters. The yield stress and consistency index are exponentially related to the concentration, whereas the behaviour index has a decreasing power law relation. Comparing the viscosities of slurry 1 and 2, reveals that the addition of kitchen waste increases the viscosity. The knowledge on the rheology thus collected can be used to predict the pressure drop in the transport of CDS and thus can be used to evaluate and design different sanitation options.

Chapter 3 is based on:

Thota Radhakrishnan, A.K., van Lier, J.B., Clemens, F.H.L.R. (2018). Rheology of Un-Sieved Concentrated Domestic Slurry: A Wide Gap Approach. *Water*, 10(10), 1287.

CHAPTER 3

Rheology: Influence of Concentration

Rheometers commonly used in measuring the rheological properties of slurries are placed into two general categories: rotational rheometer and capillary rheometers. Rheology studies are constrained by the limitations of the rheomter. The advantages and disadvantages determine the choice of rheometer to be considered. Capillary rheometers measure the rheology of a fluid through flow of the fluid in a pipe. Since the pressure drives the fluid through a pipe, the shear-rate varies along the radial direction and the flow is non-homogeneous, therefore limiting the rheometer to study only steady stress-shear rate behaviour for time independent fluids (Chhabra and Richardson, 2011). Rotational rheometers on the other hand are able to provide a constant (or nearly so) shear rate throughout the system employed. Very narrow geometries of a narrow gap coaxial cylinder or a cone-plate system provide this; they can be limiting to multiphase fluids with particulates (discussed in the following sections) which preclude the use of narrow systems (Chhabra and Richardson, 2011). Although using rheometers are a conventional means to measure the rheology of a fluid, other non-conventional methods have been applied as well. These non-conventional methods usually stem from the limitations of rheometric techniques, rheological measurements from the engineering application itself, and the need for inline measurements. Some of the non-conventional techniques to estimate the rheology are through free surface velocity of the fluid flow (AL-Behadili et al., 2018), flow from spreading of a fluid from gravity currents (Longo et al., 2013), flow in a narrow channel (Di Federico et al., 2017), and ultrasound image velocimetry of flow in pipes (Gurung et al., 2016).

Rotational rheometers, particularly the Couette-flow type, have traditionally been used to study complex fluids and have become widely accepted in recent years as the most common class of rheometer utilised in sludge rheology (Eshtiaghi et al., 2013b). Studying rheology using a Couette-flow rheometer is limited by the maximum particle size of the constituents in the slurry. Van Wazer (1963) recommends the minimum gap between the cylinders to be 10 times that of the maximum particle size in the slurry. This is to guarantee a shear flow of at least ten layers which ensures flow continuum. Despite the acknowledgement of the necessity of such a gap (Chhabra and Richardson, 2011; Slatter, 1997; Dick and Ewing, 1967),

only a few studies (rheology of similar slurries) have measured the slurry particle size for the choice of rheometer geometry (Koseoglu et al., 2012; Mori et al., 2006). This lack of attention to the particle size and distribution was also reported in the review work of Ratkovich et al. (2013). For digested and waste activated sludge, the gap size constraint is less critical, because the range of the particle size is in order of a few hundred micrometres; therefore, a common narrow gap configuration is acceptable. However, this is not the case for raw sewage sludge where particles as large as a few millimetres have been reported (Battistoni, 1997; Battistoni et al., 2000). To avoid the problem due to the size, it was suggested to work with sieved sludge where particles exceeding a certain diameter were removed (Battistoni, 1997; Battistoni et al., 2000). However, it was acknowledged that for some samples, i.e., raw sewage sludge and the organic fraction of municipal solid waste, the sieved sludge did not represent the rheological behaviour of the whole sample, since more than 30 % of the total solids were removed after sieving. Of the many articles published to characterise the rheology of wastewater slurries, to the author's knowledge, none characterise concentrated domestic slurry. For faecal sludge, the only article addressing its rheology by Woolley et al. (2014) is not comprehensive enough and is regarded to be at most a preliminary analysis. Although, Chapter 2 of this thesis presents a rheological characterisation for CDS, this was done using sieved slurry. Therefore, this paper presents a detailed rheological study of un-sieved CDS in a wide gap Couette-flow Searle type rheometer.

There are several problems that need to be overcome in studying the rheology of un-sieved slurry. Firstly, the gap-size constraint due to the large particles requires a wide gap, where the general assumptions to obtain the shear-rate from the rotation speed are not valid as they are for a conventional narrow gap. And secondly, the noise in the data requires the use of particular procedures (detailed in later sections) in obtaining the underlying rheogram. This paper details a methodology to overcome these difficulties and to measure the rheology of CDS in its complete particle composition.

3.1 Rheometry

Couette-flow rheometers consist of two coaxial cylinders with the annulus between them filled with the fluid under study. In particular, a Searle-type system has the inner cylinder rotating and the outer one stationary. To obtain the rheogram (shear-stress vs. shear-rate curve) in a Searle system, the torque and rotational velocity of the inner cylinder is measured. The shear-stress can be calculated directly from the torque. But converting the rotational velocity to the shear-rate is not straightforward since it is an ill-posed inverse problem commonly referred to as the Couette inverse problem (Ancey, 2005; Chatzimina et al., 2009; Krieger and Elrod, 1953; Leong and Yeow, 2003), and has been investigated by many researchers in the past decades. This conversion will be the focus of this study applying it to CDS.

3.1.1 Couette Inverse Problem

A Couette-flow Searle type rheometer consists of two coaxial cylinders where the inner cylinder (or bob) of radius R_i and length h rotating at a constant rotational speed of Ω and a stationary outer cylinder (or cup) of radius R_o, shown in Figure 3.1a. Balancing the forces yields the opposing torque (M) exerted on the bob by the fluid:

$$M = 2\pi h r^2 \tau \tag{3.1}$$

r being any location in the annulus, $R_i \leq r \leq R_o$. The shear-stress applied on the fluid at the bob is:

$$\tau_i = \frac{M}{2\pi h R_i^2} \tag{3.2}$$

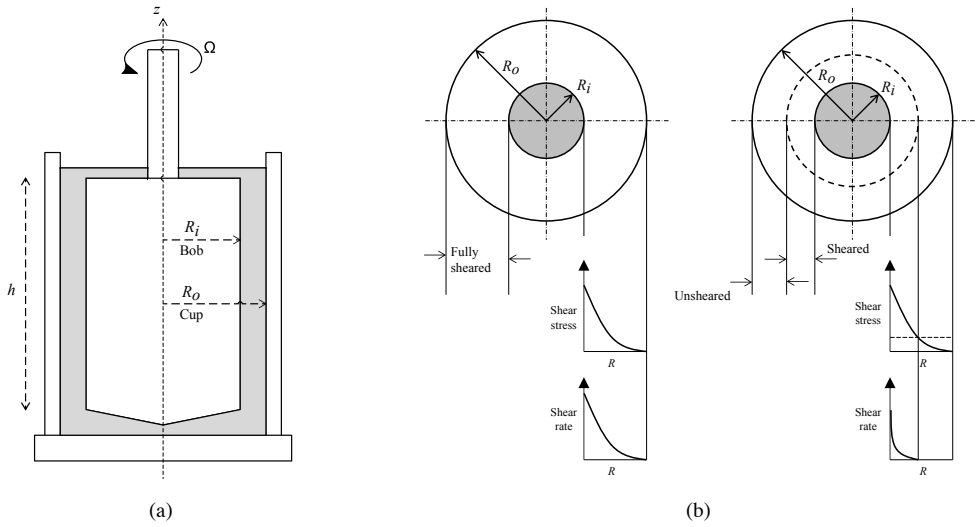

Figure 3.1: (a) Schematic representation of a Couette-flow Searle type rheometer. (b) Representing the shear-rate and shear-stress distribution for the fully and partially sheared flow modes.

Assuming a non-slip boundary condition (angular velocity is zero at the cup and at the bob is Ω) and the flow being laminar and incompressible with no normal stresses, the shear rate $\dot{\gamma}$, the shear-stress τ and angular velocity Ω, at the bob surface can be related as:

$$\Omega = \int_{R_i}^{R_o} \frac{\dot{\gamma}(r)}{r} dr = \frac{1}{2} \int_{\tau_o}^{\tau_i} \frac{\dot{\gamma}(\tau)}{\tau} d\tau \tag{3.3}$$

Solving Equation 3.3 yields in the conversion of angular velocity to the shear-rate thereby facilitating the derivation of the rheogram. The solution is dependent on the fluid behaviour $\dot{\gamma}(\tau)$, which translates to the rheological model of the fluid. Therefore, Equation 3.3 can be solved if the relation between shear-stress and shear-rate is known or an a priori assumption of the relation is required. In cases where this relation is unknown or cannot be assumed, the solution to Equation 3.3 becomes an ill-posed inverse problem. Another aspect complicating the solution to this integral, is the existence of partially sheared regions in the annulus, as seen in Figure 3.1b. For plastic materials, depending on the relative magnitude of the shear stress and the yield stress, τ_y, two flow modes are possible: Partially Sheared Flow (PSF) and Fully Sheared Flow (FSF). Under the condition where $\tau_i < \tau_y < \tau_o$, only part of the fluid close to the bob is sheared while the remaining region is stationary (PSF) as illustrated in Figure 3.1b. When $\tau_y < \tau_o < \tau_i$, the shear stress everywhere in the flow exceeds the yield value and the fluid becomes sheared in the entire annulus (FSF mode). Considering all of these complications, there have been many procedures proposed to approximate the shear-rate. A review of these procedures have been provided in Estellé et al. (2008) and

Chatzimina et al. (2009). In this paper, the method used is one proposed by Yeow et al. (2000). This method uses Tikhonov regularisation to evaluate the shear-rates. This method was selected owing to the fact that it can cope with noised data, does not require a priori knowledge about the flow behaviour, can be used for fluids with a yield stress and can be applied to both fully and partially sheared modes.

3.1.2 Tikhonov Regularisation

Yeow and co-workers (Leong and Yeow, 2003; Yeow et al., 2000) have developed a procedure for solving Equation 3.3 by treating it as a Volterra integral equation of the first kind. The integral is solved using Tikhonov regularisation, which does not require the specification of the fluid behaviour, and suppresses the propagation of eigenvalues related to 'noise' in the data when back mapping. The method followed a discretisation method and sought to derive the shear-rate by minimizing the fractional deviation between the computed shear-rate and its experimentally measured counterpart, the angular velocity. To ensure that the noise in the experimental data is not amplified, and to obtain smooth curves, a regularisation condition is imposed, which is minimising $\frac{\partial^2 \dot{\gamma}(\tau)}{\partial \tau^2}$.

Numerical Method

The shear rate $\dot{\gamma}(\tau)$ that is to be estimated is discretised as $\dot{\gamma} = (\dot{\gamma}_1, \dot{\gamma}_2, \dot{\gamma}_3 \dots \dot{\gamma}_{N_k})$ at uniformly spaced $\tau = (\tau_1 = \tau_{min}, \tau_1, \tau_1 \dots \tau_{N_k} = \tau_{max})$ and the equation that satisfies the condition to minimise the fractional deviation between the estimated shear-rate and the one experimentally measured and the regularisation condition is given by Yeow et al. (2000), shown in Equation 3.4.

$$\dot{\gamma} = (A^T A + \lambda \beta^T \beta)^{-1} A^T I \tag{3.4}$$

Where I is an appropriate identity matrix and A is a coefficient matrix given by:

$$A_{ij} = \frac{\frac{\alpha_{ij}\Delta\tau}{2\tau_j}}{\Omega_i}, \quad \begin{matrix} i = 1, 2, 3 \dots N_d \\ j = 1, 2, 3 \dots N_k \end{matrix} \tag{3.5}$$

where the number of discretisation points corresponds to N_k and the number of measured points is N_d. N_k is much larger than N_d in implementation. The discretisation step $\Delta\tau$ in Equation 3.5 is given by:

$$\Delta\tau = \frac{\tau_{max} - \tau_{min}}{N_k - 1} \tag{3.6}$$

and, α_{ij} is dependent on the numerical scheme used to approximate the integral in Equation 3.3. α_{ij} comprises the coefficient matrix from the numerical scheme, thereby using Simpson's 1/3 rule to approximate the integral $\alpha_{i1} = 1/3$, $\alpha_{ij} = 2/3$ for odd j and $\alpha_{ij} = 4/3$ for even j.

The regularisation condition, minimising $\frac{\partial^2 \dot{\gamma}(\tau)}{\partial \tau^2}$ gives rise to the tridiagonal matrix β with N_k rows in Equation 3.4.

$$\beta = \begin{bmatrix} 1 & -2 & 1 & & & & & & \\ & 1 & -2 & 1 & & & & & \\ \vdots & \vdots & \vdots & \vdots & \vdots & \vdots & \vdots & \vdots & \vdots \\ & & & & & 1 & -2 & 1 & \\ & & & & & & 1 & -2 & 1 \end{bmatrix} \frac{1}{(\Delta\tau)^2} \tag{3.7}$$

A regularisation parameter λ, shown in Equation 3.4, is used for the smoothing, which controls the extent to which the noise in the experiment is filtered at the cost of goodness of fit. As λ depends on the noise in the data, number of data and discretisation points, and the numerical scheme; an iterative procedure is adopted to determine the appropriate λ comparing the rheograms of a known non-Newtonian fluid. Further information on the derivation and implementation of the procedure can be found in the articles from Yeow and co-workers (Leong and Yeow, 2003; Yeow et al., 2000).

Recovering Yield Stress

A slurry with yield stress τ_y will not deform at a constant rate until the shear-stress applied on it is greater than its yield stress. Applying this knowledge to the integral in Equation 3.3, the lower limit becomes τ_y. Also, the discretisation step is modified to:

$$\Delta\tau = \frac{\tau_{max} - \tau_y}{N_k - 1} \tag{3.8}$$

The yield stress of the material can be determined if at least one of the measured data points is in the partially sheared flow mode. This is done by using the condition:

$$\dot{\gamma}(\tau_y) = 0 \tag{3.9}$$

The τ_y is estimated iteratively using a Newton-Raphson like method, such that the $\dot{\gamma}(\tau)$ given by Equation 3.4 satisfies the condition mentioned in Equation 3.9.

3.2 Methods and Materials

3.2.1 Experimental Procedure

The experimental procedure was two fold: One which consists of validating the translation of angular velocity to shear rate from a wide gap rheometer and the other of obtaining the rheology of concentrated domestic slurry from a wide gap rheometer.

In validating the translation of angular velocity to shear rate from a wide gap rheometer, as seen in Section 3.1.2, a test fluid that could be operated both in a narrow gap and a wide gap rheometer was needed. In our case tomato ketchup was used. The rheology of the tomato ketchup was first obtained using a narrow gap rheometer. Using this rheology, the algorithm for translating the angular velocity was adjusted and validated by tuning the regularisation parameter λ. This tuning of the parameter was so done to match the rheology obtained from the wide gap to that from the narrow gap.

For the CDS rheology, a sample of concentrated domestic slurry was collected, as shown in Section 3.2.2. This sample was then prepared to various concentrations by gravity settling, and using the supernatant as a dilutent, shown in Section 3.2.3. Using the wide gap

rheometer, as seen in Section 3.2.4, and the translation algorithm shown in Section 3.1.2, the rheograms were obtained. A Herschel-Bulkley model was used to represent these rheograms for practical purposes, and therefore the parameters for this model were obtained through parameter estimation procedures, as shown in Section 3.2.5.

3.2.2 Materials

The concentrated domestic slurry under study were collected from an experimental facility in the building of DeSaH B.V. in Sneek, the Netherlands. The facility has urine separation toilets fitted with a vacuum collection system. 5 different samples were collected and consisted mostly of human faecal waste, toilet paper, and flushed water. The vacuum pump that was used to transport the waste slurry is fitted with a cutter. The samples were drawn from a collection tank downstream of the pump. To preserve the samples and retard any biological activity, they were transported to the lab immediately after collection in a cool box at $4°C \pm 1°C$. This procedure follows the advice given in (APHA, 2005). The samples were kept in sealed containers to preserve the original moisture and avoid reactions with air. Once in the laboratory, the samples were tested within 1 day of their collection.

3.2.3 Sample Preparation

The samples collected were passed through a 2 mm mesh to remove coarse particles. The amounts of these coarse particles totalled 1 or 2 particles per 500 mL of slurry, which is considered to be negligible in this study. The low amount of coarse particles may be due to the presence of the cutter in the pump. Upon collection, the total suspended solids (TSS) in the sample was 2.6 % TSS (wt./wt.). This was then concentrated to 8.4 % TSS (wt./wt.), using gravity settling. To obtain samples of different concentrations the supernatant was used to dilute the concentrate. The different concentrations obtained were: 2.6, 3.2, 3.9, 5.1, 5.4, 6.1, 7.3 and 8.4 % TSS (wt./.wt.)

The particle size distribution (PSD) of the sample is obtained using a laser diffraction particle size analyser to assess the requirement of the gap size for the rheometer. The PSD, presented in Figure 3.2, shows that the particles present in the sample vary in size from 1 μm to about 2000 μm. The average D_{90} (representative particle size) of the sample is obtained using the cumulative size distribution, shown in Figure 3.2b, and is found to be 1108 μm. Therefore, to satisfy the continuum condition specified in Van Wazer (1963), the gap size in the rheometer must be a minimum of 11 mm.

3.2.4 Wide Gap Rheometer

The rheology measurements were performed with a MCR302 instrument from Anton Paar (Graz, Austria). Among the available bob and cup geometries, a bob (grooved) of diameter 45 mm and length 67.5 mm with a cup of diameter 74 mm is chosen. This gives a gap of the annulus to be 14.5 mm, which is more the minimum specified required (specified in Section 3.2.3). During the measurements, a lid was used to cover the sample to avoid evaporation. For assuring the no-slip boundary condition mentioned in Section 3.1.1, the bob used is grooved laterally and a thin steel cage is attached to the cup. To ensure that all samples had the same initial condition, the sample is pre-sheared for 2 min at 500 RPM prior to each investigation and then let to rest for 1 min. This procedure confirmed the repeatability of the tests. The torque was measured at various RPMs (Rotation per minute) using a RPM ramp procedure. A wide RPM range of 0 to 400 was chosen so that the fluid is partially

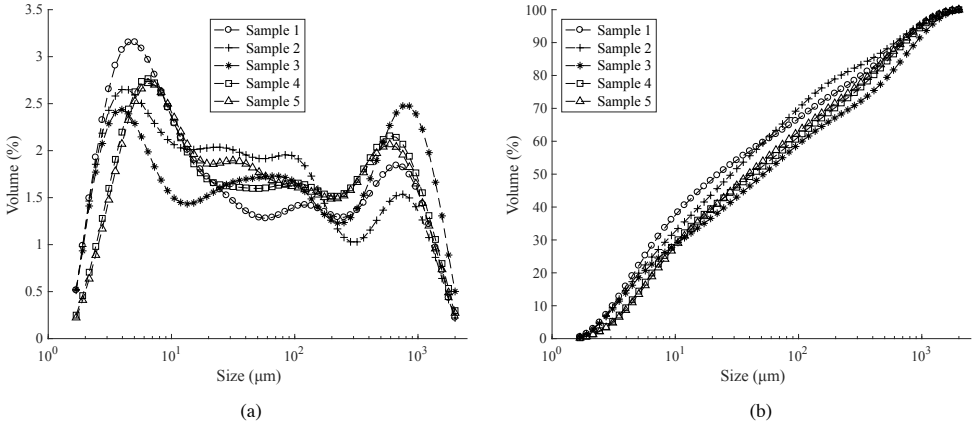

Figure 3.2: (a) Particle size distribution of 5 different samples from the collected concentrated domestic slurries (CDS). (b) Cumulative particle size distribution of the 5 samples.

and fully sheared. The steady-state torque on the bob is recorded for every set RPM on the bob. With respect to settling during the measurements, at the macro level there was no supernatant observed which indicates no settling. To obtain the measurements for a particular concentration, 5 replicate tests were performed with different samples.

3.2.5 Model Parameter Estimation

In this study, a genetic algorithm is used to estimate the parameters of the model representing their respective data (Thota Radhakrishnan et al., 2018a). This algorithm was chosen as it is a general algorithm, that is not tuned to suit a specific model. The advantage of this algorithm compared to the other usual gradient-based algorithms is that it has a low probability of being stuck in a local minimum and explores the parameter space well in general and is also able to deal with discontinuities in the goal function. More information about the implementation of the algorithm can be found in 2.1.5 and in articles from Chaudhuri et al. (2006) & Rooki et al. (2012). To evaluate the goodness of fit of the model to the data, a root mean square of the normalised residual (RMSNR, Equation 3.10) value is used. Denoting that an RMSNR value close to 0 gives a very good fit.

$$RMSNR = \sqrt{\frac{\sum_{i+1}^{N} \left(\frac{y_i - \hat{y}_i}{y_i}\right)^2}{N}} \tag{3.10}$$

where y_i is the data for fitting, $\hat{y}_i$ is from the model and N is the size of the data set. RMSNR gives the average proportionate deviation of the model from the data. The particular use of RMSNR here is to facilitate the comparison of the fit to the different data sets.

3.3 Results and Discussion

3.3.1 Choosing λ

Tomato ketchup, which has been commonly used by researchers as a test fluid, is also used here to demonstrate the validity of the method. For this purpose, the rheology of tomato ketchup from a narrow gap (the specifications of this set-up is detailed in (Thota Radhakrishnan et al., 2018a)) is used to compare the results obtained from the wide gap geometry using Tikhonov regularisation shown in Figure 3.3. It is to be noted that the shear-rate vs. shear-stress curves obtained through a narrow gap approximation using a narrow gap ($R_o/R_i = 1.08$) rheometer is considered to be an accurate enough representation of the rheology of Tomato ketchup. As mentioned in Section 3.1.2, choosing a proper regularisation parameter is the bottle neck in the here used method. In this study, the regularisation parameter is chosen such that the deviation of the rheogram obtained by the method is less than 5 % of that obtained from the narrow gap rheometer; this is shown in Figure 3.3. Thus, the obtained regularisation parameter is the one that is used throughout this paper for obtaining the rheograms of CDS. A systematic bias can be observed from the residuals between the rheograms obtained from that of the narrow gap and wide gap, as seen in Figure 3.3. For a perfect model these residues should show no autocorrelation or bias, but since the narrow gap results are approximated these biases arise.

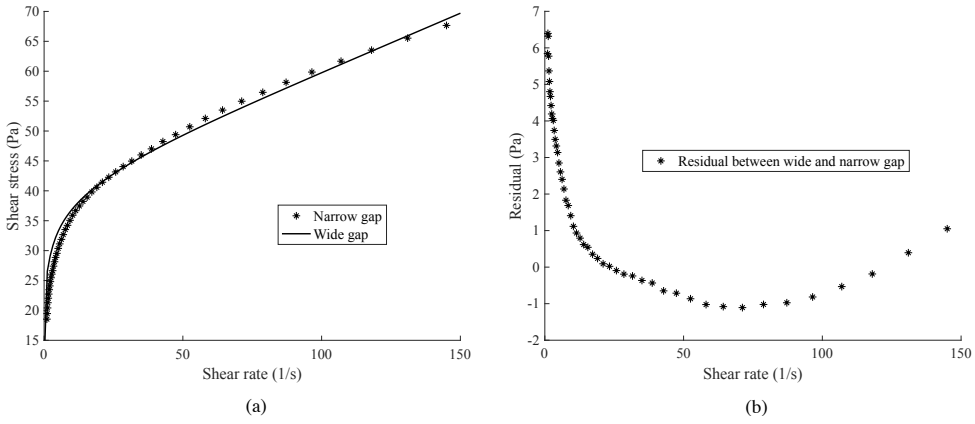

Figure 3.3: (a) Rheograms of Tomato ketchup obtained using both the narrow and wide gap geometry rheometers. (b) Residuals between the rheograms from wide and narrow gap.

3.3.2 CDS Rheograms

Measurement data of shear-stress vs. angular velocity of the un-sieved slurry at various TSS concentrations are obtained using the wide gap rheometer described in Section 3.2.4. As can be seen from the measurement data in Figure 3.4, there is much noise present. This presence of the noise in the data has been a determining factor in choosing the Tikhonov regularisation method to obtain the rheograms. It can also be observed from Figure 3.4 that

the initial points have a higher shear-stress as these points represent the partial shearing mode at lower angular velocities.

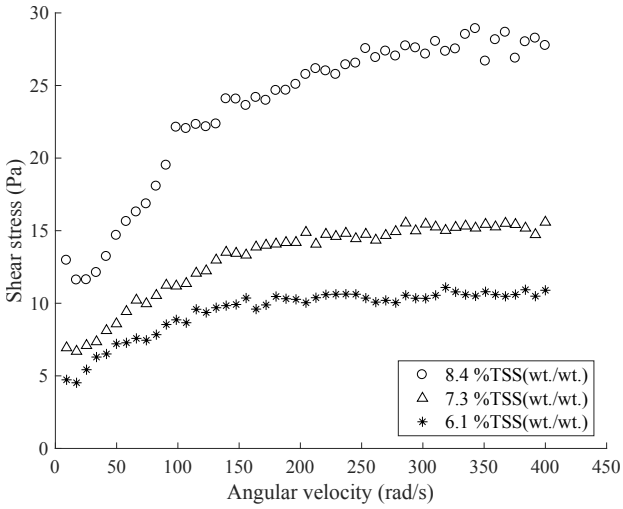

Figure 3.4: Shear-stress vs. angular velocity measurements for CDS using the wide gap geometry.

The rheograms (Figure 3.5) for the un-sieved CDS are obtained through the Tikhonov regularisation method, using the regularisation parameter determined in Section 3.3.1 and Figure 3.5. From the iteration procedure mentioned in Section 3.1.2, the yield stress of the fluid is obtained. Having measured on a wide RPM range to which also includes partially sheared flow mode, we facilitated the determined determination that of the yield stress (Section 3.1.2). as at least one measurement point in the partially sheared flow is required. A Herschel-Bulkley rheological model, shown in Equation 3.11, is known to sufficiently represent the rheology of CDS (Thota Radhakrishnan et al., 2018a). This model will also be used in this paper. As the yield stress is already known, the remaining parameters K and n of the model are estimated using a genetic algorithm, shown in Section 3.2.5, with an RMSNR value of 0.02 which denotes a 2% deviation of the model from the data.

$$\tau = \tau_y + K\dot{\gamma}^n \tag{3.11}$$

3.3.3 Effect of TSS Concentration: C

The influence of change in TSS concentration C on the rheology of the slurry is expressed through the change in rheological parameters.

Yield Stress: τ_y

The minimum shear stress that is required to overcome the flow resistance for the slurry to start flowing is the yield stress. The yield stress of the slurry when plotted against the concentration of TSS, as seen in Figure 3.6, shows an exponentially increasing behaviour. Although the same has been reported by some researchers (Eshtiaghi et al., 2013b; Seyssiecq

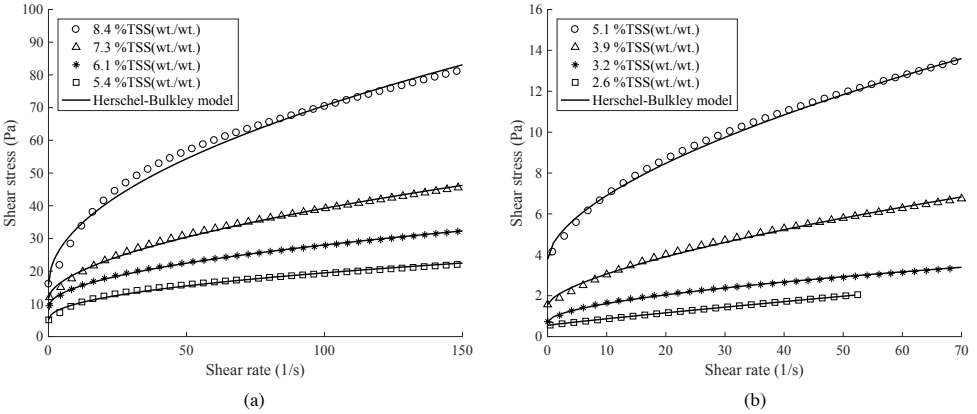

Figure 3.5: Rheograms of concentrated domestic slurries (CDS) obtained through Tikhonov regularisationregularization (a) Rheograms of concentration 5.4, 6.1, 7.3 and 8.4 % TSS (wt./wt.) (b) Rheograms of concentration 2.6, 3.9, 3.2 and 5.1 % TSS (wt./wt.).

et al., 2003) for similar slurries, in general the models used represent the yield stress vary largely. This is predominantly due to the fact that the model is built to only empirically represent the data abandoning physical reasoning. The same is true for the other parameters K and n as well. That being said, there is not much information about these parameters to give them a physical dimension, as they are in themselves an empirical representation of the rheological data. Here an attempt is made to give a semi-empirical representation to the influence of TSS concentration to the rheological parameters τ_y, K and n. This is so done by setting boundaries for these parameters, for which an explanation follows. The increasing behaviour of the yield stress with the increase in concentration can be characterised through the particle interactions. Albeit these interactions are weak physical forces, the increase in concentration increases the number of neighbouring particles. This causes the formation of particle structure, where the yield stress is applied to break and overcome it. As mentioned in previous works (Thota Radhakrishnan et al., 2018a), the yield stress is 0 at low concentrations and only above a certain concentration does it acquire a physical plausible value. This threshold concentration is known approximately to be around 3.0 % TSS (wt./wt.) (Thota Radhakrishnan et al., 2018a). The model so chosen to represent the yield stress accounts for all this information and is given in Equation 3.12 (with a RMSNR value of 0.25). This is chosen so that the value of yield stress reduces to 0 at concentration 0 % TSS, as the slurry reduces to just water and above 2.0 % TSS (wt./wt.) (a parameter found through model fitting) the presence of yield stress is established.

$$\tau_y = \begin{cases} 0.71(C - 2.0)^{1.7} & \text{for } C > 2.0 \\ 0 & \text{for } C < 2.0 \end{cases} \tag{3.12}$$

Consistency Index: K

The consistency index K that represents the inherent flow viscosity in the slurry also increases exponentially, as seen in Figure 3.7, with increasing TSS concentration C and is

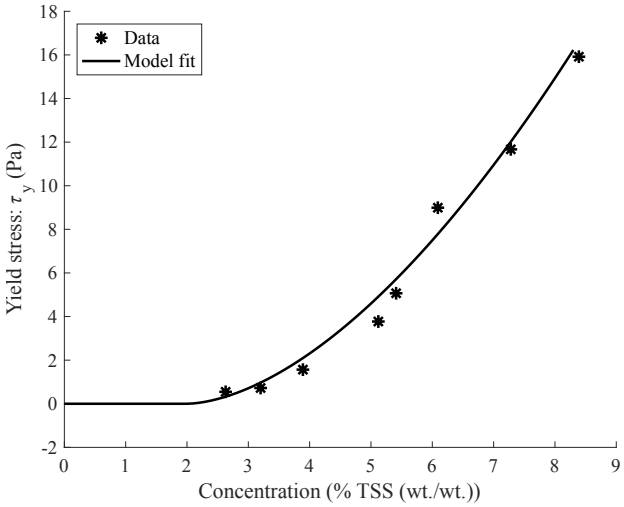

Figure 3.6: Influence of change in concentration of % TSS to Yield stress τ_y of concentrated domestic slurries (CDS).

represented using the Equation 3.13. The latter differs with Equation 3.12 used to represent the yield stress as the boundary condition for Equation 3.13 is different. As the concentration approaches 0, the consistency index reduces to a low value close to that of water, but will not become 0. This information is used to derive Equation 3.13 representing K with a RMSNR of 0.32. This has been suggested by other researchers as well (Eshtiaghi et al., 2013b; Seyssiecq et al., 2003) for similar slurries.

$$K = 0.07\epsilon^{0.5C} \tag{3.13}$$

Behaviour Index: n

The behaviour index n, represents the extent of shear thinning nature of the slurry. From Figure 3.8, that shows the influence of TSS concentration on behaviour index, it is seen that n decreases from 1 at 0 % TSS to a lower value at higher concentrations and that the change in the behaviour index is observed only after a threshold concentration (also observed in the many models reviewed by Seyssiecq et al. (2003)). Above this threshold, the behaviour index is observed to decrease with an inverse power law. To model this nature, Equation 3.14 (RMSNR 0.11) is used to represent the behaviour index and this model has been used by various other researchers (Eshtiaghi et al., 2013b; Seyssiecq et al., 2003) for similar slurries. Using this model, shown in Equation 3.14, the threshold concentration is found to be 2.6 % TSS (wt./wt.), estimated as a parameter in the model. As discussed earlier, most flow characteristics of these slurries can be attributed to the fluid particle structures. The concept of structural units (SUs) vis--vis fluid particle structures introduced by (Quemada, 1998) expresses the view that the rheological model is essentially based on the concept of effective volumes of these SUs . As for the shear thinning behaviour, it is particularly associated with the alignment of fluid particles in the direction of flow, after breaking to its constituent particles from being a composite fluid structure. As the shear-

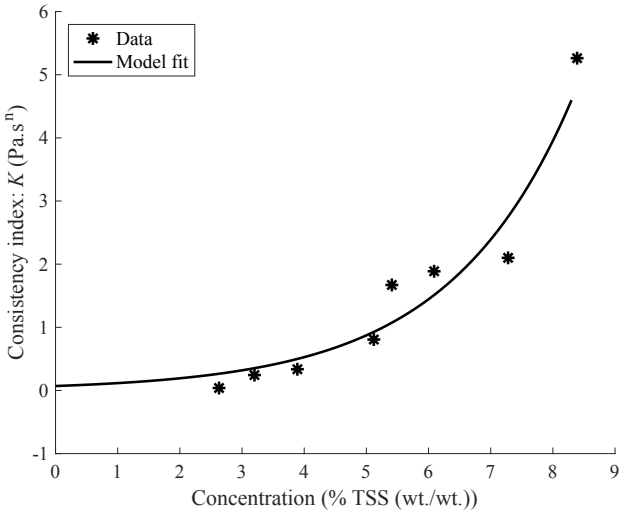

Figure 3.7: Influence of change in concentration of % TSS to consistency index K of concentrated domestic slurries (CDS).

rate increases, the amount of structures broken increases, and with the particles aligning with the flow cause the shear thinning behaviour i.e., easiness to flow behaviour. Also, as can be seen in Figure 3.8, the behaviour index tends to reach a plateau. Thereby, it can be hypothesised that the decrease in the flow behaviour index with increase in concentration although being significant in the beginning, will reach a plateau at very high concentration. The plateau at high concentration can be associated with the low significance of the fluid structures broken to that of particle-particle interaction. That is to say, although there might be a significant portion of the fluid structures broken and aligned along the flow, the inherent particle-particle interaction certainly outplays at higher concentration thereby lowering the effect of broken fluid structures.

$$n = \begin{cases} 0.65 - 0.09\ln(C - 2.57) & \text{for } C > 2.6 \\ 1 & \text{for } C < 2.6 \end{cases} \tag{3.14}$$

3.3.4 Comparing Sieved and Un-Sieved Slurries

Chapter 2 characterises the rheology of sieved CDS. On comparing it with the un-sieved slurry in this chapter (Figure 3.9), it can be seen that the apparent viscosity for the un-sieved slurry is higher. This ratio of apparent viscosity between un-sieved and sieved slurry is high at low concentrations and relatively lower at high concentrations when the shear thinning non-Newtonian behaviour is stronger. These difference can predominantly be attributed to the difference in the particle size distributions of the slurries.

3.3.5 Comparison with Other Wastewater Slurries

Slurries encountered in the different stages of wastewater treatment processes have been known to behave as non-Newtonian slurries Seyssiecq et al. (2003). A select few of the

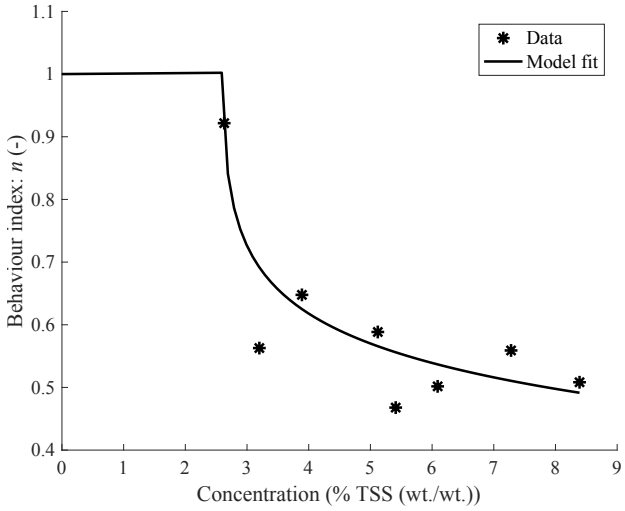

Figure 3.8: Influence of change in concentration of % TSS to behaviour index n of concentrated domestic slurries (CDS).

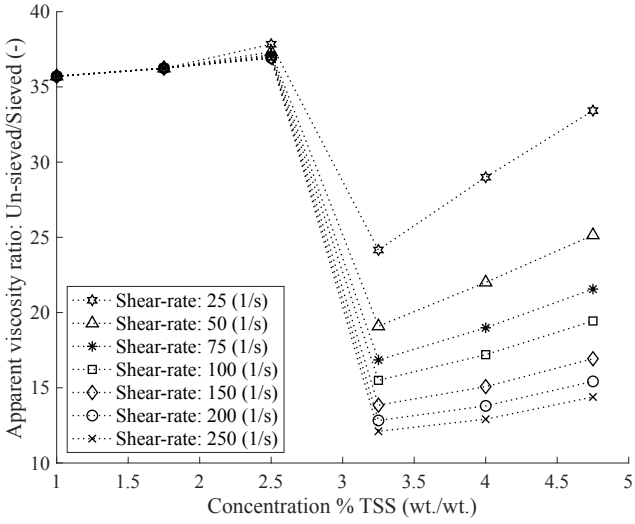

Figure 3.9: Comparison of apparent viscosities of sieved (slurry 1, Chapter 2) and un-sieved slurry.

available literature data is compared with CDS; Primary and secondary sludge from (Markis et al., 2014), and anaerobic digested sludge from (Baudez et al., 2011). On comparing these slurries with CDS (Figure 3.10) it can be seen that they have similar trends of behaving as a shear thinning slurry, and with similar tendencies to the change in concentration. In particular, on comparing the model equations of the consistency index K and yield stress

τ_y with the ones proposed of Markis et al. (2014), it is seen that the model equations and the values of the parameters are quite similar (although the values for the yield stress are higher). This again elucidates that the slurries in comparison behave similarly (with respect to its non-Newtonian behaviour).

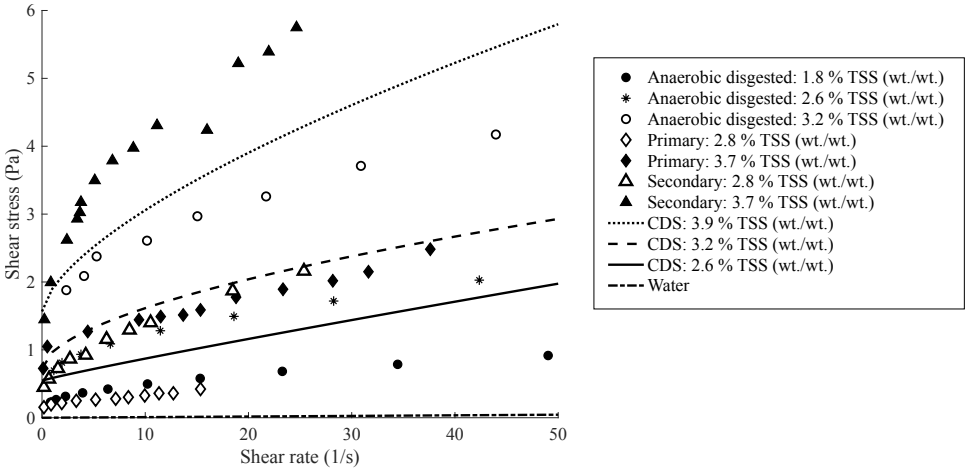

Figure 3.10: Comparison of the rheograms of concentrated domestic slurries (CDS) (this study) and similar wastewater sludges: Anaerobic digested (Baudez et al., 2011), primary and secondary sludge (Markis et al., 2014).

3.4 Conclusions

The rheology of CDS is fundamental in designing transport systems to carry them. A rotating rheometer is commonly used for this purpose. The geometry of the rotating rheometer to be used is highly dependent on the size of the particles in the slurry. As the slurry has large particles present in them, the choice of geometry is crucial. For this purpose, the rheology of un-sieved concentrated domestic slurry is measured using a wide gap rheometer. To obtain the shear-rates from a wide gap rotating rheometer it is essential to choose an appropriate mathematical method, and for this purpose a Tikhonov regularisation method is used. This particular method (Tikhonov regularisation) is chosen as it copes with the noisy data and yield stress present in the fluid. This method is validated using a test fluid, tomato ketchup, and the regularisation parameter (essential to the method) is obtained using the same fluid. The obtained rheology of the un-sieved slurry presents a complete information on the flow characteristics of concentrated domestic slurry. This complete information is crucial in providing design specification of slurry handling systems. A Herschel-Bulkley rheological model is used to represent the rheology of the slurry. The influence of change in concentration of TSS on the rheology is studied through its influence on the parameters of the rheological model. The yield stress and consistency index of the Herschel-Bulkley model increase exponentially and are represented through their respective exponential models. Similarly, an attempt has been made to represent the behaviour index through an inverse power law model. It is observed that the yield stress in the slurry is only physically meaningful above

2 % TSS (wt./wt.) and the behaviour index above 2.6 % TSS (wt./wt.). These equations provide practitioners with usable forms of information to design slurry handling systems.

Part II

Flow Characterisation

Chapter 4 is based on:

Thota Radhakrishnan, A.K., van Lier, J.B., Clemens, F.H.L.R. (2016). Experimental design to study concentrated domestic slurry transport hydraulics. Presented at the 8^{th} *Sewer Processes Network conference*, Rotterdam, the Netherlands, 31 August - 2 September 2016.

Thota Radhakrishnan, A.K., Alidai, A., Pothof, I.W.M., Clemens, F.H.L.R. (2015). Predicting The Onset Of Secondary Flows In The Rheological Measurement Of Domestic Slurry. Presented at the 10^{th} *Urban Drainage Modelling Conference*, Mont-Saint-Anne, Qubec, Canada, 20 - 23 September 2015.

CHAPTER 4

Slurry Loop Experimental Set-up

Understanding the flow characteristics of concentrated domestic slurries is essential in establishing design guidelines for its transport in pipelines. Domestic slurries originating from sanitation systems that employ source separation and thereby making use of vacuum toilets and kitchen food waste disposers are concentrated with a TSS content of 0.9 - 2.7 % (wt./wt.). With the implications of sediment formation and shorter transport lengths (Thota Radhakrishnan et al., 2018b) makes it difficult for conventional gravity sewers to accommodate these slurries. Pipelines are used to transport these slurries from its collection to the place of treatment. However, due to the knowledge gap in estimating the energy (pressure) loss incurred in the transportation of these slurries, it is difficult to establish the required pipe and pump sizing for the transport system. This gap can be bridged by studying the transport characteristics of CDS and developing a transport model to establish guidelines required to estimate the pipe and pump sizing for the pipeline systems. The aim of the second part of the thesis is to establish the design guideline.

At the core of estimating the pressure losses for the flow of CDS is its rheology, which has already been established in Chapter 2 and Chapter 3. CDS is found to behave as a non-Newtonian fluid. In particular it has a yield stress and has a shear-thinning behaviour. To study the transport characteristics of CDS, a large quantity is required. It is already know that CDS is hazardous and not stable with time owing to bacterial decomposition (APHA, 2005). Considering the constraints related to working with CDS, a model slurry in lieu of CDS is used in the following experiments. This model slurry ideally has similar rheological characteristics with respect to its non-Newtonian behaviour. Therefore, it is aimed to study the flow characteristics of non-Newtonian fluids in general, having similar rheological characteristics as CDS.

Flow Characteristics

To bridge the knowledge gap of the flow characteristics, the experiment pipeline loop was set-up with the following objectives:

- Investigate the incurred transport pressure loss of non-Newtonian slurries.
- Examine the relation between pressure loss incurred on transportation of non-Newtonian slurries to its rheological characterisation.
- Investigate laminar to turbulent flow transition of non-Newtonian slurries.
- Predict laminar to turbulent flow transition of non-Newtonian slurries.

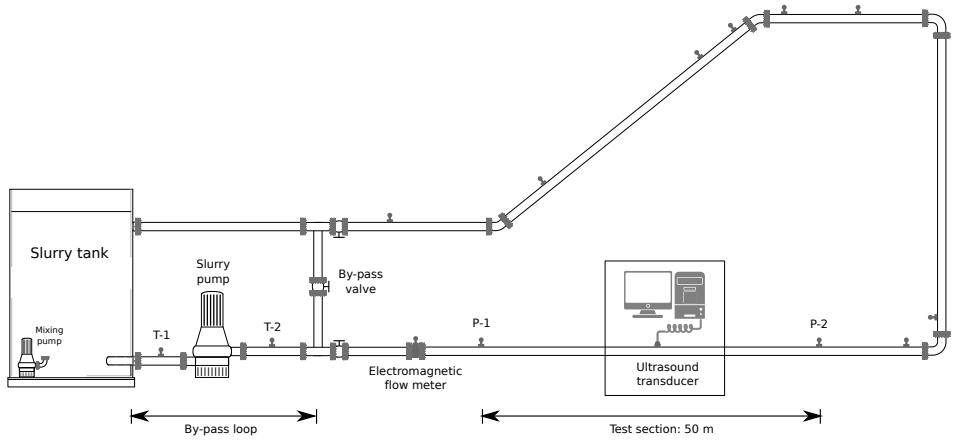

Figure 4.1: Schematic representation of the experimental set-up. T-1, T-2: Temperature sensor, P-1, P-2: Pressure sensor.

Outline

A detailed description of the experimental set-up is presented first. This set-up will serve to provide the basis for the measurements performed and presented in Chapters 5 and 6. Instead of non-Newtonian domestic slurry, a non-Newtonian clay slurry is used in these measurements, the properties of which are presented in Section 4.1.2. The flow of slurries is initially characterised through pressure losses in Section 4.2. Further characterisation of the flow is done using ultrasound imaging presented in Section 4.3.

4.1 Experimental set-up

All the measurements reported in this study were performed in a 200 m long closed-loop recirculation pipeline system with an inner diameter of 100 mm. The set-up is schematically represented in Figure 4.1. The set-up consists of a horizontal, vertical and an inclined section of 2 °. Only the horizontal section will be part of this study. A variable frequency centrifugal wastewater (slurry) pump (NT 3153, Xylem) is used to maintain the flow of the slurry. The desired flow rate is achieved by setting an appropriate outlet pressure or pump rotor rotation frequency. A slurry tank (Figure 4.2) of approximately 4 m^3 capacity upstream of the pump contains the slurry for the measurements. The slurry tank, with two outlets at the bottom

and two inlets at the top, is capable of generating a vortex when a cross inflow-outflow to the tank is selected. This vortex is instrumental in keeping the slurry continuously mixed in order to obtain a constant composition of the slurry. To aid the mixing, a submersible pump is fitted inside at the bottom of the tank opposite the outlets to further stimulate the mixing process.

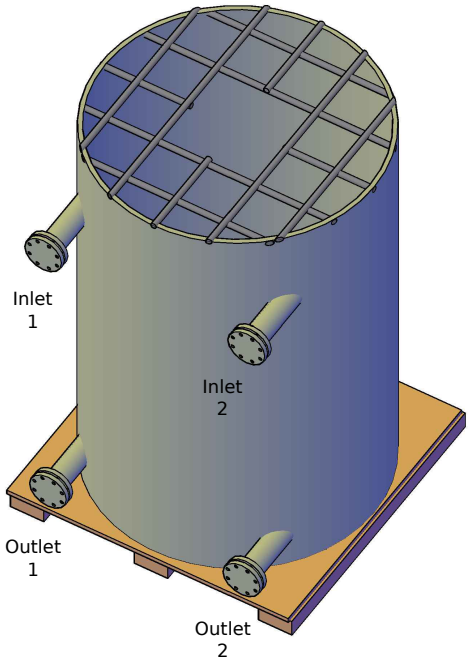

Figure 4.2: Slurry tank with two outlets at the bottom and two inlets at the top

To ensure a completely developed velocity profile at the test sections, the entry and exit lengths (L_e) are to be considered. The minimum L_e required to be satisfied is that for the laminar flow, as it is known that the L_e for a turbulent flow is shorter than that for a laminar flow (Bewersdorff and Thiel, 1993; Bogue, 1959; Chen, 1973; Froishteter and Vinogradov, 1980; Soto and Shah, 1976). The ratio of entry length to pipe diameter L_e/D is widely accepted to scale with $Re/30$ (Durst et al., 2005; Poole and Ridley, 2007). Therefore, for the cases of laminar and transition flow regimes, with $Re \geq 3000$ the acceptable entry length would be 100 ($= L_e/D$) pipe diameters. The test section (Figure 4.1) made of PVC is located 50 m downstream of the pump (with a L_e/D of 500). The pressure drop across the test section is measured using a pressure transducer placed at either ends of the test section. To ensure completely developed flows, the test section has an entrance length of 20 m from the bends (L_e/D: 200) and an exit length of 15 m from the bends (L_e/D: 150). This exceeds the required entrance and exit lengths as mentioned above.

4.1.1 Measuring Instruments

The following measuring instruments were using in the set-up. The range and measurement uncertainty of the instruments in presented in Table 4.1. All measuring instruments were tested and calibrated by in-house reference measurements and standards.

Pressure

The pressure drop across the test section is measured using two submersible pressure transducers P-1 and P-2 (PDCR5031, GE) placed at either ends of the test section. These sensors measure the absolute pressure. They contain a micro-machined silicon piezoelectric resistive pressure sensor which provides a linearised output voltage proportional to the pressure measured with an accuracy of 0.04 % over its full scale range of 0-6 bar.

Temperature

Temperature affects the rheology of the slurry, therefore it is important to monitor the changes in temperature. The temperature of the flowing slurry is measured before and after the pump using a temperature sensor (STS-PT100, Ametek) with an accuracy of 0.04 % (4.1).

Flow rate

The average volumetric flow rate is measured using an electromagnetic flow meter (Optiflux 2300C, Krohne) which is placed 10m upstream of the test section. The flow meter is especially suitable for slurries and wastewater.

Table 4.1: List of instruments

Instrument	Measuring range	Uncertainty (based on 2σ)
Electromagnetic flow meter	0 to 115 m^3/h	0.2 % over full scale
Pressure sensor	0 to 6 bar	0.04 % over full scale
Temperature sensor	0 to 50 $^\circ C$	0.04 % over full scale

4.1.2 Model Slurry

The slurry that is chosen for this study is based on Kaolin clay, of the type used for making ceramics. As the flow characteristics are the focus of this study, only similarities pertaining to the rheology are prioritised for the choice of the model slurry. This particular slurry has a similar non-Newtonian property with respect to that of CDS. It behaves as a near Newtonian fluid at low concentrations and as a shear-thinning fluid with a yield stress at high concentrations (Table 4.2). The slurry is formed through the suspension of the clay particles in water. In this study, 5 different concentrations of clay slurries are used and these are labelled S1, S2, S3, S4 and S5 and their respective concentrations are given in Table 4.2. The particle size distribution of the particulates suspended in water is examined using Microtrac Bluewave diffraction analyser (Malvern Instruments Ltd., UK) equipped with Microtrac FLEX 11 Software and is given in Figure 4.3. The suspended particulates were in the range of 5-55 micrometres and have a D_{85} of $38\mu m$. For most of the work the

shear dependence of the slurry is considered to dominate other fluid behaviour like visco-elasticity and thixotrophy. The rheology of the slurry (Table 4.2) was obtained using a rotational rheometer. An MCR302 instrument from Anton Paar equipped with a standard cup and bob (cup diameter: 29.29 mm, bob diameter: 27 mm, bob length: 40.5 mm) was used for this purpose. As the rheology is dependent on temperature, a Peltier temperature control system was used to set and maintain the temperature with an accuracy of $\pm 0.1°C$. The concentration and temperature of the different slurry samples used in the rheometer for determining the rheological characteristics are the same as the one used in the loop experiment. The slurry's non-Newtonian behaviour is dependent on the concentration of solids, as can be seen from Table 4.2 and Figure 4.3b. At low concentrations, the slurry is typically a power law fluid and at high concentrations it behaves as a Herschel-Bulkley fluid: it has a non-zero yield stress.

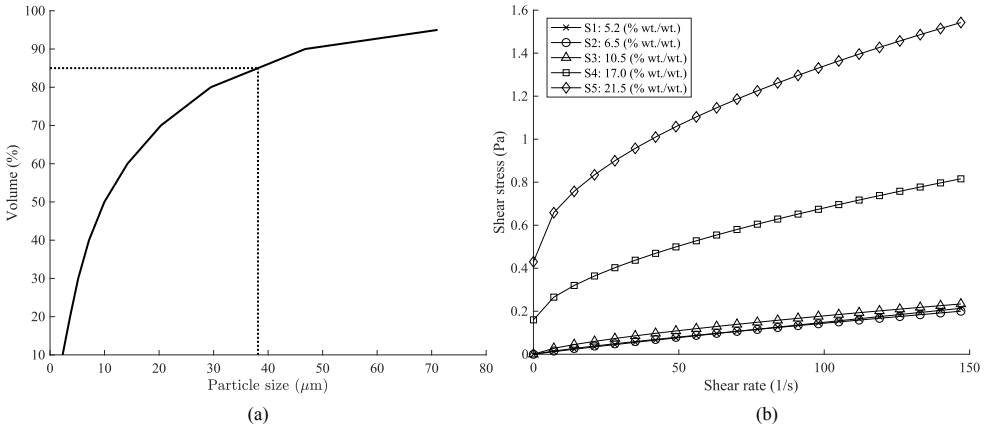

Figure 4.3: Cumulative particle size distribution of suspended slurry particulates in water with a D_{85} of $38\mu m$.

Table 4.2: Slurry characteristics: Rheology

Slurry	Concentration	Yield Stress: τ_y	Consistency Index: K	Behaviour Index: n	Density: ρ
-	% TSS (wt./wt.)	Pa	$mPa.s^n$	–	kg/m^3
S1	5.2	0	1.96	0.94	1029
S2	6.5	0	2.88	0.85	1039
S3	10.5	0	7.11	0.70	1067
S4	17.0	0.16	32.84	0.60	1113
S5	21.5	0.43	83.04	0.52	1146

4.1.3 Experimental Procedure

The system was initially filled with water and the pressure drop across the test section was measured at various flow rates. For measurements at different concentration of slurry (S1 to

S5, Table 4.2), a known amount of clay powder is added to the tank and mixed in-situ. The initial mixing is done through a shorter section (Figure 4.1, by-pass loop) of the pipeline by means of a by-pass valve for 3-4 hours and then through the entire flow loop for another 3-4 hours. During both the mixing and measurements, the small circulation pump and vortex inside the tank ensures complete mixing of the suspension inside the tank. Slurry samples from the tank are taken both during mixing and measurements to determine the slurry concentration and its rheology. During each measurement cycle, the temperature of the slurry varied less than 0.5 °C and the concentration varied less than 0.75 % TSS (wt./wt.). The recorded temperature of the slurry is also used to set the temperature of the slurry during its rheological measurements.

For each concentration, the measurements of the flow pressure drop and velocity profile was measured for different flow rates (bulk flow velocity of 0.4 m/s till 3.8 m/s). The desired flow rate was set by choosing the appropriate outlet pressure and pump rotor frequency.

To determine the occurrence of settling of the clay particles during the flow of slurry, the Rouse number for a low flow rate is used. The Rouse number for the given clay particles in the slurry was calculated to be around 0.18 at a flow velocity of 0.21 m/s, which was the lowest achieved flow velocity for slurry S5 (Rouse, 1939). Under these conditions, the mode of transport is said to be wash load, which is considered to be a fully suspended flow without the formation of a sediment bed (Rouse, 1939; Einstein et al., 1940). Therefore, under the given condition, no settling occurs during the measurements.

4.1.4 Data Acquisition and Processing

After allowing time for complete mixing (by checking slurry samples from the tank) as mentioned in Section 4.1.3, the data acquisition is carried out. The data is acquired from all the sensors and recorded simultaneously on a computer. The data from these sensors are recorded at the rate of 1 kHz. Each test case measurement of a certain slurry concentration and a flow rate were performed for around 20 minutes. This time frame provided enough measurements with steady-state situation for each test case. A tool in Matlab was created to visualise the data, and select steady-states in the data. The recorded pressure, temperature and flow rate data was averaged over 600 seconds.

4.1.5 Uncertainty

The Fanning friction factor f is used to characterise the energy losses incurred during the flow of the slurries. The energy loss is calculated based on the pressure drop (Equation 4.1) along the test section.

$$f = \frac{\Delta P}{L}\frac{D}{2\rho V^2}; \qquad \Delta P = (P_1 - P_2) \tag{4.1}$$

The uncertainty in f is calculated using Gauss's law of error propagation (Taylor, 1997):

$$\sigma_f^2 = \left(\frac{\partial f}{\partial P_1}\right)^2 \sigma_{P_1}^2 + \left(\frac{\partial f}{\partial P_2}\right)^2 \sigma_{P_2}^2 + \left(\frac{\partial f}{\partial V}\right)^2 \sigma_V^2 \tag{4.2}$$

assuming that the parameters are independent, Equation 4.2 becomes:

$$\sigma_f^2 = \left(\frac{D}{2L\rho V^2}\right)^2 \sigma_{P_1}^2 + \left(\frac{-D}{2L\rho V^2}\right)^2 \sigma_{P_1}^2 + \left(\frac{-2(P_1 - P_2)}{2L\rho V^3}\right)^2 \sigma_V^2 \tag{4.3}$$

The uncertainty in the pressure P and average flow velocity V is a combination of the uncertainty of the instrument and the uncertainty from the process itself. The uncertainty of the instruments is given in Table 4.1. The uncertainty from the process is due to the signal fluctuations arising from sensing and transmission. Assuming that the calculated standard deviation is that of the entire population (i.e. no other independent samples), the uncertainty in Pressure and Velocity is given by Equation 4.4.

$$\sigma_{measurement}^2 = \sigma_{instrument}^2 + \sigma_{process}^2 \tag{4.4}$$

The uncertainty of the friction factor as a ratio of its standard deviation to itself is plotted in Figure 4.4 against the velocity for a representative case of Slurry S5. The maximum incurred error is 7 %, which will be taken into consideration in further analysis that follows.

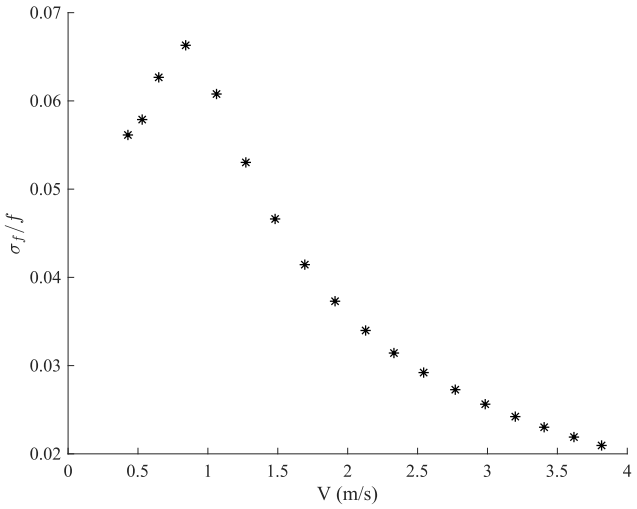

Figure 4.4: Uncertainty in the friction factor

4.2 Transport pressure loss

The results from the pressure drop measurements are presented and discussed in this section. Firstly, the results from the flow characterisation of water is presented, after which the results from the slurry flow is presented.

The measurement data for water is plotted in Figure 4.5 using friction factor f and Reynolds number. For Newtoniain fluids, the Reynolds number $Re = \frac{DV\rho}{\mu}$. The measured data correspond to the turbulent flow regime with $Re > 30000$. On plotting the Blasius equation for turbulent flow, it coincides with the measurements of water. These data serve to validate the experimental set-up.

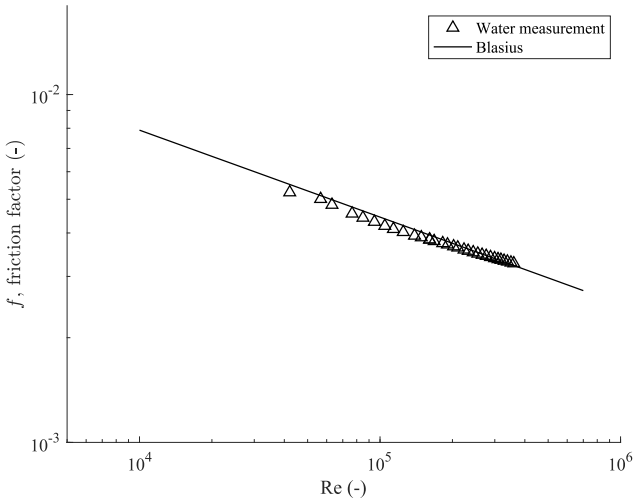

Figure 4.5: Friction factor vs. Reynolds number for the flow of water (measurement)

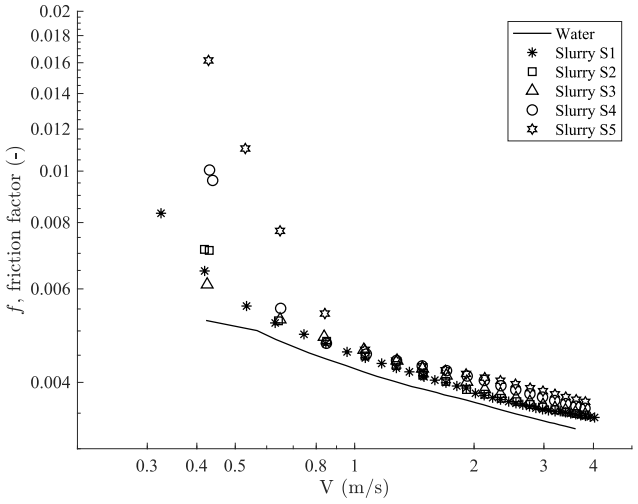

Figure 4.6: Friction factor vs. flow velocity for the flow of water (measurement)

With respect to the flow of slurry, the average flow velocity is used instead of the Reynolds number to access the initial results. The usage of the Reynolds number for non-Newtonian slurries will be discussed in Chapter 5 and 6. The initial analysis of the results from the slurry experiment are presented in Figure 4.6. This figure represents the plot of the friction factor versus the average flow velocity. Assessing these results alongside that of water (with only turbulent flow), it can be seen that there are two distinct regions in the plot, of laminar and turbulent flow with a sharp change from one to the other. The friction factor of water is lower than that of the slurries. Comparing the flows of different slurry concentrations, the

friction factor in the turbulent flow regime is mostly similar whereas the friction factor in the laminar region is highest for slurry S5 (21.5 % TSS (wt./wt.)) and decreases with the decrease in concentration. A broader analysis of the pressure drop results is presented in Chapter 6.

4.3 Ultrasound Imaging Velocimetry

Flow characterisations predominantly have been done using measurements that are external to the flow of the slurries such as pressure and flow rate. Internal flow characterisations, along with the external measurements give a complete understanding of the slurry flow. In this study Ultrasound Imaging Velocimetry (UIV) is used for this purpose. This method is particularly chosen as it is a non-intrusive diagnostic equipment and applicable to optically inaccessible fluids (as are the slurries in this study).

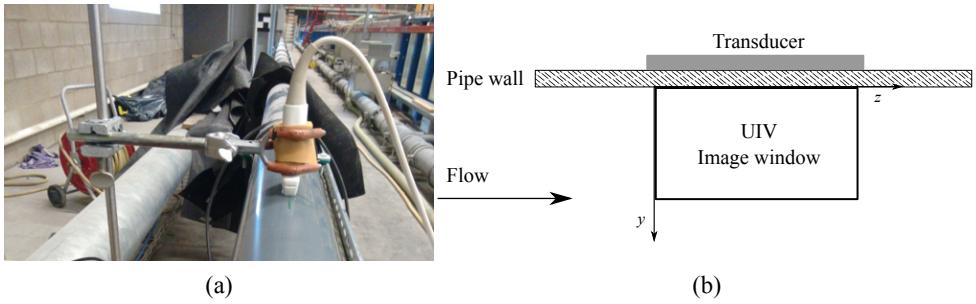

Figure 4.7: (a) Ultrasound imaging transducer aligned streamwise along the pipe. (b) Schematic representation of the coordinate system on the test section for UIV measurement.

4.3.1 UIV System

UIV (for details see Poelma (2017)) is used to obtain the velocimetry data for studying the transition in slurry flow. The system consists of an ultrasound imaging module and Particle Image Velocimetry (PIV) processing software. The imaging module is an Ultrasonix SonixTOUCH research system (Analogic Ultrasound, Canada) with a linear transducer (L14-5/38 mm aperture). The transducer centred to operate at a frequency of 10MHz has a linear array of 128 piezo-electric elements and is positioned at the centre of the pipe test section aligned length wise on the outer upper wall (Figure 4.7a). Aquasonic 100 (Parker laboratories, Fairfield, NJ, USA) gel is used to couple the transducer to the pipe wall. The radio frequency signals reflected from the flowing slurry are sampled at the rate of 40 MHz and stored in raw format for analysis. With the system set to run in research mode, this allows control to set the specifications of the ultrasound image acquisition parameters. The raw imaging data was acquired over 7-8 s at a frame rate of 400 frames per second. This high frame rate was obtained by setting the system to operate only with 64 elements (half of the available elements) of the transducer and limiting the image depth to 2.5cm from the upper outer wall of the pipe. The maximum flow velocity of the experiments is limited by the upper limit of the maximum detectable particle displacement for the UIV method. Note: This 2-D time

series velocity profile extends only 2.5 cm in depth (being 50 % of the pipe's radius) into the pipe from the outer upper pipe wall.

For convenience, two coordinate systems are used. The coordinate system (z, y) used in representation of the flow field is shown in Figure 4.7b. In the (z, y), the streamwise flow velocity component is z and the radial distance from the wall perpendicular to the axis of the pipe is y. This coordinate system will be used to represent only the flow fields. For the analysis of these flow fields, the coordinate system (z, r) will be used, where r is the radial distance from the axis of the pipe perpendicular to the axis.

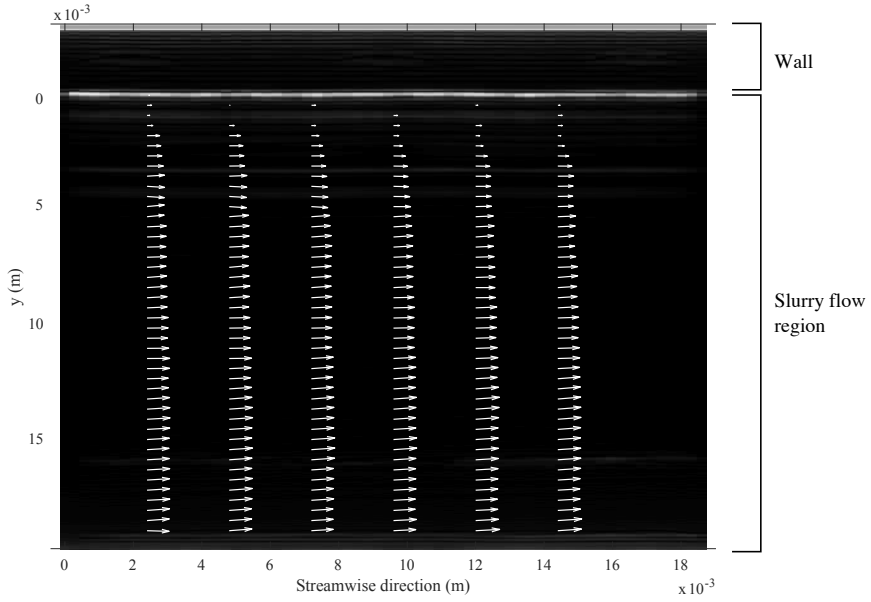

Figure 4.8: Derived flow field projected on an ultrasound image. The velocity vectors in the wall region due to non-stationary echoes, which are discarded and the vectors in the slurry flow region are used for analysis.

4.3.2 PIV Method

Custom PIV software (details can be found in Poelma et al. (2012)) was used to obtain the velocimetry data from the ultrasound images. Utrasound images contain speckles that are quite apparent. These speckles are a result of interference from many suspended clay particles in the slurry. Despite this, the estimation of the local displacements of the scatterers are possible if the displacement is small. Therefore, by tracking these particles the quantification of the slurry flow is done. The custom PIV software mentioned above uses cross-correlation between image pairs to determine the local displacement. The algorithm selects a sub-region of the ultrasound image. In this region an interrogation window is extracted from both the image pairs that are a best match between both image pairs. The best match is determined using cross-correlation, and the highest peak in this cross-correlation is chosen as the best pair. The pixel displacement between these interrogation windows in the image pair and the

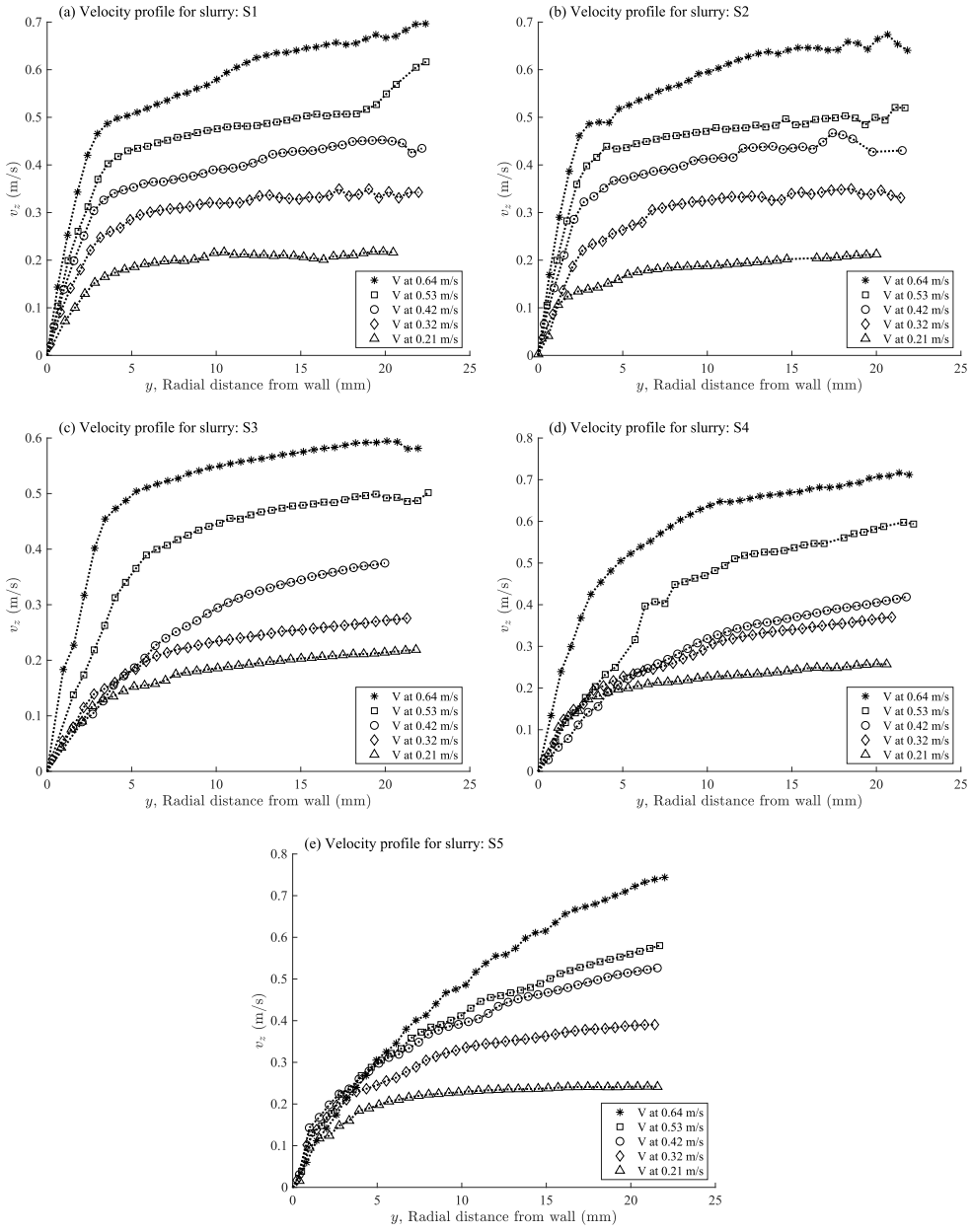

Figure 4.9: Velocity profiles for the different flows of slurries and average flow velocity.

time step between them is used to quantify the motion. Applying this over the entire image and all consecutive image pairs over the recorded data gives a time-series of 2-D velocity profile at the centre-plane of the pipe. Outliers in the velocity field were detected using a

median test. These outliers were replaced using an interpolation of the neighbouring vectors.

4.3.3 Velocimetry

Ultrasound images were obtained at 400 Hz over an interval of 7 seconds approximately. Applying the PIV cross-correlation method mentioned in Section 4.3.2 to the time-series sequence of the images, a 2D velocity vector field is obtained for each slurry in Table 4.2) at different flow velocities. Figure 4.8 shows a typical flow field obtained using the above mentioned method. The figure shows a unidirectional flow with both the presence of a wall and the slurry flow regions. The location of the wall in the velocity field is detected by superimposing the derived velocity profile on to the ultrasound image. Applying the no-slip boundary condition, at the point where velocity profile approaches zero, the wall location is identified. The velocity vectors in the wall region due to non-stationary echoes which are common for PVC pipes are discarded.

Using the flow field, a velocity profile across the cross section of the pipe is obtained for the different cases of various slurry concentration and average flow velocity V. These velocity profiles are shown in Figure 4.9. Due to the limitation of the acquisition frame rate, the maximum flow velocity for which the velocity profiles were acquired is 0.64 m/s. With a minimum flow velocity of 0.21 m/s and a maximum of 0.64 m/s, the range of different flow regimes for the different slurries is determined. A close look at the different profile structures of the obtained velocity profiles in Figure 4.9 gives this indication of different flow regimes. A detailed study of these regimes, their observation and identification will be discussed in Chapter 5.

4.4 Outlook: Chapter 5 & 6

To study the flow characterisation of non-Newtonian slurries a pipeline loop was built. This pipeline loop was equipped with pressure sensors and temperature sensors to accurately measure the pressure drop across the test section along with the temperature of the slurry flowing. These measurements were carried out for various concentrations of slurries and flow velocities. Using the results from the flow of water, the experimental set-up was validated. The friction factor was plotted vs. the flow velocity for the slurries. Further analysis of these pressure drop data are presented in Chapter 6 along with a model that represents them.

Along with the flow characterisation of slurry flows using pressure losses, a non invasive method of characterising the flows using its flow fields is presented. This method used ultrasound imaging techniques to capture time-series images and employs PIV techniques to obtain a flow field. Further, the flow field was used to obtain velocity profiles through which the slurry flows were characterised. These flow fields were then used to analyse the transition from laminar to turbulent flow, which is presented in Chapter 5.

Chapter 5 is based on:

Thota Radhakrishnan, A.K., Poelma, C., van Lier, J.B., Clemens, F.H.L.R. (2019). Laminar-turbulent transition of a non-Newtonian fluid flow. *Journal of Hydraulic research*, submitted.

CHAPTER 5

Laminar-Turbulence Transition

Flows of non-Newtonian fluids or slurries are commonly found in a variety of process systems. The flow of slurries in wastewater treatment plants is a commonly encountered example. Characterising their flow regime is an important factor in the overall hydraulic design and the operation of the equipment handling them. Predicting the flow regime as laminar, transitional or turbulent has been a major part of the study on non-Newtonian flows in the recent decades. As the gap between theoretical understanding and experimental findings of Newtonian fluids closes, non-Newtonian fluids are starting to become a new realm of fluids waiting to be explored, with transition in their flow forming a fundamental importance.

5.1 Transition

Studying the transition of flow from laminar to turbulent has two aspects to it; 1) identifying the conditions under which transitions occurs and 2) the possibility of predicting these transitions. Both are discussed in the following sections.

5.1.1 Characterising transition

Transition from laminar to turbulent flow is known to occur through intermittent flow structures which evolve from disturbances in the flow. A number of classic experimental works (Darbyshire and Mullin, 1995; Draad et al., 1998; Güzel et al., 2009a; Lindgren, 1969; Nishi et al., 2008; Wygnanski et al., 1975; Wygnanski and Champagne, 1973) have focussed on studying the transitional regime and have shown that two distinct flow structures exist: puffs and slugs. The occurrence of these structures depends on the Reynolds number ($Re = \frac{DV\rho}{\mu}$); puffs occur at relatively low Reynolds numbers and slugs at a higher Reynolds numbers. As for Newtonian fluids, through the experimental studies performed in circular pipes that have already been mentioned, it is seen that puffs are found when $Re \lessapprox 2700$ and slugs are found when $Re \gtrapprox 3000$.

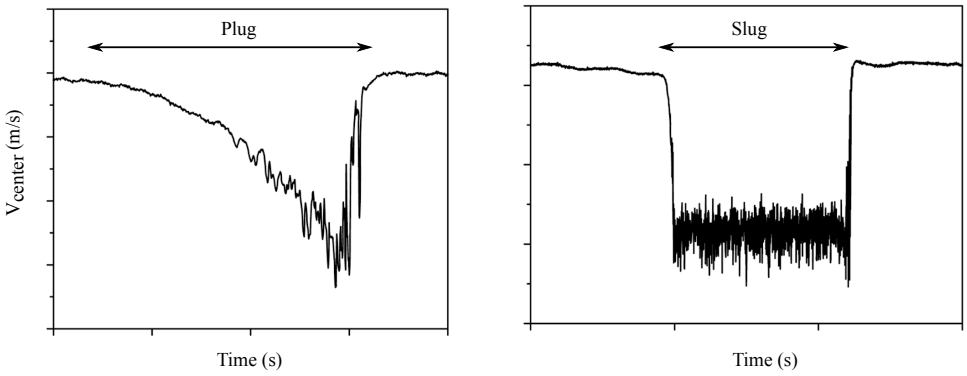

Figure 5.1: Velocity trace (adopted from Nishi et al. (2008)) at the centre of the pipe showing the presence of puff (left) and slug (right).

To characterise puffs and slugs, changes in the local velocity are often used. Puffs are identified as having a saw-toothed velocity trace (gradually decreasing, followed by a more sudden jump back to the undisturbed velocity), see e.g. Nishi et al. (2008); Wygnanski and Champagne (1973). These puffs represent isolated patches of turbulent flow and are dissipated downstream along the flow (Figure 5.1, left). On the other hand, the velocity trace of the slugs is identified as having a square shape (Figure 5.1, right), with properties similar to that of fully developed turbulence within them (Nishi et al., 2008). Its leading edge is found to travel faster than the average flow velocity and its trailing edge, thereby increasing in length as it travels downstream.

5.1.2 Predicting transition

For Newtonian fluids, transition can be predicted in practical applications based on the well-established critical Reynolds number (2100-2300 for pipe flows). There is a wide range of theories and models available to predict this onset of transition (Avila et al., 2011; Eckhardt et al., 2007), and such a range is due to the difficulty that transition as a phenomenon is not very well defined and occurs over a range of Reynolds numbers (Darbyshire and Mullin, 1995; Draad et al., 1998). For non-Newtonian fluids, a complicating factor is the representation of the fluid behaviour in simple rheological models. The models are only a simplified representation of a small set of measured quantities, i.e. measuring only the shear stress vs. shear rate while ignoring other information - such as the type of fluid and the particles involved (in the case of a slurry). As a consequence, the Reynolds number is no longer defined in a trivial manner, as there is no longer a single value that represent the viscosity. Nevertheless, there is a need for models that predict/describe the transition in non-Newtonian fluids/slurries. The ones mostly commonly referred to in literature are described below. These models can be categorised as either Reynolds number based or Stability parameter-based models.

Reynolds number based

Hedstrom (1952) proposed the intersection method wherein the transition is defined as to occur at the Reynolds number associated with the intersection of the (extrapolated) laminar

and turbulent friction factor curves. Although simple, the result is highly dependent on the choice and accuracy of the turbulent model (friction factor curves, e.g. Blasius friction curve) and is regarded as an ambiguous criterion.

Metzner and Reed (1955) analysed data from a series of pipe flow experiments of different non-Newtonian fluids and pointed out that the flow curves deviated from the laminar flow curve at approximately the same ratio of viscous to inertial forces. Considering the Fanning friction factor as a stability parameter, they proposed that transition would take place at $f \approx 0.0076$. To calculate the friction factor, the Metzner-Reed Reynolds number Re_{MR} (Equation 5.1) is used, and at transition it corresponds to a value of ≈ 2100. The parameters in Equation 5.1 are derived as n representing the slope of a logarithmic plot of $\frac{D\Delta P}{4L} versus \frac{8V}{D}$, which is found to be nearly constant for most non-Newtonian fluids over a wide range of shear stresses. K' is the coefficient from the integration of the expression representing the wall shear rate as a function of the pressure drop and the volumetric flow rate, which finally leads to $\frac{D\Delta P}{4L} = K'(\frac{8V}{D})^{n'}$. The Re_{MR} is based on power-law fluids; for Herschel-Bulkley fluids the parameters in Re_{MR} are dependent on the yield stress, which imposes complications.

$$Re_{MR} = \frac{8V^2\rho}{K'(\frac{8V}{D})^n}, \qquad K' = K\left(\frac{1+3n}{4n}\right)^n \tag{5.1}$$

Slatter (1995) proposed a Reynolds number (Equation 5.2) accounting for a solid plug at the centre of the pipe flow due to the presence of yield stress in the fluid. The unsheared plug at the centre is treated as a solid plug and its flow is subtracted from the mean fluid flow to determine the effective flow velocity of the annular, sheared region (Equation 5.3).

$$Re_S = \frac{8\rho V_{ann}^2}{\tau_y + K(8V_{ann}/D_{shear})^n} \tag{5.2}$$

$$V_{ann} = \frac{Q_{ann}}{A_{ann}} = \frac{Q - Q_{plug}}{\pi(R^2 - R_{plug}^2)} \tag{5.3}$$

To obtain the effective flow velocity in the annulus, the volumetric flow rate in the plug is obtained using Equation 5.4, where the radius of the plug is determined using Equation 5.5.

$$Q_{plug} = A_{plug}\frac{D}{2K^{(1/n)}\tau_w}\frac{n}{n+1}[(\tau_w - \tau_y)^{(n+1)/n}] \tag{5.4}$$

$$R_{plug} = \frac{\tau_y}{\tau_w}R \tag{5.5}$$

Among the Reynolds number-based models, the ones by Slatter and Metzner-Reed model will be considered for this study. The Hedstrom method is not considered, since an assumption must be made on the turbulence flow model which is not in the scope of the study. Nevertheless, the Hedstrom method will be used as a verification step, to validate the identified transition through the measured pressure drop.

Stability parameter based

Ryan and Johnson (1959) approached transition through a local stability parameter on the balance of stabilizing and destabilizing forces. The stability parameter is based on the energy-dissipation of disturbances, where the energy exchanges are represented as shear stresses.

This stability parameter represented as Z_{RJ} is a function of the ratio of input energy to energy dissipation for a fluid element as shown in Equation 5.6. Transition occurs at the boundary between stable laminar and stable turbulent pipe flow where the parameter reaches a critical point represented as $\frac{\partial Z_{RJ}}{\partial y} = 0$ and Z_{RJ} takes the value 808, which is set to be the predictive criterion. This value is derived through the transition of Newtonian fluids and assumed to be true for all fluid types.

Ryan and Johnson (1959) approached transition through a local stability parameter on the balance of stabilizing and destabilizing forces. The stability parameter is based on the energy-dissipation of disturbances, where the energy exchanges are represented as shear stresses. This stability parameter, represented as Z_{RJ}, is a function of the ratio of input energy to energy dissipation for a fluid element as shown in Equation 5.6. Transition occurs at the boundary between stable laminar and stable turbulent pipe flow where the parameter reaches a critical point represented as $\frac{\partial Z_{RJ}}{\partial y} = 0$ and Z_{RJ} takes the value 808, which is set to be the predictive criterion. This value is derived through the transition of Newtonian fluids and assumed to be valid for all fluid types.

$$Z_{RJ} = \frac{r\rho v_z}{\tau_w}\frac{\partial v_z}{\partial y}, \qquad at \frac{\partial Z_{RJ}}{\partial y} = 0 \tag{5.6}$$

Hanks and co-workers (Hanks, 1969, 1963; Hanks and Dadia, 1971; Hanks and Ricks, 1974) derived a similar criterion as Ryan and Johnson (1959), through the perspective of angular momentum transfer. The proposed stability criterion is seen to represent the coupling ratio between the rate of change of angular momentum of a deforming fluid element and its rate of momentum loss by frictional drag. At transition, the fluid element is seen to become unstable to rotational disturbance and thus giving rise to turbulent eddies through the non-linearity of the momentum transfer process. The critical value of the stability parameter was determined to be 404, exactly half of that derived by Ryan and Johnson (1959). Equation 5.7 represents the derived stability criterion, where $w = \nabla \times v$ is the vorticity vector from the velocity vector v and $\nabla.\tau$ is the divergence of the deviatoric stress tensor. For a rectilinear pipe flow, Equation 5.7 reduces to Equation 5.8. This is derived using the Fanning friction factor to represent the average flow velocity in terms of the rheological model. In practise, Equation 5.8 is used setting $Z_H = 404$, to derive the transition critical flow velocity.

$$Z_H = |\rho v \times w|/|\nabla.\tau| \tag{5.7}$$

$$Z_H = \frac{Re}{16}\left(\frac{v}{V}\right)\left(-\frac{d(v/V)}{d(r/r_w)}\right) \tag{5.8}$$

Mishra and Tripathi (1971) pointed out that transition occurs through a step-wise process. The consecutive steps are described as follows: two-dimensional waves, three dimensional waves, a turbulent spot and propagation of the turbulent spot to the entire field. The formation of the turbulent spot coincides with the point where the rate of change of the mean velocity is at its maximum. With this, they accordingly proposed that the average kinetic energy per unit volume in the fluid and the shear stress at the wall to be the important factors governing the transition. Through this they derived a stability parameter as the ratio of the kinetic energy per unit volume of the fluid and the wall shear stress and also postulate that it should remain the same for all purely viscous non-Newtonian fluids.

Among the stability parameter-based models the one of Hanks and co-workers will be considered for this study. This is due to reason that all the models are very similar at the

implementation and that only the theory behind the model development is different. Also, the Hanks model is very well documented for the use of Herschel-Bulkley fluids (being the main rheological model considered in this study) while the other two are not well documented and pose difficulties in its implementation for Herschel-Bulkley fluids.

It is not claimed that the previous discussion encompasses a complete list of the predictive methods that have been proposed. Some that have not been mentioned are either modifications or extensions of the ones discussed. Readers interested in these are referred to literature (e.g. Güzel et al. (2009a)).

Studying and examining laminar turbulent transition in the flow of fluids including non-Newtonian fluids have been made possible through many experimental techniques. These techniques include Hot wire anemometry (Nishi et al., 2008; Wygnanski and Champagne, 1973), Laser Doppler Anemometry/Velocimetry (Draad et al., 1998; Escudier and Presti, 1996; Güzel et al., 2009a; Peixinho et al., 2005), stereoscopic-PIV (Van Doorne and Westerweel, 2007) and more recently Ultrasound Imaging Velocimetry (UIV) (Hogendoorn and Poelma, 2018). The choice of the experimental technique in most cases certainly depends on the test fluid properties and the capability to be intrusive or not. In the case of hot-wire anemometry and laser doppler anemometry, the information of the flow obtained is a time series of a particular point in the flow. Whereas, the UIV technique gives information about the flow field within a time range. This technique is both non-invasive and applicable to optically inaccessible fluids. The work of (Hogendoorn and Poelma, 2018) states the applicability of using UIV as a technique to acquire flow fields of fluids with particles and observe transition in them. Given the applicability of the UIV technique, this will be used in this study.

This study aims to investigate laminar-turbulent transition and verify models that predict this transition in non-Newtonian fluids. A flow loop is built to achieve fully-developed steady state flows of non-Newtonian fluid in a circular pipe, the set-up is detailed in section 4. Using this set-up, the pressure drop along the pipe is measured at various flow rates for different concentrations of a non-Newtonian slurry. Along with this the instantaneous velocity field is quantified to investigate laminar-turbulent transition using Ultrasound Imaging Velocimetry (UIV) (Section 4.3). It must be noted that the data set obtained is both unique considering such a large flow loop and novel when taking into account the UIV method applied. The velocimetry data will be used to identify and investigate the formation of intermittent fluid structures present during transition and identify transition. Considering the availability of many predictive model candidates (Section 5.1.2), the aim of this paper, is to verify the available predicting methods for transition in non-Newtonian fluids.

5.2 Observing transition

The resulting vector fields obtained from the PIV (Section 4.3.3) processing were used to identify the occurrence of flow regime transition. Transition is visualised by plotting a single array of the velocity vectors along the radial direction as a function of time, which illustrate an evolution of the transition characteristics i.e. slugs and puffs. A median filter is applied on the velocimetry data to replace the outliers present in the data. As the large-scale structures dominate, the median filter will not hinder the analysis. As a representative case, the different cases of slurry 4 is illustrated in Figures 5.2 & 5.3 and these representative cases will form the core of the discussion that follows. Other data sets for the same conditions, as

well as the other cases, showed similar behaviour and we focus here on these exemplary data sets. The data for the other cases is available in the appendix (Appendix Figures B.1 to B.10). In Figure 5.2, the radial component of the velocity vector is plotted and in Figure 5.3, the axial component (streamwise direction) of the velocity vector is plotted. Using Taylor's hypothesis, the time-series can be interpreted as a spatial sequence (although it is stressed that the image does not represent a true instantaneous snapshot) of the evolution of the structures.

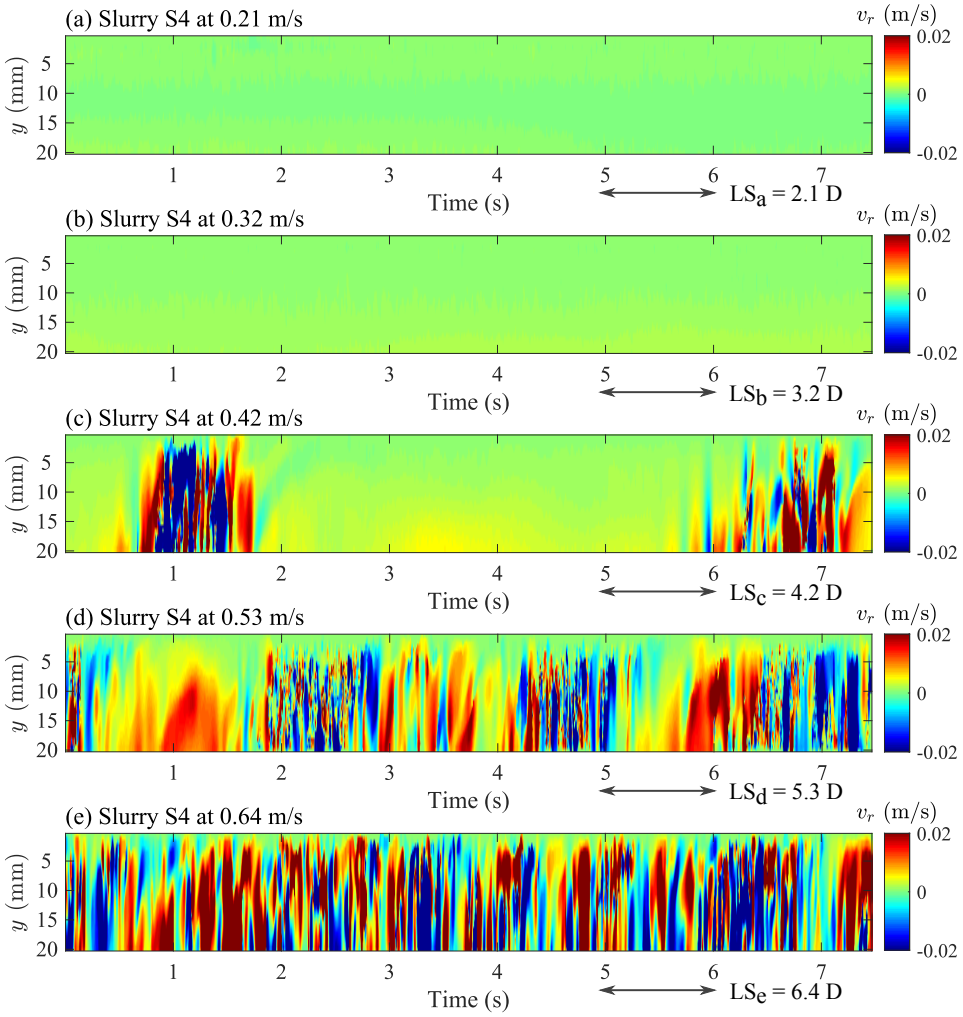

Figure 5.2: Observing transition through the ultrasound velocimetry data. Plot of the radial component of the velocity vector against time as an estimate for the cross-sectional plane for slurry 4. The length scale (LS) with respect to time is given as a factor of diameter ($LS = \frac{t.V}{D}$).

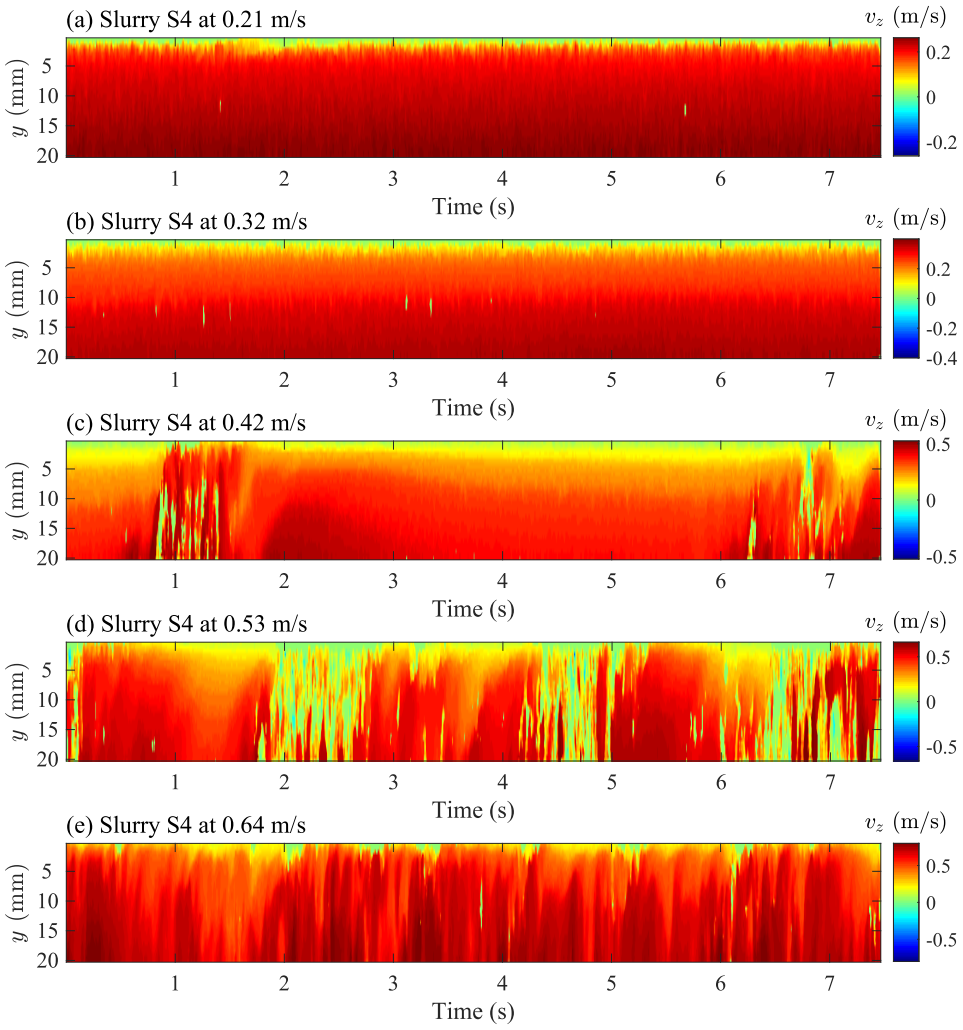

Figure 5.3: Observing transition through the ultrasound velocimetry data. Plot of the axial component of the velocity vector against time as an estimate for the cross-sectional plane for slurry 4.

An initial observation from the Figures 5.2 & 5.3, is the presence of intermittent structures (Figure 5.2 c, d and Figure 5.3 c, d). For further analysis of the intermittent structures, the mean of the velocity components along the radial direction is plotted against time (Figure 5.4). The centre line velocity trace is generally used in characterising these intermittent structures, but due to the limitation of the depth of the flow field in study, the mean of the velocity components that encompasses all the radial positions is used. The plot of the mean also provides an appropriate indication of the intermittent structures, as they are deviations that are seen from the mean flow (Figure 5.4). Analysing the mean plot (Figure 5.4), it

can be seen that the intermittent structures are similar to the ones observed in previous studies (Güzel et al., 2009a; Nishi et al., 2008; Wygnanski and Champagne, 1973). These intermittent structures are caused by localised perturbations. They induce turbulence at localised sections of the pipe as puffs and slugs. The length of these structures are found to be about 5 diameters for puffs and 10 diameters for slugs. This size is particularly low compared to lengths of 30 diameters reported in earlier studies (Eckhardt et al., 2007; Wygnanski and Champagne, 1973). Figures 5.4c and 5.4h show the presence of structures that appear gradual and dissipate. These structures are characterised as puffs. Figures 5.4d and 5.4i show the presence of slugs which appear as a sharp deviation from the mean flow and persist for a short period of time and then sharply deteriorates. It is also noted that within the structure of slugs characteristics similar to turbulence can be seen. These intermittent structures could also be observed in the plots of Figures 5.2 and 5.3.

Through the occurrence of the intermittent structures, it is identified that transition does not occur at a single stage, as it rather occurs over a range of velocities with different characteristics. The state-of-the-art characterisation of transition is through puffs and slugs as already mentioned in section 5.1.1. In this study, a different approach is applied to characterise these transitions. Different stages of transition are identified, based on a combination of the occurrence of puffs and slugs. Figure 5.2, 5.3 (combined with the information from the figures in the Appendix) show these stages through the time evolution plots of the velocity component, as not all the measured cases undergo all the transition stages, only a few representative cases are considered. One of the stages can be identified with the occurrence of puffs (Figure 5.2c and 5.3c), where the flow is mostly laminar with the occurrence of occasional puffs and fluctuations. Another stage can be identified with the occurrence of slugs (Figure 5.2d and 5.3d) which can also be viewed as turbulent flow with some less intense regions. Using these characteristics of transition as a criterium for identifying transition, the cases that undergo transition are shown in Table 5.1.

Table 5.1: Identified flow regimes through the plotting of ultrasound velocimetry data and predictability of the transition models, S: Slatter, MR: Metzner-Reed and H: Hanks where the shading in green shows positive and red shows negative predictability.

V	S 1			S 2			S 3			S 4			S 5		
0.64	Turbulent			Turbulent			Turbulent			Turbulent			Transition		
	S	MR	H	S	MR	H	S	MR	H	S	MR	H	S	MR	H
0.53	Turbulent			Turbulent			Turbulent			Transition			Laminar		
	S	MR	H	S	MR	H	S	MR	H	S	MR	H	S	MR	H
0.42	Turbulent			Turbulent			Transition			Transition			Laminar		
	S	MR	H	S	MR	H	S	MR	H	S	MR	H	S	MR	H
0.32	Turbulent			Turbulent			Transition			Laminar			Laminar		
	S	MR	H	S	MR	H	S	MR	H	S	MR	H	S	MR	H
0.21	Transition			Transition			Laminar			Laminar			Laminar		
	S	MR	H	S	MR	H	S	MR	H	S	MR	H	S	MR	H

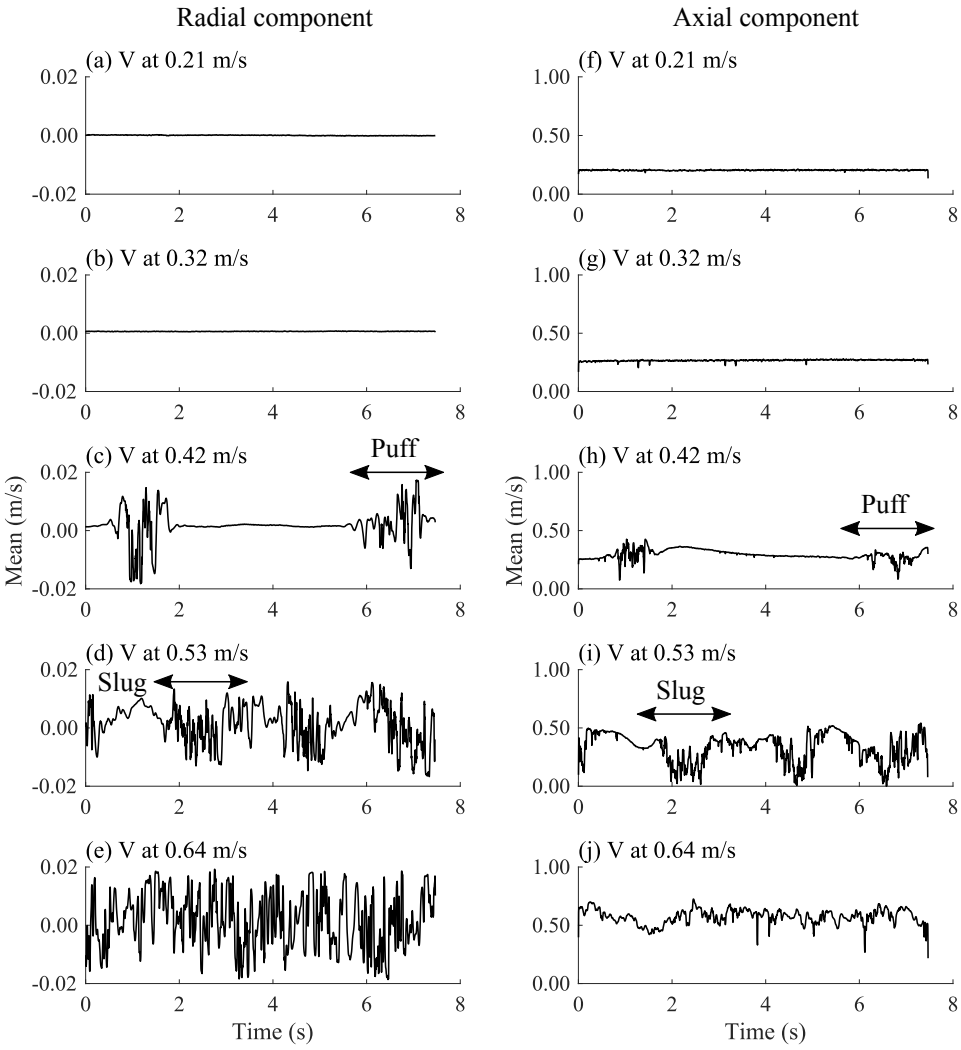

Figure 5.4: Plot of the mean of the velocity component along the radial direction against time. The radial component is used in figures a, b, c, d, e and the axial component in f, g, h, i, j.

5.3 Analysing transition

After the qualitative observation of transition through the visualisation of the transition structures, it is useful to analyse transition through statistical means and physical quantities to differentiate it with laminar and turbulent regimes. By such an approach, the identified cases of transition can be verified through other metrics. For this, (1) the intersection of the laminar and turbulent friction factor curves from the measure pressure drop is used mark

the transition, and (2) the changes in turbulence intensity with respect to the increase in mean flow rate can also indicate transition.

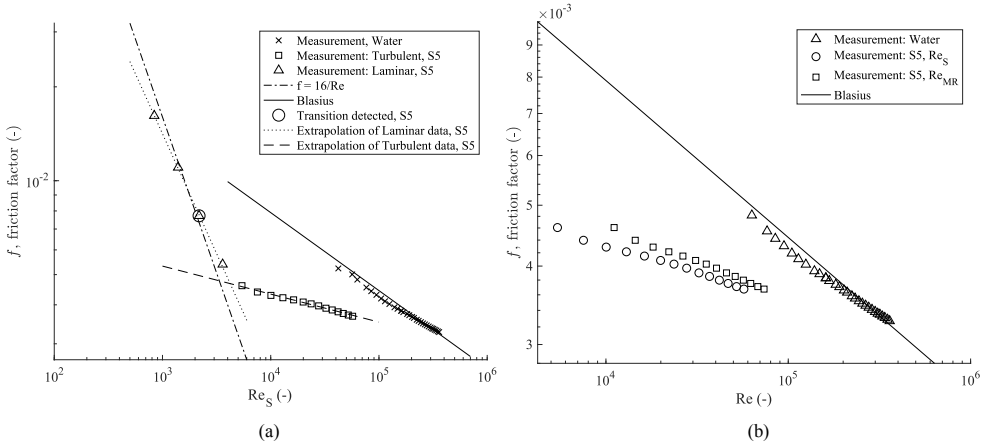

Figure 5.5: (a) Friction factor vs. Reynolds number curve for the flow of slurry S5. (b) Friction factor and Reynolds number for the turbulent data set for slurry S5.

5.3.1 Friction factor curves

Transition can be identified/verified from the plotting the friction factor versus Reynolds number curves. Transition is assumed to occur at the intersection of the laminar and turbulent friction factor curves (Hedstrom, 1952). The Slatter-Reynolds number is used here, as it considers both the shear thinning behaviour of the fluid and the presence of yield stress. As a representative case, the friction factor curve for the case of slurry S5 (Fig. 5.5a) is plotted as it is the only case that contains enough measurements in the laminar flow regime. From the figure, it can be seen that there is a sharp change in the data. Considering the lower Re set of points before the sharp change to be laminar flow, and the higher Re points as turbulent flow, the intersection of the extrapolated laminar and turbulent curves indicates the point of transition. Before further analysis, it is instructive to examine the friction factor curve. On plotting $f = 16/Re$, the laminar Fanning friction factor curve, it can be seen that the slurry measurements considered to be laminar fall on or close to the Fanning curve. But a striking result is obtained on plotting the Blasius turbulent curve. The Blasius curve is above the slurry measurements considered to be turbulent. This may be attributed to the use of the Slatter-Reynolds number, as it is a particular representation of the viscous forces through rheology. To rule out any suspicion over measurement errors, the measured friction factor for the flow of water in the same setup is plotted in the same figure. The friction factor for water falls right on the Blasius curve. A plausible explanation for this would be that, although the Slatter-Reynolds number is used for water, it ultimately reduces to the standard Reynolds number as $\tau_y = 0$ and $n = 1$ for water. These results could certainly rule out measurement errors. Further, on plotting the friction factor versus Metzner-Reed Reynolds number (Figure 5.5b) considering only the turbulent data set of slurry S5, the data are shifted with respect to the data using the Slatter Reynolds number. This is to underline that the formulation of the Reynolds number for non-Newtonian fluids plays a huge role in

discrepancies that arise.

The observed point of transition for this slurry (S5, Table 5.1) is at 0.64m/s (for this pipe diameter). There is no UIV data for slurry flow above this velocity due to the limitations of the equipment mentioned earlier (Section 4.3). On comparing the point of transition identified from the intersection of the friction factor curves with the one already observed for this slurry, it can be seen that the transition predicted at 0.64 m/s is close to the point of transition from the friction factor curves and lies on the extrapolated laminar curve.

5.3.2 Turbulence intensity

This occurrence of transition was further studied through the turbulence intensity, $I(v'/V)$. As a representative case, Figure 5.6 shows the turbulence intensity versus mean flow velocity for slurry S4 using the velocity trace at 20mm from the pipe wall. The turbulence intensity for the velocity component in the flow direction v_z when plotted against the mean axial velocity (Figure 5.6) shows peaks at the same velocities where transitions were identified through the visualisation of the flow field (Table 5.1). The sharp changes in peaks in turbulence intensities as a criteria for transition has also been used by Güzel et al. (2009a). On plotting the turbulence intensity for the v_r velocity component (Figure 5.6), a steady increase in the turbulence intensity is seen on the onset of transition. Table 5.1 shows the measured cases of transition, which correspond to the data points where there is a sharp increase in turbulence velocity. These sharp changes in turbulence intensity that occur at the onset of transition is due to the definition of the turbulence intensity itself: it considers both the laminar parts of the velocity trace (low to no fluctuations) and the puffs & slugs (high fluctuations) in the calculation of v'. As the standard deviation between the laminar part and the part with the intermittent structures of the velocity trace has a large difference, the v' at transition has a high value. This in general tends to give a sharp change in the turbulence intensity at transition. Therefore, this can be considered as an intrinsic property of the velocity trace at transition.

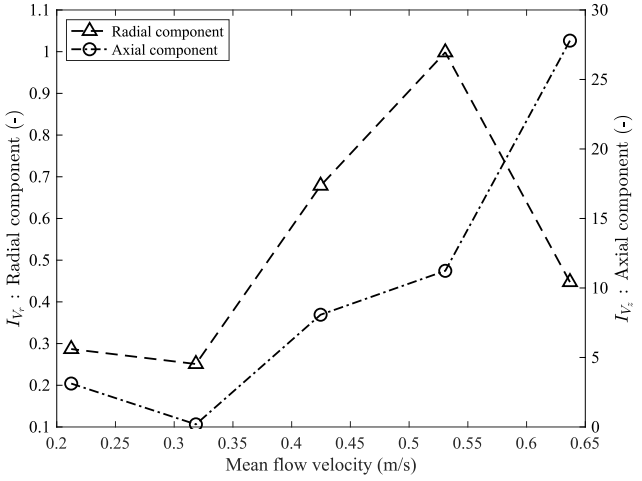

Figure 5.6: Plot of turbulence intensity using the velocity trace at 20mm from the pipe wall for slurry S4 using both the radial and axial velocity component.

Therefore, it is concluded that the cases of transition that were identified using the visualisation of the flow field from the UIV measurements correspond to the cases identified by other means (friction factor curve intersection, autocorrelation, turbulence intensity), which can be considered to be its verification.

5.4 Predicting transition

Cases of transition presented in Table 5.1 for the flow of slurry are the ones that were identified using the velocimetry plots and verified using other physical quantities mentioned in Section 5.3. From section 5.1.2, three different transition models are selected: the Slatter Reynolds number, Metzner-Reed Reynolds number and Hanks stability criterion. To apply the selected transition predicting models mentioned in Section 5.1.2, the transition velocity V_{trans} is used (Table 5.2). The transition velocity is used as opposed to only Reynolds number, as the models used are varied and the transition velocity is common to all three of them. The rheology of the respective slurries (Table 4.2) is used to calculate these transition velocities. While the models predict only one transition velocity per slurry, the experimental measurements give us a range at which transition occurs as portrayed in Table 5.1.

Table 5.2: Transition velocity V_{trans} estimated by the different candidate models for the slurries.

	Predicted V_{trans} (m/s)		
Slurry	Slatter	Metzner-Reed	Hanks
S1	0.04	0.04	0.04
S2	0.05	0.05	0.05
S3	0.09	0.08	0.10
S4	0.39	0.22	0.34
S5	0.64	0.36	0.53

Using the transition velocities (Table 5.2), the flow regimes of each case and its predictability of the transition models is shown in Table 5.1. Among the models studied here, the Reynolds number-based model by Slatter performs best in predicting the transition and flow regimes for fluids with yield stress and lower behaviour index (S4 and S5) as well as predicting the flow regimes slurries that are only shear-thinning (S1, S2, S3). The second best is the stability parameter-based model of Hanks. The Metzner-Reed model performs the least. On the other hand, for slurries that are only shear thinning (zero yield stress, slurries S1, S2, S3) all the models seem to fail in predicting the transition. The transition velocity predicted for these slurries is less than the ones measured, therefore predicting a transition earlier than observed in reality. For slurries with a yield stress, the reason for the Slatter and Hanks model to perform better could be found in the fact that it uses the Yield stress, while it is not incorporated in the Metzner-Reed model. For slurries that are only shear-thinning it is interesting to note that all the models predict more or less the same transition velocity. This could be attributed to the reduction of the Reynolds number-based models for weakly shear-thinning fluids to the standard Reynolds number and predict the same transition velocity. As for the Hanks models, this could also be true as it uses the transition criteria used is similar to the Reynolds number-based models.

Therefore, it is concluded that the Slatter Reynolds number-based model for fluids with a low behaviour index and yield stress can predict transition correctly. The Slatter Reynolds number model has the advantage that it can easily be implemented compared to the stability parameter based models.

5.5 Conclusion and outlook

A test facility containing a pipe-loop was constructed to investigate and flow of non-Newtonian slurries and its transition from laminar to turbulent flow. To obtain images of the flow an ultrasound transducer was used. Using this imaging technique, it was demonstrated that ultrasound imaging velocimetry (UIV) can be performed to obtain velocity measurements in slurry flows that are usually inaccessible to optical techniques. It is also demonstrated that using UIV measurements, it is also possible to obtain transition and turbulent statistics. UIV has also provided a new insight in transition through a novel visualisation of the intermittent structures (puffs and slugs) that are formed during transition.

Transition was observed and identified through the visualisation of the flow field with time. The cases wherein transition was observed were later verified by application of physical and statistical metrics. These verification metrics included intersection of the laminar and turbulent friction curves, autocorrelation of the flow field and turbulence intensity. These verification metrics not only assisted in verifying the observed transition, but also in characterising them. It is worth mentioning that the length of the intermittent structures are about 5 times the pipe diameter for the puffs and about 10 times the pipe diameter for the slugs. With the turbulent intensity, it is also seen that there is a sharp rise in its value upon transition. Through these, it is also concluded that transition occurs as a multistep process.

The transition velocity V_{trans}, was used to access the models used to predict transition. Among them, the Reynolds number-based model of Slatter is assessed to be the best in predicting transition for fluids with an yield stress and low behaviour index. This is followed by the stability parameter-based model of Hanks in terms of its predictability, while the one of Metzner-Reed is least favorable. The Slatter model also has its advantage in its ease of implementation.

Considering the promising results, the UIV technique has certainly a solid future in the field of multiphase flow studies. Especially with its capability to be a non-intrusive diagnostic instrument and its applicability to optically inaccessible fluids. With the possibility to obtain longer time series and deeper intrusion (possibly a complete cross-section) in the pipe, its potential to investigate turbulence and transition is high. The realm of non-Newtonian fluids is still burgeoning. As most non-Newtonian fluids are opaque, the use of UIV could yield more understanding of turbulence and transition its flows, and hence provide a basis for improving CFD models for non-Newtonian fluids.

Chapter 6 is based on:

Mehta, D., Thota Radhakrishnan A.K., van Lier, J.B., Clemens, F.H.L.R. (2019). Assessment of semi-empirical models for estimating frictional losses incurred in the turbulent flow of non-Newtonian slurries through closed circular pipes. *Journal of Hydraulic research*, submitted.

Mehta, D., Thota Radhakrishnan A.K., van Lier, J.B., Clemens, F.H.L.R. (2019). Sensitivity Analysis of a Wall Boundary Condition for the Turbulent Pipe Flow of HerschelBulkley Fluids. *Water*, 11(1), 19.

Mehta, D., Thota Radhakrishnan A.K., van Lier, J.B., Clemens, F.H.L.R. (2018). A Wall Boundary Condition for the Simulation of a Turbulent Non-Newtonian Domestic Slurry in Pipe. *Water*, 10(2), 124.

Mehta, D., Thota Radhakrishnan, A.K., van Lier, J.B., Clemens, F.H.L.R. (2018). Numerical and CFD-based modelling of concentrated domestic slurry in turbulent flow through circular pipes. Presented at the *11th Urban Drainage Modelling Conference*, Palermo, Italy, 23 - 26 September 2018.

Mehta, D., Thota Radhakrishnan, A.K., van Lier, J.B., Clemens, F.H.L.R. (2017). Concentrated domestic slurry in pipes: a computational analysis. Presented at the *14th International Conference on Urban Drainage*, Prague, Czech Republic, 10 - 15 September 2017.

CHAPTER 6

Modelling Non-Newtonian Flow

Implementing new sanitation systems effects in the concentrating of the domestic slurries waste stream. Transportation of these slurries require design guidelines that enable them to be conveyed from the point of origin to a suitable treatment location. An important parameter in the design of a waste water transport system for concentrated domestic slurry, is the drop in pressure due to the frictional losses incurred by the slurry transport. This makes the knowledge of the pressure drop and the relationship it bears with the slurry's rheology, volume flow rate, temperature etc., a prerequisite for design. Concentrated domestic slurries in general are non-Newtonian in nature. This implies that general non-Newtonian fluid flow characteristics are also applicable to CDS. This enables the use of a non-Newtonian model slurry in lieu of CDS to understand its flow characteristics. An experimental set-up is built to study the flow characteristics of non-Newtonian fluids, with a clay slurry used as a model slurry. The details of this is found in Chapter 4

Experiments provide ample information about the flow characteristics of non-Newtonian fluids. These flow characteristics include the pressure losses incurred. That being said, it is also important to numerically extended the results and conclusions from the experiments to cover a range of rheological parameters and flow conditions. These numerical extensions are in effect a simple relation between the pressure loss incurred during flow and the rheological parameters, flow conditions and dimensions of the pipe. This relation would enable the design of the pipe transport system.

This chapter concerns the numerical analyses on the flow of non-Newtonian slurries through circular pipes, in a turbulent regime. It discusses various semi-empirical relations and their possible extensions, to quantify the frictional losses incurred by a slurry under turbulent flow conditions, from basic information on the slurry's rheology and flow velocity along with their capabilities and limitations.

On the other hand, with the constant increase in computational capacity and power Computational fluid dynamics (CFD) have been frequently used to extend the flow mea-

surements, to avoid repetitive and costly experimentation. CFD is also used in this study to study its capability of predicting the flow characteristics.

The outline of this chapter is as follows. Firstly, a brief overview of the flow of non-Newtonian fluid is discussed. Then, a summary of existing semi-empirical models and their extension to include the non-Newtonian behaviour under study is given. Finally, the chosen models are used to quantify the wall shear-stress incurred by the slurry under experimental conditions and the results are reported with an error analysis to assess which model functions most consistently and accurately.

6.1 Non-Newtonian fluids

For a Newtonian fluid, the shear-stress is directly proportional to the strain-rate, where the constant of proportionality depends only on the temperature and pressure. This relation mathematically reads,

$$\boldsymbol{\tau} = \mu\boldsymbol{\gamma} \tag{6.1}$$

where μ is the molecular viscosity that depends on the temperature and pressure, $\boldsymbol{\tau}$ is the stress tensor and $\boldsymbol{\gamma}$ is the strain-rate tensor defined as,

$$\boldsymbol{\gamma} = \Delta\vec{u} + \Delta\vec{u}^T \tag{6.2}$$

where $\vec{v}$ is the velocity vector and $\Delta\vec{u}$ its gradient tensor. A non-Newtonian fluid on the other hand, follows a relationship that reads,

$$\boldsymbol{\tau} = \eta(|\boldsymbol{\gamma}|)\boldsymbol{\gamma} \tag{6.3}$$

wherein the function $\eta(|\boldsymbol{\gamma}|)$ is not related to $\boldsymbol{\gamma}$ but its second invariant $|\boldsymbol{\gamma}|$, called the shear-rate $\dot{\gamma}$. One can obtain the shear-rate from the strain-rate tensor using,

$$\dot{\boldsymbol{\gamma}} = \sqrt{trace(\boldsymbol{\gamma}^T\boldsymbol{\gamma})} \tag{6.4}$$

In eq. 6.3, η is the apparent viscosity that unlike the molecular viscosity, depends not only on the fluid's temperature and pressure but also the flow conditions such as the shear rate and even the duration of the shear (Chhabra and Richardson, 2011).

Herschel and Bulkley (1926) report the behaviour of certain non-Newtonian fluids that show two irregular properties. Firstly, these fluids require a minimum stress called the yield stress, to flow at all. Secondly, once the yield stress is exceeded causing the fluid to flow, the apparent viscosity of the fluid reduces with increasing shear rate; a property now called pseudoplasticity or shear-thinning. Owing to the mentioned properties, the fluids studied by Herschel and Bulkley (1926) are now known as Herschel-Bulkley (HB) or yield pseudoplastic fluids. Eq. 6.3, in the case of an HB fluid reads,

$$\tau = \tau_y + K\dot{\gamma}^n \tag{6.5}$$

where τ_y is the yield stress, K is the consistency index and n is the behaviour index. Further details on these parameters can be found in Chapter 2 and 3. It is important to note that the shear-stress and shear-rate terms in eq. 6.5 are scalars and given that a HB fluid only flows once the yield stress is exceeded, the equation is only valid given the condition $|\tau| = \tau \geq \tau_y$; else if $\tau < \tau_y, \dot{\gamma} = 0$. Eq. 6.5 can also be expressed in three dimensions in full tensorial notation as 6.6,

$$\boldsymbol{\tau} = (\frac{\tau_y}{|\boldsymbol{\gamma}|} + K(\boldsymbol{\gamma}^{n-1}))\boldsymbol{\gamma} \tag{6.6}$$

Under laminar condition the flow of non-Newtonian fluids in closed pipes can be describes using Figure 6.1. Figure 6.1 considers a longitudinal section of a circular pipe with its wall shown as the thick black lines. The pipe has a radius R and a diameter D. Taking the flow to be from the left to right along the axis marked as z, consider a cylinder of radius $r < R$ of length L that is coaxial to the pipe and inside it; its longitudinal section is shown with dotted line.

The pressure drop across this imaginary cylinder is Δp. This pressure drop is the result of the shear-stress acting along the curved surface of the cylinder against the direction of the flow, indicated in Figure 6.1 as τ_{rz} 6.7.

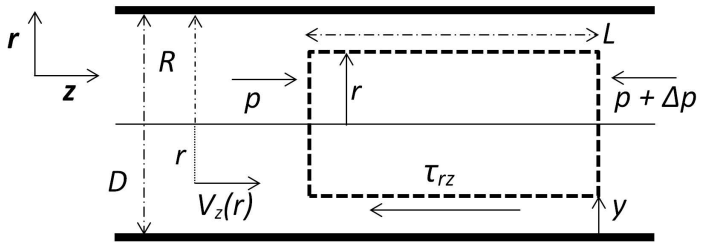

Figure 6.1: A schematic of the longitudinal section of circular horizontal pipe (Chhabra and Richardson, 2011).

$$\tau_{rz} = (\frac{\Delta p}{L})(\frac{r}{2}) \tag{6.7}$$

Further using eq. 6.7 one can obtain the shear-stress at the wall:τ_w by replacing r with R. An important quantity that determines the shear stress is the flow velocity V that is defined as,

$$V = \frac{Q}{\pi R^2} \tag{6.8}$$

where Q is the volumetric flow rate that can be obtained by integrating the radial distribution of the axial velocity or $v(r)$ across incremental annuli of radius r and thickness dr as,

$$Q = \int_0^R 2\pi r v(r) dr \tag{6.9}$$

For a laminar flow of an HB fluid, eq. 6.5, 6.7 and 6.9 provide an implicit relation between $v(r)$ and τ_w (Skelland, 1967).

$$v(r) = \frac{nR}{n+1}(\frac{\tau_w}{K})^{\frac{1}{n}}\{(1-\zeta)^{\frac{n+1}{n}} - (\frac{r}{R} - \zeta)^{\frac{n+1}{n}}\} \tag{6.10}$$

where $\zeta = \tau_y/\tau_w$. Using eq. 6.10, the wall shear-stress is calculated for a set of rheological parameters, flow velocity and pipe diameter. However, this cannot be done for turbulent flows. Over the year, various semi-empirical methods have been proposed that enable the quantification of wall shear-stress for non-Newtonian fluids of various types, in turbulent flows. The next section will discuss some of these methods, which are relevant or could be modified to be relevant for the analyses of HB fluids.

6.2 Semi-empirical models

Heywood and Cheng (1984) and Assefa and Kaushal (2015) provide a review of various semi-empirical pipe flow models for both laminar and turbulent regimes of various non-Newtonian fluids. This article considers the models proposed by (TOMITA, 1959), (Dodge and Metzner, 1959) (DM), (Torrance, 1963), (Wilson and Thomas, 1985; Thomas and Wilson, 1987) (WT) and (Slatter, 1995). Of these models only WT, Torrance and Slatter included the yield stress in their formulations. Tomita and DM derived their models for power-law fluids (Table 2.2), which do not possess a yield stress but have a behaviour index that is not unity. This section provides a description of these models and discusses their accuracy in terms of quantifying the wall shear stress. For brevity, references will not be repeatedly quoted. More details on the topics discussed here are well-summarised in Skelland (1967).

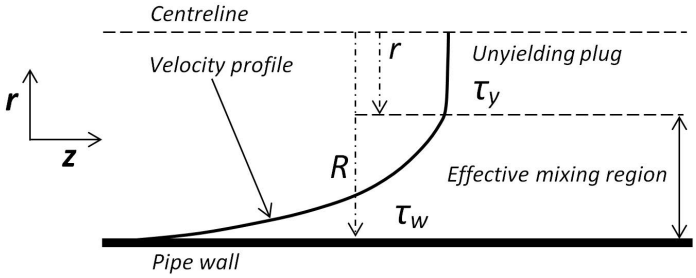

Figure 6.2: The velocity profile of a fluid with a non-zero yield stress inside a circular pipe (Mehta et al., 2018).

Before proceeding with the description of the models, it is imperative to have an understanding of the flow of fluids with a non-zero yield stress (BP or HB fluids) in circular pipes.

Figure 6.2 depicts a possible velocity profile of fluid with a non-zero yield stress. As per eq. 6.7, at the centreline where r = 0, the shear stress is also 0. Further, eq. 6.7 dictates that the shear-stress is directly proportional to the radial distance from the centreline. Therefore, the shear-stress reduces from its maximum value at the wall to zero at the centreline. In doing so, there would exist a region near the centreline, within which the shear-stress would be less than the yield stress of the fluid. As a result, an unyielding region is formed near the centreline and the fluid within this region is transported as a **plug**.

The radial distance at which the plug is formed r_p , can be obtained by setting τ_{rz} as τ_y at $r = r_p$ and τ_{rz} as τ_w at $r = R$, which results in,

$$\zeta = \frac{\tau_y}{\tau_w} = \frac{r_p}{R} \tag{6.11}$$

6.2.1 Tomita

Tomita derived two models, one for power-law fluids and the second for Bingham plastic fluids, which have a behaviour index n = 1 but possess a non-zero yield stress. The approach begins by relating the average flow velocity to the rheological parameters in laminar flow condition. Following this, by representing the pressure gradient as a sum of laminar and turbulent contributions, which is subsequently solved to provide a relation between the

pressure drop and velocity profile. In general, the wall shear-rate is used to determine the wall shear-stress which relates to the pressure drop for a flow of fluid. The details of the derivation of Tomita's flow model for BP and PL fluids are presented in Appendix C.1. Following the same procedure and assumptions a relation for the fanning friction factor for HB fluid is derived. The derivation for which is also provided in Appendix C.1. The resulting relation eq. 6.12 will be used in this study (hereafter referred to as TO-HB).

$$\frac{1}{\sqrt{f_{HB}}} = (A - \frac{(1-\zeta)(\zeta+3)}{2\kappa})\sqrt{\frac{H(\zeta,n)(1-\zeta)}{2}} + B\sqrt{\frac{H(\zeta,n)(1-\zeta)}{2}} ln(Re_{HB}\sqrt{f_{HB}}) \tag{6.12}$$

6.2.2 Dodge & Metzner

Dodge and Metzner (1959) (DM) proposed a semi-empirical relationship between the wall shear-stress and the average flow velocity for PL fluids based on extensive dimensional analysis supported by experiments to determine the relevant constants. Their aim was to relate the Fanning friction factor defined by eq. C.7 to the generalised Reynolds number proposed by Metzner and Reed (1955).

Chilton and Stainsby (1998) (CS) extended a part of the analysis by Metzner and Reed (1955) on the generalised Reynolds number (originally meant for laminar flows) and proposed a relevant Reynolds number of turbulent HB fluids. Using experimental data, CS established that the proposed Reynolds number is physically more representative of transitional and turbulent behaviour than the generalised Reynolds number by Metzner and Reed (1955).

The approach put forth by DM is extended to HB fluid, by incorporating a suitable Reynolds number. The details of the approach, assumptions and the derivation is presented in Appendix C.2. The resulting eq. 6.13 from this extension will be considered in this study and shall be referred to as DM-HB.

$$\frac{1}{\sqrt{f_{HB}}} = \frac{4}{(n')^{0.75}}\sqrt{1-\zeta} log(N_{Re-Gen_{HB}} f_{HB}^{1-\frac{n'}{2}}) - \frac{0.4}{(n')^{1.2}}\sqrt{1-\zeta} \tag{6.13}$$

Further, CS suggested a similar equation based on eq. C.65 as

$$\frac{1}{\sqrt{f_{HB}}} = 4log(Re_{CS}\frac{1}{n^2}\frac{1}{(1-\zeta)^4}\sqrt{f_{HB}}) - 0.4 \tag{6.14}$$

which shall be called CS-HB from hereafter and will also be used in this study.

6.2.3 Torrance

As one of the older-known expressions for HB fluids, Torrance (1963) proposed

$$\frac{1}{\sqrt{f_{HB}}} = (0.45 - \frac{2.75}{n}) + \frac{1.97}{n} ln(1-\zeta) + \frac{1.97}{n} ln(Re_{Bi}(\frac{3n+1}{4n})^n f_{HB}^{1-\frac{n}{2}}) \tag{6.15}$$

where f_{HB} is the Fanning friction factor defined using eq. C.7 and the Reynolds number Re_{Bi} is the generalised Reynolds number for a PL fluid used by Bird (Bird et al., 1983, 1987) (can be derived from N_{Re-Gen} proposed earlier by Metzner and Reed (1955)),

$$Re_{Bi} = \frac{1}{8^{n-1}} \frac{D^n V^{2-n} \rho}{K} (\frac{4n}{3n+1})^n \tag{6.16}$$

It is immediately noticeable that although Torrance's equation includes the contribution of the yield stress that separates an HB fluid from a PL fluid, the Reynolds number used in the equation does not encompass the yield stress. However, it is likely that eq. 6.15 could still provide accurate results at high Reynolds numbers at which, the effect of the yield stress would perhaps be negligible.

6.2.4 Wilson and Thomas

Wilson and Thomas (Wilson and Thomas, 1985; Thomas and Wilson, 1987) proposed the following relationship between the wall shear stress arising from an HB fluid and its flow conditions.

$$\frac{V}{v_\tau} = 2.5ln(\frac{\rho D v_\tau}{\eta_w}) + 2.5(\frac{(1-\zeta)}{(1+n\zeta)} \frac{(1+n)}{2}) + \frac{(1+n\zeta)}{(1+n)} + (1.25\zeta^2 + 2.5\zeta - 11.6) \tag{6.17}$$

where v_τ is the friction velocity defined as,

$$v_\tau = \sqrt{\frac{\tau_w}{\rho}} \tag{6.18}$$

WT derived eq. 6.17 by relating the thickness of the viscous sublayer that represents the dissipation of energy due to friction, with the ratio of the area under the rheogram of an HB fluid to that of a Newtonian fluid for the same shear-rate and the wall shear-stress.

6.2.5 Slatter

Slatter (1995) carried out a comprehensive series of experiments with a wide range of HB fluids. First, the Reynolds number to determine the transition for HB fluids was modified to,

$$Re_S = \frac{8\rho V_{ann}^2}{\tau_y + K(\frac{8V_{ann}}{D_{ann}})^n} \tag{6.19}$$

The denominator of the right-hand side of eq. 6.19 is similar to the constitutive relation for an HB fluid i.e. eq. 6.5 but with the shear-rate defined in terms of V_{ann} and D_{ann} which are,

$$V_{ann} = \frac{Q - Q_p}{\pi(R^2 - r_p^2)} \tag{6.20}$$

$$D_{ann} = 2(R - r_p) \tag{6.21}$$

Q_p is the volume flow rate through the plug, which can be obtained using eq. C.32 in the case of an HB fluid. The above expressions were further modified to account for the particle roughness within the HB fluids under consideration by Slatter. This roughness was related to the representative size of the particles d_{85}. The d_{85} is the particle diameter at which 85% of the slurry's sample mass is comprised on particles smaller in size than d_{85}. For details on the procedure used to determine the representative size, the readers are referred to Slatter (1995). A different Reynolds number was defined to account for the particle roughness effect as

$$Re_R = \frac{8\rho v_\tau^2}{\tau_y + K(\frac{8v_\tau}{d_{85}})^n} \tag{6.22}$$

such that $Re_R < 3.32$ pertains to a smooth pipe flow (fully-developed turbulent) for which the following relationship holds,

$$\frac{V}{v_\tau} = 2.5ln(\frac{R}{d_{85}}) + 2.5ln(Re_R) + 1.75 \tag{6.23}$$

On the other hand, for a rough pipe flow i.e. $Re_R \geq 3.32$,

$$\frac{V}{v_\tau} = 2.5ln(\frac{R}{d_{85}}) + 4.75 \tag{6.24}$$

The use of either eq. 6.23 or eq. 6.24, requires information on the wall shear stress to calculate v_τ and therefore, must be solved implicitly. Thus, both of them are used to estimate the wall shear stress for the experimental test cases considered in this article.

6.3 Computational Fluid Dynamics

With the development of computational resources, analyses of many industrial flows are being increasingly made as numerical computations of the NavierStokes (NS) equations. In contrast to the approaches mentioned in Section 6.2, a Computational Fluid Dynamics (CFD) based approach involves solving the modified Navier-Stokes (NS) equations (Eq. 6.25).

$$\begin{aligned} \frac{\partial \overline{v_i}}{\partial x_i} &= 0 \\ \rho\overline{v_j}\frac{\partial \overline{v_i}}{\partial x_j} &= -\frac{\partial \overline{p}}{\partial x_j} + \frac{\partial}{\partial x_j}(\overline{\eta\dot{\gamma}_{ij}} - \rho\overline{v_i'v_j'} + \overline{\eta'\dot{\gamma}'_{ij}}) \end{aligned} \tag{6.25}$$

Turbulent flows display a range of length and time scales; resolving all of these is not feasible at high Reynolds numbers (Ferziger and Peric, 2012). Therefore, these scales are mathematically altered (a process called decomposition) to reduce the range of length and time scales to a manageable quantity while ensuring that the decomposed scales represent the macroscopic properties of the flow under consideration. In the current context, the terms modified in the NS equation refers to a process through which the NS equations could me made tractable by solving for only the most relevant turbulent features in a flow. One such modification known as Reynolds averaging, provides an insight into the flow's features averaged over a number of instances of the flow using what are better known as the Reynolds-Averaged Navier-Stokes (RANS) equations. The solution to eq. 6.25 requires a closure for $-rho\overline{v_i'v_j'}$ (Reynolds stress). RANS methods model Reynolds stresses in terms of the known velocity field (the ensemble-averaged v in this case) to close eq. 6.25. Wilcox (1998) presents a detailed description of RANS models, of which the $k-\epsilon$ (Launder and Spalding, 1983) and the Reynolds stress model (RSM; see Launder et al. (1975) and references therein) is used in this article.

For the flow of any fluid, as the flow increases, the effects of viscosity diminishes (Pope and Pope, 2000). In the presence of walls, which is the case in this study which concerns a wall bounded flow, all flows slow down to zero velocity at the wall (the no-slip condition). In doing so, even a turbulent flow passes through a laminar region near the wall (Schlichting,

1960). Therefore, RANS models that are meant for the analysis of fully turbulent flows require a correction to model the transition into a laminar regime and ultimately zero velocity. Such empirical corrections have permitted the use of RANS models for a range of industrial applications.

Mehta et al. (2018) proposed a wall boundary condition that could be used in combination with the RANS equations to estimate the wall shear-stress in a circular pipe carrying an HB fluid in a turbulent flow. The derivation of this condition followed a similar approach put forth by Launder and Spalding (1983) and using the theory of Prandtl (1925, 1933) to obtain a relation between the wall shear-stress and the velocity near the wall for a Herschel-Bulkley fluid. The result of which was eq. 6.26 where it was assumed that τ_y did not affect the assumption that laminar stresses are much lower than the turbulent stresses in the core turbulent region. Implying that τ_y is much lower compared to τ_w.

$$\frac{v}{(\frac{\tau_w-\tau_y}{\rho})^{\frac{1}{2}}} = \underbrace{\frac{1}{n\kappa} ln(y^n \frac{\rho}{K} \varepsilon (\frac{\tau_w-\tau_y}{\rho})^{\frac{2-n}{n}})}_{\psi_1} \tag{6.26}$$

Further, if τ_y would be compared to τ_w, implying the existence of a region that does not yield but flows as a plug at the centre of the pipe. In turbulent flow, this plug is not as smooth as is shown in Figure 6.2 for a laminar flow. Upon considering this unyielding plug, eq. 6.27 is obtained following a similar procedure as eq. 6.26. Details on the derivation of the wall function could be found in Mehta et al. (2018)

$$\frac{v}{(\frac{\tau_w-\tau_y}{\rho})^{\frac{1}{2}}} = \underbrace{(\frac{1}{1-\zeta}) \frac{1}{n\kappa} ln(y^n \frac{\rho}{K} \varepsilon (\frac{\tau_w-\tau_y}{\rho})^{\frac{2-n}{n}})}_{\psi_1} \tag{6.27}$$

It was found that the proposed specified shear boundary condition (ψ_1), the RSM is observed to deliver more accurate results with fluids that have a smaller behaviour index or $n \lessapprox 0.6$, alluding to a stronger non-linear behaviour. On the other hand, $k\epsilon$ seems to work better with fluids that have a value of $n > 0.8$. Further, modifying the wall boundary condition (ψ_2) to account for the influence of a fluid's yield stress (τ_y) when it is comparable in magnitude to the wall shear-stress (τ_w), both RSM and $k\epsilon$ are observed to be accurate when used with ψ_2, depending on the value of n. It is fair to mention that the accuracy of these numerical methods depends to a great extent on the rheological input. Therefore, in line with these findings, appropriate choices are made according to the slurry in study to model its turbulent pipe flow using CFD.

Details of the solver, numerics and mesh for performing the CFD are provided in Appendix D. Details for which can be found in the work of Mehta et al. (2018, 2019). Results will be presented here for comparison with experimental data and the semi-empirical models.

6.4 Comparing Experiments, CFD and Semi-Empirical models

The measurements obtained from the pressure loss experiments mentioned in Chapter 4 for the clay slurries as non-Newtonian slurries are analysed here. These measurements are compared with the results obtained from the semi-empirical models described in Section 6.2

and CFD in Section 6.3. Table 6.1 lists the abbreviations used for the various models and methods considered here.

Table 6.1: Abbreviations for various models and methods used for the comparison

Method or Model	Abbreviation	Remarks
Tomita Power Law	TO-PL	Eq. C.29
Tomita Herschel-Bulkley	TO-HB	Eq. 6.12
Dodge & Metzner Power Law	DM-PL	Eq. C.48 with $\tau_y = 0$
Dodge & Metzner Herschel-Bulkley	DM-HB	Eq. 6.13
Chilton & Stainsby Herschel-Bulkley	CS-HB	Eq. 6.14
Torrance	TR	Eq. 6.15
Wilson & Thomas	WT	Eq. 6.17
Slatter smooth	SS	Eq. 6.23
Slatter rough	SR	Eq. 6.24
CFD - RANS	CFD	Using $k-\epsilon$ and RMS with ψ_1 and ψ_2
Experimental data	EX	Pressure loss experiments from Section 4.2, for slurries S1, S2, S3, S4, S5

The results are presented as plots of the wall shear-stress τ_w (Pa) against the pseudo-shear rate $8V/D$ in s^{-1}. While interpreting the results obtained with RANS (CFD), it is important to bear in mind the limitations of the numerical methods involved. These are illustrated in Mehta et al. (2019) as a sensitivity analysis of the wall boundary conditions proposed in Mehta et al. (2018).

For conciseness, only the results for S3, S4 and S5 are discussed here using Figures 6.3, 6.4 and 6.5. These cases are chosen as they rightly represent the different non-Newtonian rheological types.

Analysis of the plots in Figures 6.3, 6.4 and 6.5 show that CFD provides accurate results in all cases, deviating less than 15 % at high pseudo-shear rates. For the model by Tomita, TO-PL and its proposed extension to HB fluids, TO-HB, only deliver accurate results for S3 (also for S1 and S2 but not shown here). These two cases concern no yield stress, making them PL fluids. However, in the other cases, both TO-PL and TO-HB provide similar results with nearly overlapping plots. Using the approach of Dodge % Metzner, DM-PL and its proposed extension to HB fluids, DM-HB, show a behaviour similar to Tomita, with the PL and HB solutions overlapping each other. The CS-HB approach deviates from experimental data as the pseudo shear rate increases. All the other remaining approaches namely TR, WT, SS and SR produce similar results at low shear rates but tend to deviate from each other as the shear increases (increasing flow velocity).

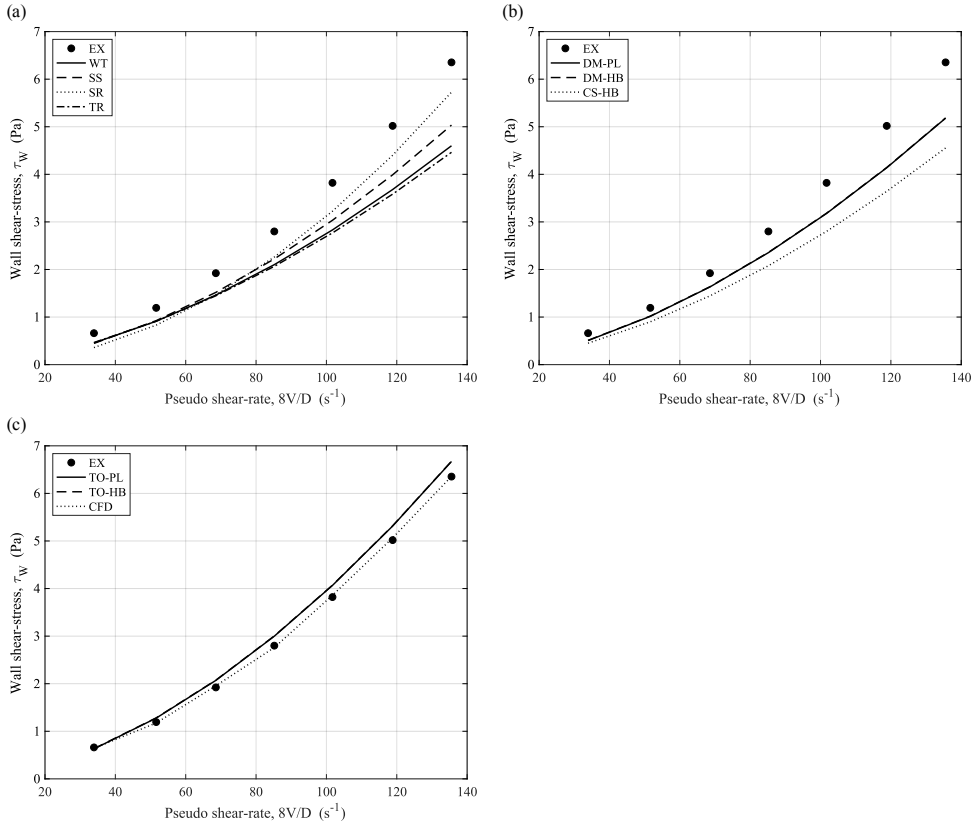

Figure 6.3: Plot of wall shear-stress against pseudo shear-rate calculated for the different models for slurry S3.

The similarity between the PL and HB approaches of the TO and DM models could be attributed to the interesting hypothesis presented in the original article by Dodge and Metzner (1959). Dodge & Metzner explained that their PL model was applicable to non-power law fluids such as HB fluids too. They proved mathematically that the resulting mean velocity in the pipe is dependent mostly on the shear-rates occurring a radial distances $r/R > 0.8$ or the shear occurring in the immediate vicinity of the wall. The region away from the pipe's wall and towards the centerline, where the effect of the yield stress for HB fluids is apparent due to the reducing shear stress, in fact, contribute to less than 7% of the mean flow that results. This in turn implies that accounting for the yield stress as an extra parameters for HB fluids as part of the DM approach, may not add any value to the DM model. By extension, the same applies to the HB extension of Tomita's PL model, in which, the incorporation of the yield stress does not alter the estimates of the wall shear stress. The results presented in Figures 6.3, 6.4 and 6.5 can serve as a proof of the idea put forth by DM.

Finally, the concerns for the other models, their accuracy cannot be assessed easily as the trends in the estimates they provide are not consistent across the test cases discussed here. Thus, to gain more insight into the accuracy of all the models considered in this study, an

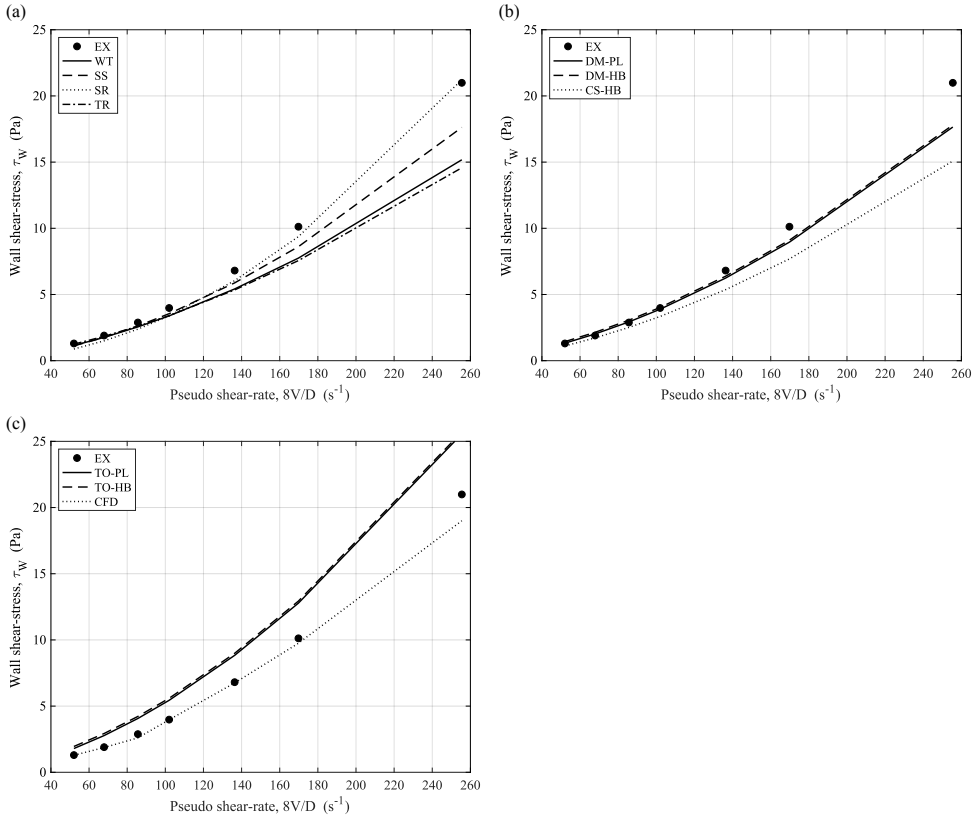

Figure 6.4: Plot of wall shear-stress against pseudo shear-rate calculated for the different models for slurry S4.

error analysis is used which provides the predictability of model's capability for estimating the pressure losses.

6.5 Predictability

To provide a more meaningful insight into the usability of the various numerical models, it is essential to have knowledge of their predictability. In this study, various models were used to estimate the wall shear-stress for certain experimental condition of flow velocity, rheology and the resulting gradient for a range of non-Newtonian fluids. However, the uncertainty in the experimental determination of the flow parameters itself was not taken into account. Further, the trends in the accuracy of the estimates with the various models cannot be assessed qualitatively using the results discussed in the previous section. Therefore, as an alternative, one could calculate the predictability with which, a model can estimate the wall shear-stress for a set of experimental conditions, themselves determined with a fixed uncertainty.

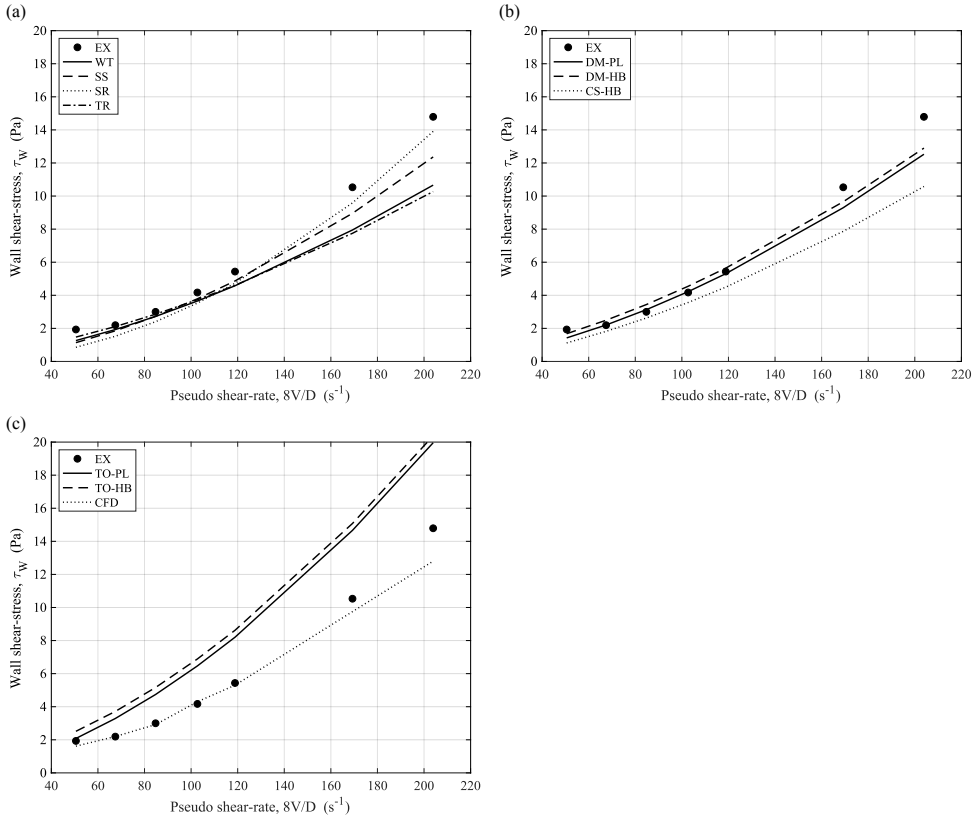

Figure 6.5: Plot of wall shear-stress against pseudo shear-rate calculated for the different models for slurry S5.

This is done using the amount of overlap area of the probability distribution curves used to represent both the experimentally determined wall shear-stress (Section 4.1.5) and the ones estimated through the numerical models (using the uncertainties of the parameters). This by no means provides definitive estimation of the predictability of the numerical model, but only serves as a tool to compare the different numerical models in this study. Using this approach the predictabilities are obtained as listed in Table 6.2.

Although the predictability is best with CFD, the overall values of the all the numerical methods discussed in this article are in fact, very low, with 0.27 being the maximum. It is interesting to note that the Dodge & Metzner approach based on dimensional analysis is nearly as accurate as CFD. Further, Slatter's approach despite being calibrated for a dataset which is not included in this error analysis, is as accurate as Dodge & Metzner's approach. All the other semi-empirical models demonstrate little accuracy in their estimates. The lowest accuracy is that of the Tomita model, which in fact is based on the treatment of turbulent non-Newtonian flows as though they were mathematically satisfying laminar flow conditions (Skelland, 1967).

Table 6.2: Predictabilities with various models and methods

Method or Model	Predictability	Predictability with velocity envelope ($v > 1.5m/s$)
CFD	0.27	0.61
Dodge & Metzner	0.22	0.27
Slatter	0.22	0.27
Torrance	0.14	0.19
Wilson & Thomas	0.13	0.18
Tomita	0.07	0.11

Despite the above results, it is fair to mention that the CFD approach proposed in Mehta et al. (2018), works accurately only within a well-defined envelope that is described in Mehta et al. (2019). This operational envelope is bound by highly turbulent flows and hence, high flow velocities (more than 1.5 m/s or $8V/D$ more than 200); and a value of yield stress that must be comparable with the wall shear-stress. Accounting for these nuances and implementing the operational envelope to the analysis, the predictability with in the velocity envelope is mentioned in Table 6.2. Upon restricting the velocity range of the data set taken into account, all the models show improved predictability. However, CFD in particular, shows a two-fold improvement.

6.6 Discussion

It is important to note that the models considered here do not fully represent the physical phenomena concerning the turbulent flow of a non-Newtonian fluid. Being semi-empirical in nature, the models based on simplification of the turbulent flow such as Tomita's model that uses the laminar velocity profile to determine the extent of the plug region, tend not to be very accurate. Nonetheless, it is interesting to note that the extension of Tomita's PL model to HB fluids following the incorporation of the yield stress, does not alter the estimates. This solely is attributed to the shear-stress near the wall has a greater contribution to the velocity profile which is dominated by the fluid behaviour indices rather than the yield stress, as rightly hypothesised by Dodge and Metzner (1959).

On the other hand, the Wilson and Thomas model based on the fundamentals of turbulence and boundary layer thickness, is more accurate than Tomita's model for the cases considered in this article. Slatter's model that was calibrated for a set of experiments not included in error analysis, has an accuracy that is comparable with CFD.

CFD itself shows enhanced accuracy within the operational envelope determined using a strict sensitivity analysis (Mehta et al., 2019). However, it is fair to mention that the CFD approach mostly enforces a relation that the wall shear-stress must bear with the velocity field near the wall, to satisfy the universal law of the wall modified to account for the viscosity of a non-Newtonian fluid. An experimental campaign that could support this relationship is still lacking, although the method itself has been validated for a wide range of test-cases concerning HB fluids, available in literature (Mehta et al., 2018). Perhaps one reason why the CFD approach works well is that it complied with Dodge & Metzner's idea that a more fundamental treatment of the shear-stress near the wall region is central to a

better estimation of the flow that results.

6.7 Conclusions and Outlook

Based on the results outlined in this article, it is concluded that despite a number of approaches proposed so far, the numerical estimation of wall shear-stress for turbulent flow of non-Newtonian fluids in circular pipes still remains a challenge. Semi-empirical models are often based on the over-simplification of the physical aspects of non-Newtonian turbulent flows. Further, the use of a restricted set of experiments for the determination of any empirical parameters, does hinder the ability of such models to be versatile. In this regards, extending Slatter's model to experiments beyond the ones considered in its formulation, could perhaps make the model more robust and accurate, and hence, worth investigating.

Although CFD holds promise in terms of its capacity to estimate frictional losses, it requires further development in terms of incorporating the fundamentals of non-Newtonian turbulence, which themselves require thorough experimental investigation, given the lack of literature on the subject.

Part III

Implementation and Outlook

Chapter 7 is based on:

Thota Radhakrishnan, A.K., Langeveld, J., van Lier, J.B., Clemens, F.H.L.R. (2018). Challenge of Transport: Exploring the Limit of Gravity Sewers to Transport Concentrated Domestic Slurries. Presented at the *11th Urban Drainage Modelling Conference*, Palermo, Italy, 23 - 26 September 2018.

Thota Radhakrishnan, A.K., van Lier, J.B., Clemens, F.H.L.R. (2017). Effect of temperature on the transport of concentrated domestic slurry. Presented at the *4th Water Research Conference*, Waterloo, Canada, 10 - 13 September 2017.

CHAPTER 7

Outlook & Perspectives

In chapters 4 - 6 the models used for design of the transport system for CDS was described. The models, although verified, were developed in a controlled environment, whereas in reality (systems in practise) only a few parameters can be controlled, leaving a disordered system. This disorder emanates from many factors such as intermittent flows, settling of the suspended particles, inclusion of a gases phase in the flow and flow through bends (upward or downward). Therefore in reality, the practitioner is faced with different practical problems for the design. To put the theoretical framework in perspective to its usage, the following discussions are made.

7.1 Theoretical framework

A brief outline of the design equations from the theoretical framework that follow the discussion later are presented here. These are gathered from the conclusions of the previous chapters.

The information of the rheology from Chapters 2 and 3 are summarised here. Along with it, the 1-D models that have been validated to predict the pressure losses and transition to turbulence is also presented. It must be noted that these systems operate under pressure for a completely closed conduit (pipe) to convey CDS.

7.1.1 Rheology

The rheology of the concentrated domestic slurry (CDS) is represented using a Herschel-Bulkley rheological model as,

$$\tau = \tau_y + K\dot{\gamma}^n \tag{7.1}$$

where the parameters τ_y, K and n depend on the TSS concentration (C, % wt./wt.) and temperature of the slurry. The equations of the parameters as a function of concentration is given as,

$$\tau_y = \begin{cases} 0.71(C-2.0)^{1.7} & \text{for } C > 2.0 \\ 0 & \text{for } C < 2.0 \end{cases} \tag{7.2}$$

$$K = 0.07\epsilon^{0.5C} \tag{7.3}$$

$$n = \begin{cases} 0.65 - 0.09\ ln(C-2.57) & \text{for } C > 2.6 \\ 1 & \text{for } C < 2.6 \end{cases} \tag{7.4}$$

The yield stress described in equation 7.2 has a boundary condition where the value of τ_y is only physically meaningful above a TSS concentration of 2.0 % (wt./wt.). Similarly, the behaviour index n as given in equation 7.4 is influenced by changes in the TSS concentration above 2.6 % (wt./wt.). The consistency index K approaches to the viscosity of water as TSS concentration approaches zero.

Using the above equations, the expression representing the rheology of CDS can be obtained. It should be noted that the above equations provide the rheology of CDS at 20 $°C$. To obtain the rheology (or apparent viscosity) at a different temperature, the following equation is used:

$$\frac{\mu_{app,T_1}}{\mu_{app,T_2}} = \epsilon^{E(\frac{1}{T_1}-\frac{1}{T_2})}, \qquad E = 7.5°C \tag{7.5}$$

The density of the slurry is based on the expression presented in equation 7.6. This expression depends on the density of CDS without water (dry) ($\rho_{CDS_{dr}}$) which is between 1090 - 1100 kg/m^3.

$$\rho = \frac{1}{\frac{1-0.01C}{\rho_{water}} + \frac{0.01C}{\rho_{CDS_{dry}}}} \tag{7.6}$$

7.1.2 Pressure Loss

The energy losses in the transport of CDS that are mainly studied here are the pressure losses incurred due to the friction against the wall. These energy losses differ depending on the flow regime as laminar or turbulent flow.

Laminar flow

The Navier-Stokes equation provides a starting point for the derivation of the laminar flow equation. Following a similar procedure as used to derive the Hagen-Poiseuille equation for Newtonian flows, the following solution is derived for non-Newtonian fluids. Using the Herschel-Bulkley rheological model, the following flow equation are obtained (Chilton and Stainsby, 1998):

$$\frac{\Delta P}{L} = \frac{4K}{D}(\frac{8V}{D})^n(\frac{3n+1}{4n})^n(\frac{1}{1-X})(\frac{1}{1-aX-bX^2-cX^3})^n \tag{7.7}$$

where X is given by

$$X = \frac{\tau_y}{\tau_w} = \frac{4L\tau_y}{D\Delta P} \tag{7.8}$$

and the constants a, b, c as

$$a = \frac{1}{(2n+1)}; \qquad b = \frac{2n}{(n+1)(2n+1)}; \qquad c = \frac{2n^2}{(n+1)(2n+1)} \tag{7.9}$$

Turbulent flow

The Slatter (1995) model is used for this. A particle roughness Reynolds number (Equation 7.10) is defined using the d_{85} (representative size of the particles).

$$Re_R = \frac{8\rho v_\tau^2}{\tau_y + K(\frac{8v_\tau}{d_{85}})^n} \tag{7.10}$$

If $Re_R < 3.32$, the flow pertains to a smooth pipe flow (fully-developed turbulent) for which the pressure losses are determined using:

$$\frac{V}{v_\tau} = 2.5ln(\frac{R}{d_{85}}) + 2.5ln(Re_R) + 1.75 \tag{7.11}$$

On the other hand, for a rough pipe flow i.e. $Re_R \geq 3.32$, the pressure losses are determined using:

$$\frac{V}{v_\tau} = 2.5ln(\frac{R}{d_{85}}) + 4.75 \tag{7.12}$$

It should be noted that equations 7.10 and 7.11, requires information on the wall shear stress to calculate $v_\tau = \sqrt{\tau_w/\rho}$ and therefore, must be solved implicitly.

7.1.3 Predicting Transition

The preferred flow regime to transport suspended particle slurries (including CDS) is that of turbulent flow as the eddies provide adequate radial velocity to prevent a sediment bed from forming and adequate momentum mass-transfer to keep the suspended solids well mixed during flow. To identify the velocity at which transition to turbulence occurs, the Slatter (1995) equation is used.

The following equation comprise together in establishing the Slatter Reynolds number. Transition to turbulence is predicted to occur at Re_S above 2100.

$$Re_S = \frac{8\rho V_{ann}^2}{\tau_y + K(8V_{ann}/D_{shear})^n} \tag{7.13}$$

where the annular velocity is calculated using

$$V_{ann} = \frac{Q_{ann}}{A_{ann}} = \frac{Q - Q_{plug}}{\pi(R^2 - R_{plug}^2)} \tag{7.14}$$

and

$$Q_{plug} = A_{plug}\frac{D}{2K^{(1/n)}\tau_w}\frac{n}{n+1}[(\tau_w - \tau_y)^{(n+1)/n}] \tag{7.15}$$

with the radius of the plug given as

$$R_{plug} = \frac{\tau_y}{\tau_w}R \tag{7.16}$$

To solve the equations to determine the value of the Reynolds number, information on the wall shear-stres τ_w is required. Therefore, when solving for turbulent flow, the wall shear-stress is obtained as described in section 7.1.2. Similarly, when solving for laminar flow, the wall shear-stress is obtained as described in section 7.1.2.

7.2 Application & Analysis

It is essential that an analysis of the pressure drop data is done to get an understanding of the implications on the slurry transport systems. On adopting a new sanitation system, domestic slurries are concentrated as discussed in Chapter 1. The dilution and temperature of the resulting slurry vary depending on the extent of source separation and installation of various new sanitation concepts such as food waste disposer and type of vacuum toilets, i.e. amount of water per flush.

As changes in the implementation of the NS concepts affect the dilution of CDS, it also affects the transport pressure losses incurred. A feasible transport system varies with the adopted NS system in the household. Thereby, also giving rise to the possibility of adjusting the dilution to suit the CDS transport system. The final dilution of the slurries can thereby be adjusted by changing various parameters of the new sanitation system, for e.g. vacuum flush water volume and FWDs.

In the following sections, the effect of change in concentration and temperature on the incurred pressure loss is discussed.

7.2.1 Change in Concentration

Using the pilot projects in Sneek, Leeuwarden (Chapters 2 & 3) as a case study, the CDS concentrations from the different slurry streams from NS systems is investigated. Upon examining, the streams from the NS systems implemented with source separation, food waste disposers and vacuum toilets, the average CDS concentrations is approximately 0.9 % TSS (wt./wt.). The concentration of TSS in slurries that arise from vacuum toilets with urine is approximately 1.8 % (wt./wt.). When urine separation is implemented, the slurry concentration is approximately 2.7 % TSS (wt./wt.).

To understand the implication of these different dilutions, the pressure loss data as a function of average flow velocity is gathered for the different slurry concentration. The pressure loss for water is also included for analysis. This is done using the equations discussed in Section 7.1. As a representative case, the pressure losses for slurries with the above mentioned 3 concentrations are obtained for transport using a 200mm[‡] diameter pipe. The results are shown in Figure 7.1, where both the turbulent and laminar regime is plotted for which the transition velocities are indicated. Although these results have been obtained for a particular pipe diameter of 200 mm, the pressure losses can be scaled for different pipe diameters using the Reynolds number as indicated in section 7.1.2. As indicated, there are two transition velocities that are estimated. One using the Slatter's Reynolds number mentioned in Section 7.1.3 and the other using the intersection of the laminar % turbulent flow curves.

Firstly, the pressure loss curve for water is the lowest. But, interestingly the curve that has the highest pressure loss is the one of 1.8 % TSS and not of 2.7 % TSS. In fact, the curve of 2.7 % TSS is lower than that of 0.9 % TSS. This is noted to be due to the lower

[‡]The pipe diameter used in the pilot project in Sneek is 75 mm. But as a case study here the 200 mm pipe diameter is used for the ease of discussion. The effects of using a different pipe diameter for the conveyance could be easily estimated using the Reynolds number in the equations applicable to estimate the pressure drop.

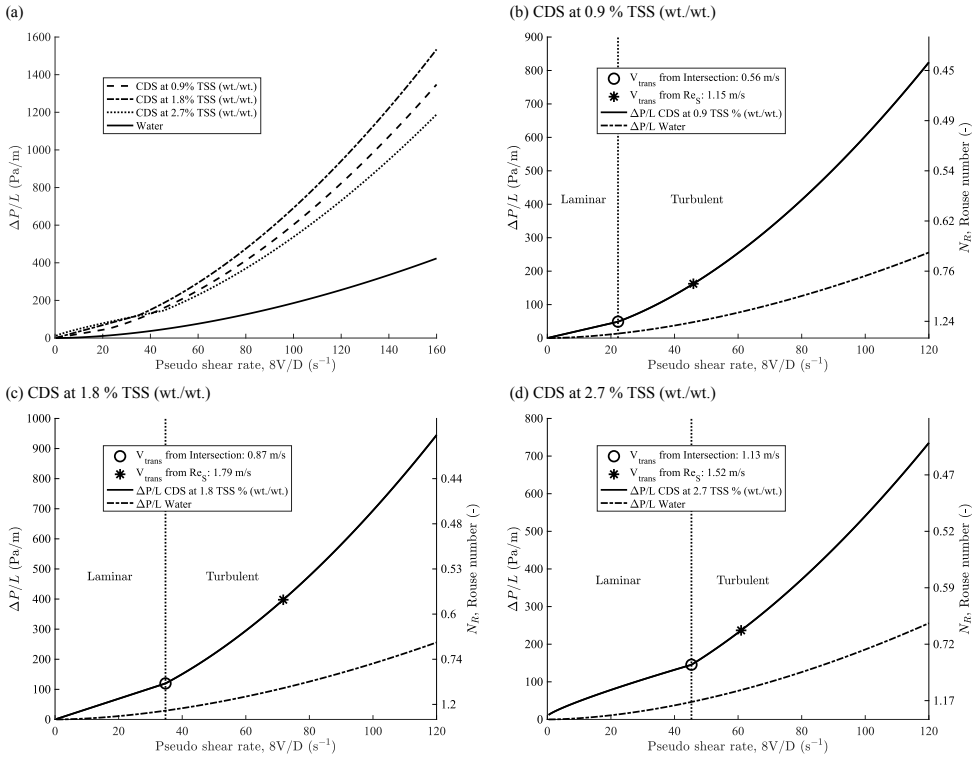

Figure 7.1: (a)Plot of the pressure loss per unit length ($\Delta P/L$) for different concentrations of TSS with both laminar and turbulent flow regimes. (b) Plot of $\Delta P/L$ against average flow velocity for CDS at 0.9 % TSS with the transition velocities V_{trans} from the intersection of laminar and turbulent flow curves indicated. The Rouse number is also indicated on the right axis for the respective flow situations. (c) Plot of $\Delta P/L$ against average flow velocity for CDS at 1.8 % TSS. (d) Plot of $\Delta P/L$ against average flow velocity for CDS at 2.7 % TSS. Note: Pipe diameter for all cases D is 0.2 m.

behaviour index and higher yield-stress present in the slurry with 2.7 % TSS, which provides a drag reduction. With respect to the transition velocities, the V_{trans} estimated using the intersection method and that from Re_S varies largely. As mention in Chapter 5, transition is not a point process but rather a step process. This discrepancy could therefore refer to the different stages of transition or rather the uncertainty in pinpointing transition using the Reynolds number which arguably flawed in its representation for non-Newtonian fluids. However, both the transition velocities are rather high and in practise, transporting these slurries at high velocities is expensive. To understand the consequence of transporting CDS below these velocities, the Rouse number is used.

The Rouse number (N_R) (Rouse, 1937, 1961) is a non-dimensional number used to estimate the concentration profile of sediment or suspended particulate transport (Equation 7.17). The Rouse number N_R is defined as the ratio of the sediment fall velocity w_s and the

upward velocity on the sediment given by the product of the von Karmann constant κ (= 0.40) and the shear velocity u_*. The mode of transport (Mofjeld, 1988) can be estimated using the resulting value of the Rouse number for a given flow as partially suspended flow for $1.2 < N_R < 2.5$, completely suspended for $0.8 < N_R < 1.2$ and wash load for $N_R < 0.8$. Despite the preferred regime being turbulent, constraints hold for practitioners in designing and if a laminar regime is preferred over turbulence the Rouse number must atleast be below 1.2 to avoid sedimentation.

$$N_R = \frac{w_s}{\kappa u_*} \tag{7.17}$$

On further examining the results obtained for the calculation of the Rouse numbers for the flow of slurries in Figure 7.1, it is observed that at flows below the transition threshold (in laminar regime) the Rouse number at certain velocities is below 1.2 and thus could be used for the design of the system. It must be noted that the settling velocities used in these calculations are primitive and only an estimate. To further understand the consequences of the laminar regime, it is preferable that research is carried out to understand the settling nature of these slurries at high concentration and in the context of a non-Newtonian fluid.

With respect to the current practise, designing the transport pipeline for new sanitation systems with design guidelines for water could be unfavourable as it under predicts the pressure loss incurred and the V_{trans} by a very large margin than the least concentrated slurry encountered.

Collection tanks are used as an intermediate in most current design cases (e.g. pilot project in Sneek, Chapter 2) between collection and transport. They accumulate CDS over a period of time before being transported to the local treatment plant. The suspended solids settle over time forming either a gradient of concentration in the tank along its depth or a bed of solids at the bottom. Although, Sedimentation also occurs in the collection pipes due to being operated under intermittent flow, it is not within the scope of this work. In either cases, high and low concentrations of suspended solids are encountered when these collected slurries are later transported. The concentration gradients may occur even if mixing is provided in the collection tanks. In tackling this situation, flow characteristics for a range of CDS concentrations can be used in designing these systems.

7.2.2 Change in Temperature

In Chapter 2, it was established that slurry rheology has a strong correlation with temperature. Its influence therefore must be analysed. As a representative case, the influence of change in temperature is analysed for the flow of CDS at 1.8 % TSS in a 200mm diameter pipe at different temperature as shown in Figure 7.2.

The influence of temperature on pressure loss is evident from Figure 7.2. This is so due to the influence of temperature on the rheology of the fluid. This influence of temperature is also on V_{trans}. Although the influence is less (< 5 %) with changes at high temperatures, at lower temperatures this influence is prominent (> 5 %).

In reality, temperature changes do occur mostly likely with the implementation of different source-separation schemes. With the inclusion of food waste disposers, connection to the kitchen sink might increase the temperature of the slurry incoming from the FWD.

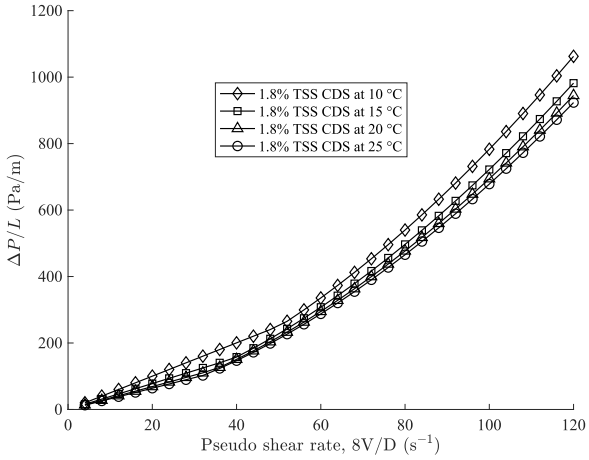

Figure 7.2: Plot of the pressure loss per unit length ($\Delta P/L$) for CDS at 1.8 % TSS at different flow temperatures with pipe diameter D as 0.2 m.

Therefore, it is indeed compelling to account for the changes in temperature of the slurry in transport.

7.2.3 Flow through pipe components

The entirety of this work has focussed much on the horizontal flow characteristics of non-Newtonian fluids. Pressurised sewer systems conveying CDS will most likely contain many bends and it is also well known that bends contribute to much of the pressure losses incurred. Although, flow through bends being out of scope for this work, a preliminary study of the losses through the 90° bend (Chapter 4) in the built slurry loop experimental set-up was analysed.

The minor loss coefficient which is generally used to represent the losses incurred in components is approximately 0.2 - 0.4 for a 90° bend calculated for the flow of water. In our case, for the flow of the clay slurries (Chapter 4, 5 and 6), the minor loss coefficient (Figure 7.3) has a broader range at low velocities between 0 and 0.2 and narrows down to approximately 0.15 at high velocities. This observation shows that the losses are highly dependent on the flow velocity. Despite this being a preliminary study, attention must be paid to these losses and the influence of the non-Newtonian behaviour. Following up with this knowledge is highly important as these components contribute largely to the pressure losses incurred.

7.2.4 Occurrence of a gaseous phase

Domestic slurries are biologically active and degrade with time. This biochemical degradation causes the production of many gasses that are either built up upon collection, intermittent storage and/or transportation of these slurries. It is therefore essential to understand its influence on the transport characteristics of the slurries.

A preliminary study was conducted to understand the influence of gasses on the flow of

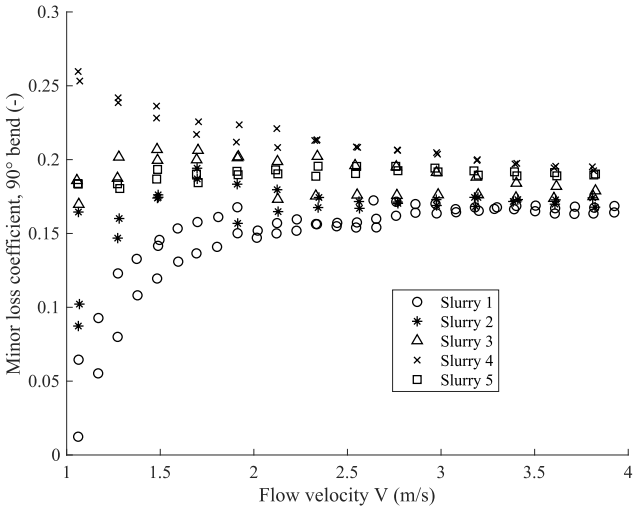

Figure 7.3: Plot of minor loss coefficient for a regular flanged 90° elbow fitting against flow velocities for the different clay slurries mentioned in Chapter 4.

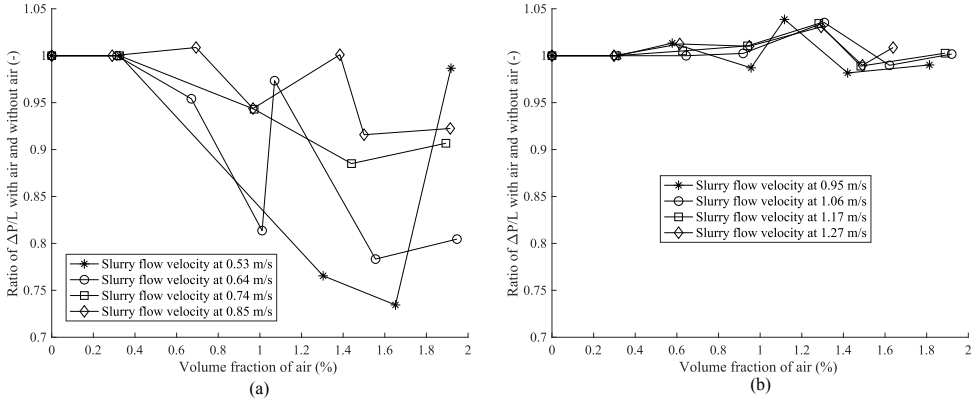

Figure 7.4: Ratio of pressure losses from the flow of slurries with air and without air plotted against volume fraction of air at different flow velocities. Concentration of slurry is 21.5 % TSS (Clay slurry, Chapter 4).

slurries. This was followed up using the slurry loop (Chapter 4) with the non-Newtonian clay slurries (Slurry 5 at 21.5 % TSS). Pressurised air was let in using calibrated airflow meters. The effect of this is presented in Figure 7.4. It is found at low flow velocities of the slurry (near laminar and transition, Chapter 5), the influence of the gaseous phase is high. This being that, the flow of air decreases the pressure losses for the flow of slurry. And at high slurry flow velocities, there is no significant effect.

A study on the effect of the gaseous phase in the transport of wastewater (CAPWAT, Pothof and Clemens (2010, 2011)) concluded that the capacity is largely reduced in some

scenarios of sloping pipes. This is caused by energy losses from gas pockets. Although, this is well established for dilute wastewater, it is still unknown for CDS. The production of gaseous phases are unavoidable and therefore it merits to further investigate its influence on the flow of slurries.

7.3 Discussion

In the previous sections, several results were laid forth on the estimated pressure drop incurred in the flow of CDS at different concentrations and temperatures. These results also extend to the transition velocity, at which transition to turbulence occurs. In this section, the results obtained are discussed with the perspective of its applicability in designing new sanitation systems. It also extends to discuss the current state of understanding of these systems.

At the outset, it is important to discuss the design considerations and dilemmas. The implementation of NS system as an alternative to conventional systems is backed by its ability to cost-effectively recover resources such as energy, nutrients and water. The other incentives for implementing NS systems is the possible avoidance of consuming large amounts of fossil fuels in conventional treatment.

At this point, it is very well established that the TSS concentration and temperature influence the energy consumed (or pressure loss) in the transport of CDS. Therefore, in order to optimise the overall energy balance in NS systems, concentration and temperature are to be considered as variables for optimisation. The dependence on temperature in the range of 5 - 25 °C is evident from section 7.2.2. Temperature of CDS depends solely on the flush water temperature and the heat lost or gained from the connecting pipes to the point of collection. Addressing these particular constraints is rather ambitious and out of scope of this study. Rather, what is more important in this issue is the TSS concentration, as its influence is stronger than that of temperature changes. Thereby, assuming that the temperature of CDS remains constant and beyond control, the variable that will be discussed here is that of TSS concentration.

The concentration of the source separated CDS stream arising from houses depends on the new sanitation features that are installed. This could include vacuum toilets with or without urine separation and food waste disposers. This is inclusive of the dependence of the amount of flush water used in vacuum toilets and food waste disposers. Some of the possible TSS concentration on average of these streams are 0.9 % TSS (wt./wt.) vacuum toilets & food waste disposers installed, 1.8 % TSS (wt./wt.) with vacuum toilets and 2.7 % TSS (wt./wt.) for vacuum toilets with urine separation.

In order to obtain an optimised conveyance system for CDS, the energy consumed must be low. At first glance, considering the results obtained in the previous sections, transporting lower TSS concentration slurries incur lower energy losses (check Figure 7.1). With respect to energy balance, a feasible system should be able to recover at least the energy that is consumed for conveyance. But, on the other hand, it is known that energy recovery from concentrated slurries is more efficient than dilute slurries (Chapter 1). Also, from Figure 7.1, it is seen that the incurred pressure loss for fluids with a yield stress and a shear thinning behaviour is lower than that of a fluid with only shear thinning. This implies that there could exist a "break even point" at higher concentrations with respect to energy consumed

upon transport and energy recovered upon treatment. This can only be ascertained through an optimisation study considering global systems approach that includes all the elements of the new sanitation system and the way of implementation.

Considering the transition to turbulence and flow of slurries at laminar flow regimes; it is seen that the V_{trans} for the probable concentrations (mentioned earlier) of CDS is considerably high (100 times that of water). However, flowing below the V_{trans} might result in the settling of the suspended particles. Nonetheless, the settling of the particles could be prevented if the Rouse number is low enough (< 1.2). Another flow scenario is that of intermittent flow. Intermittent flow cause particles to settle down in the pipe at no flow intervals. The re-suspension of the particles is possible when the flow is re-initiated and the corresponding wall shear-stress is high enough to clear the bed. This wall shear-stress is generally achieved at turbulent flow, where eddies activate re-suspension. Further, the cohesive nature of the particles may produce further complications to the re-suspension of the particles. A detailed study into the settling of the suspended particles, cohesivity of the suspended particles and its re-suspension could provide definite answers to this.

Domestic waste slurries are generally known to be biologically active. This causes the slurries to produce gases upon biological degradation. The production and accumulation of these gases poses another threat to the capacity of the transportation system (Pothof and Clemens, 2010, 2011). It is established from the work of Pothof and Clemens (2010, 2011) that the flow of gasses with water in downward slopes in some cases cause a large reduction in the capacity of the system. Although, this is now well established and quantified for water, it is still unknown for CDS. A complete design guideline would require it to consider the implications of gas production and accumulation.

7.4 Conclusion

A brief summary of the established theoretical framework in designing the transport system was provided. This considered both the energy losses and the minimum flow velocity requirement for turbulent flow. Using these, an analysis of its implication on the practical implementation of these systems is discussed. This discussion included the influence of slurry temperature and TSS concentration on the energy losses and V_{trans}.

Although various aspects of the design of the transport system have been established, there still exists many open questions. These include the identification of the adequate dilution of CDS for a feasible design of new sanitation, understanding the settling and re-suspension of the cohesive particles of CDS, flow through minor pipe components and the influence of gas production and accumulation in the transport of CDS.

For a feasible design of the new sanitation system, the flow velocity must meet the requirements for which the particles stay suspended ($N_R < 1.2$) and the energy consumed for transportation is low. On the other hand the chosen flow velocity is dictated by the concentration of the suspended particles which depends on the flush water quantity used in vacuum toilets and FWDs.

CHAPTER 8

Conclusion and Recommendations

Critical analysis of the current sanitation systems have indicated the lost opportunity in recovering energy, nutrients and water from wastewater streams. This has lead to the introduction of a shift in the sanitation paradigm, introducing source separation, vacuum toilets, food waste disposers, decentralisation and resource recovery. "New Sanitation" consists of different elements i.e., collection, transportation and treatment. Although collection and treatment are well studied, transportation has been vastly overlooked.

Accessing the New Sanitation system as a whole, leads to a better understanding about its feasibility and applicability. The much over-looked element in new sanitation, the transport systems, which bridge the collection and treatment, is the focus of this thesis. The objective of this thesis is to understand the rheological and transport characteristics of concentrated domestic slurry; thereby, establishing a model that predicts the pressure (energy) losses incurred in the transport of these slurries. Finally, an approach for implementing a new sanitation transport system is proposed, considering the revealed slurry characteristics.

8.1 General conclusions

Pressure losses are estimated using a 1-D flow equation, modelling the flow of non-Newtonian fluids using its rheology. There have been many models established to estimate the pressure losses across the wide spectrum of non-Newtonian fluid behaviour. These include for Bingham, shear-thinning and Herschel-Bulkley fluid behaviours. In contrast, literature on the rheological characterisation of CDS have been very limited. Although, the rheology of primary and secondary sludge in the treatment process have been studied, this cannot be directly applied to CDS. This knowledge gap hinders the designing of transport systems for CDS.

8.1.1 Rheology

Rheological characterisation of CDS showed that its non-Newtonian behaviour is akin to yield shear-thinning or Herschel-Bulkley type. Thereby, a Herschel-Bulkley model is used to describe the rheology of CDS. Analysis of the rheogram data showed that the rheology is highly influenced by temperature and TSS concentration. With respect to the temperature, the viscosity decreases with increase in temperature. This influence is modelled using an Arrhenius type equation considering the apparent viscosity.

As for the TSS concentration, the viscosity increases with increase in TSS. To model this effect, the influence is reflected through the rheology model (Herschel-Bulkley) parameters. The yield stress and consistency index increase exponentially in effect to the TSS concentration and are represented through their respective exponential models. Similarly, the behaviour index is represented through an inverse power law model. It is observed that the yield stress in the slurry is only physically meaningful above 2 % TSS (wt./wt.) and the behaviour index above 2.6 % TSS (wt./wt.).

The particle size distribution of the suspended solids in CDS is also found to play a crucial role in influencing the rheology. This effect is particularly seen in the addition of ground kitchen waste using food waste disposers in the kitchen. Addition of GKW changes the effective particle size of the slurry (for example d_{85}). It is seen that the viscosity increase with the increase in the effective particle size: d_{85}.

8.1.2 Flow characterisation

Laminar-turbulent transition being a very important aspect of flow characterisation, occurs as a multi stage process. It occurs through the emergence of intermittent flow structures: puffs and slugs. The length of the intermittent structures was observed to be about 5 times the pipe diameter for the puffs and about 10 times the pipe diameter for the slugs. Among the models used to predict transition, the Reynolds number-based model of Slatter is assessed to be the best for fluids with a yield stress and low behaviour index. This is followed by the stability parameter-based model of Hanks in terms of its predictability, while the one of Metzner & Reed is least favourable. The flow energy losses incurred is the other important aspect of flow characterisation. In estimating these losses, it is found that the Slatter model is highly preferred with respect to its predictability and its ease of implementation.

In translating these results to the design of a feasible transport system for CDS, it is important to establish an optimum dilution of CDS. As it is observed that the pressure loss incurred for the flow of water and to that of CDS differ by a large margin, the dilution (TSS concentration) is the single most important factor as it influences the rheology and hence the pressure drop greatly. The energy losses is found to increase greatly with the increase in TSS concentration, but at the onset of yield-stress, it reduces significantly but it is still higher than that incurred for the flow of water. The optimum dilution would have to justify the energy consumed upon transportation or avoidance of energy use elsewhere.

8.2 Recommendations for research and application

The various aspects of transport design models having been established, there still exists many open questions; in particular, the identification of the adequate dilution of CDS for a

feasible design of new sanitation systems. The design envelop and uncertainty within which the system will function, given the many parameters of the system, is still unknown. To provide this, the work in this thesis is hindered by the limited samples used for the rheological characterisation. With the precise rheology measurement protocol that is already established in this work, an experimental campaign that includes a broad spectrum of CDS samples could therefore establish this envelope. This also extends to include the influence of adding ground kitchen waste to the CDS. At this point, the knowledge of the influence is limited to the consequences to the PSD and not on the design envelope. To account for this, a rheological characterisation of CDS with GKW from a wide range of food waste disposers and kitchen wastes must be performed. This experimental campaign would provide an envelop of the rheological parameters to represent CDS with GKW, which in turn provides clarity on the uncertainty bounds of the transport characteristics.

Despite the many number of approaches to estimate the wall shear-stress (pressure losses) for the turbulent flow of non-Newtonian fluids, it still remains a challenge. Models and approaches are often based on over-simplification of the physical phenomena of non-Newtonian turbulent flow. Semi-empirical models are determined for a restricted set of experiments, which hinders its ability to be versatile over the many non-Newtonian behaviours. In this regard, extending Slatter's model to experiments beyond the ones considered in its formulation, could perhaps make the model more robust and accurate, and hence, worth investigating. Although CFD holds promise in terms of its capacity to estimate frictional losses, it requires further development in terms of incorporating the fundamentals of non-Newtonian turbulence, which themselves require thorough experimental investigation and understanding. Considering that many non-Newtonian fluids (industrial) are opaque, techniques used in this work such as UIV, could render it fit for purpose in investigating these fundamentals of non-Newtonian turbulent and transitional flow.

In light of the promising results from the UIV measurements, the technique has certainly a solid future in the field of multiphase flow studies. Especially with its capacity to be a non-intrusive diagnostic instrument and its applicability to optically inaccessible fluids. With the possibility to obtain longer time series and deeper intrusion (possibly a complete pipe cross-section), its potential to investigate the fundamentals of turbulence and transition is encouraging.

The classic representation of the friction losses using the friction factor vs. the Reynolds number charts are found to be least favourable for non-Newtonian fluids. The ambiguity with the representation of the Reynolds number for non-Newtonian fluids stems from the representation of the viscous forces. As opposed to Newtonian fluids, non-Newtonian fluids do not have a definitive viscosity, but a shear dependent viscosity. Moving away from the Reynolds number, a pseudo shear-rate could be a probable candidate for representing the friction losses. However, this adoption to a different representation should only be based on solid fundamental physics rather than mere comfort. Only an exhaustive survey of different possible representations could determine this.

The possibility of implementing some elements of new sanitation systems in conventional systems is also worth exploring. This broadens the envelope of opportunities for the development of resource recovery options. Some of the important questions to examine are the adoption of vacuum toilets and/or food waste disposers using gravity sewers. This could possibly also include some aspects of sources separation. However, the prospect of adopting gravity sewers is hindered by the settling of the suspended particles and shorter transport

lengths for slurries with a significant amount of suspended solids. The issue of settling of the suspended particles and its re-suspension also affects the possibility of intermittent or discontinuous flow. The prospect of CDS being transported through gravity sewers or intermittent flow could be known by understanding the settling properties, cohesive nature of the suspended particles and also its re-suspension when settled.

8.2.1 Future of New Sanitation

The implementation of new sanitation systems depend largely on the advantages it provides over the conventional systems. The efficiency of energy recovery and avoidance of energy use along with the feasibility of nutrient recovery and re-purposing them play a vital role. In addition, by separating the black water streams, by far most (antibiotic resistant) pathogens and medicine residues from the large pool of water, making application of proper technologies to address these more feasible. As such, the new sanitation system isn't a single complete solution, rather it is made of various different solutions to tackle different problems. It is this attribute that makes the concept of new sanitation system an attractive alternative. Various sub-concepts of the new sanitation systems could be adopted where needed, rather than as a whole.

A very often raised concern about new sanitation system is that, will it replace the existing conventional system? From the point of view of this thesis, it is another type of system that could very well co-exist with the current systems in environments where it could be a very practical and feasible option. This is akin to saying that no single mode of transport has replaced the other, but rather has found its part in the entire ecosystem of transportation.

Bibliography

Abu-Jdayil, B., Banat, F., and Al-Sameraiy, M. (2010). Steady rheological properties of rotating biological contactor (RBC) sludge. *Journal of Water Resource and Protection*, 2(1):1–7.

AL-Behadili, A. J. M., Sellier, M., Nokes, R., Moyers-Gonzalez, M., and Geoghegan, P. H. (2018). Rheometry based on free surface velocity. *Inverse Problems in Science and Engineering*, pages 1–21.

Ancey, C. (2005). Solving the Couette inverse problem using a wavelet-vaguelette decomposition. *Journal of Rheology*, 49(2):441–460.

Ansys, I. (2011). ANSYS Fluent 14.0 Theory Guide. *Southpointe, Canonsburg, PA, USA*.

APHA (2005). *Standard methods for the examination of water and wastewater*. American Public Health Association (APHA), Washington, DC, USA.

Ashley, R. M., Bertrand-Krajewski, J. L., Hvitved-Jacobsen, T., and Verbanck, M. (2005). Solids in sewers: Characteristics, effects and control of sewer solids and associated pollutants. *Water Intelligence Online*, 4:9781780402727.

Assefa, K. M. and Kaushal, D. R. (2015). A comparative study of friction factor correlations for high concentrate slurry flow in smooth pipes. *Journal of Hydrology and Hydromechanics*, 63(1):13–20.

Avila, K., Moxey, D., de Lozar, A., Avila, M., Barkley, D., and Hof, B. (2011). *The onset of turbulence in pipe flow*, volume 333. American Association for the Advancement of Science.

Baroutian, S., Eshtiaghi, N., and Gapes, D. J. (2013). Rheology of a primary and secondary sewage sludge mixture: Dependency on temperature and solid concentration. *Bioresource technology*, 140:227–233.

Bartosik, A. (2006). Modelling of a turbulent flow using the Herschel-Bulkley rheological model. *Inzynieria Chemiczna i Procesowa*, 27(3):623–632.

Bartosik, A. (2010). Application of rheological models in prediction of turbulent slurry flow. *Flow, turbulence and combustion*, 84(2):277–293.

Battistoni, P. (1997). Pre-treatment, measurement execution procedure and waste characteristics in the rheology of sewage sludges and the digested organic fraction of municipal solid wastes. *Water Science and Technology*, 36(11):33–41.

Battistoni, P., Fava, G., Stanzini, C., Cecchi, F., and Bassetti, A. (1993). Feed characteristics and digester operative conditions as parameters affecting the rheology of digested municipal solid wastes. *Water Science and Technology*, 27(2):37–45.

Battistoni, P., Pavan, P., Mata-Alvarez, J., Prisciandaro, M., and Cecchi, F. (2000). Rheology of sludge from double phase anaerobic digestion of organic fraction of municipal solid waste. *Water Science and Technology*, 41(3):51–59.

Baudez, J. C., Markis, F., Eshtiaghi, N., and Slatter, P. (2011). The rheological behaviour of anaerobic digested sludge. *Water research*, 45(17):5675–5680.

Baudez, J. C., Slatter, P., and Eshtiaghi, N. (2013). The impact of temperature on the rheological behaviour of anaerobic digested sludge. *Chemical Engineering Journal*, 215:182–187.

Bewersdorff, H.-W. and Thiel, H. (1993). Turbulence structure of dilute polymer and surfactant solutions in artificially roughened pipes. In *Further Developments in Turbulence Management*, pages 347–368. Springer.

Bird, R. B., Armstrong, R. C., and Hassager, O. (1987). Dynamics of polymeric liquids. Vol. 1: Fluid mechanics.

Bird, R. B., Dai, G. C., and Yarusso, B. J. (1983). The rheology and flow of viscoplastic materials. *Reviews in Chemical Engineering*, 1(1):1–70.

Bogue, D. C. (1959). Entrance effects and prediction of turbulence in non-Newtonian flow. *Industrial & Engineering Chemistry*, 51(7):874–878.

Bolzonella, D., Pavan, P., Battistoni, P., and Cecchi, F. (2003). The under sink garbage grinder: a friendly technology for the environment. *Environmental Technology*, 24(3):349–359.

Braun, R. and Wellinger, A. (2003). Potential of co-digestion. In *IEA Bioenergy, Task*, volume 37.

Brewer, T. and Pringle, Y. (2015). Beyond Bazalgette: 150 years of sanitation. *The Lancet*, 386(9989):128–129.

Buckingham, E. (1914). On physically similar systems; illustrations of the use of dimensional equations. *Physical review*, 4(4):345.

Byrd, R. H., Schnabel, R. B., and Shultz, G. A. (1987). A trust region algorithm for nonlinearly constrained optimization. *SIAM Journal on Numerical Analysis*, 24(5):1152–1170.

Chatzimina, M., Gerogiou, G., and Alexandrou, A. (2009). Wall Shear Rates in Circular Couette Flow of a Herschel-BulkleyFluid. *Applied Rheology*, 19(3):34288.

Chaudhuri, A., Wereley, N. M., Radhakrishnan, R., and Choi, S. B. (2006). Rheological parameter estimation for a ferrous nanoparticle-based magnetorheological fluid using genetic algorithms. *Journal of intelligent material systems and structures*, 17(3):261–269.

Chen, R.-Y. (1973). Flow in the entrance region at low Reynolds numbers. *Journal of Fluids Engineering*, 95(1):153–1581.

Chhabra, R. P. and Richardson, J. F. (2011). *Non-Newtonian flow and applied rheology: engineering applications*. Butterworth-Heinemann.

Chilton, R., Stainsby, R., and Thompson, S. (1996). The design of sewage sludge pumping systems. *Journal of Hydraulic Research*, 34(3):395–408.

Chilton, R. A. and Stainsby, R. (1998). Pressure loss equations for laminar and turbulent non-Newtonian pipe flow. *Journal of hydraulic engineering*, 124(5):522–529.

Darbyshire, A. G. and Mullin, T. (1995). Transition to turbulence in constant-mass-flux pipe flow. *Journal of Fluid Mechanics*, 289:83–114.

Davidson, P. (2015). *Turbulence: an introduction for scientists and engineers*. Oxford University Press.

Di Federico, V., Longo, S., King, S. E., Chiapponi, L., Petrolo, D., and Ciriello, V. (2017). Gravity-driven flow of HerschelBulkley fluid in a fracture and in a 2D porous medium. *Journal of Fluid Mechanics*, 821:59–84.

Dick, R. I. and Ewing, B. B. (1967). The rheology of activated sludge. *Journal - Water Pollution Control Federation*, pages 543–560.

Dodge, D. W. and Metzner, A. B. (1959). Turbulent flow of nonNewtonian systems. *AIChE Journal*, 5(2):189–204.

Draad, A. A., Kuiken, G. D. C., and Nieuwstadt, F. T. M. (1998). Laminarturbulent transition in pipe flow for Newtonian and non-Newtonian fluids. *Journal of Fluid Mechanics*, 377:267–312.

Durst, F., Ray, S., Ünsal, B., and Bayoumi, O. A. (2005). The development lengths of laminar pipe and channel flows. *Journal of fluids engineering*, 127(6):1154–1160.

Eckhardt, B., Schneider, T. M., Hof, B., and Westerweel, J. (2007). Turbulence transition in pipe flow. *Annu. Rev. Fluid Mech.*, 39:447–468.

Einstein, H. A., Anderson, A. G., and Johnson, J. W. (1940). A distinction between bedload and suspended load in natural streams. *Eos, Transactions American Geophysical Union*, 21(2):628–633.

Escudier, M. P. and Presti, F. (1996). Pipe flow of a thixotropic liquid. *Journal of non-newtonian fluid mechanics*, 62(2-3):291–306.

Eshtiaghi, N., Baudez, J., and Slatter, P. (2013a). Rheological behaviour of anaerobic digested sludge: impact of concentration and temperature. In *AD 13: Recovering (bio) Resources for the World*, pages 1–4. International Water Association (IWA).

Eshtiaghi, N., Markis, F., and Slatter, P. (2012). The laminar/turbulent transition in a sludge pipeline. *Water Science and Technology*, 65(4):697–702.

Eshtiaghi, N., Markis, F., Yap, S. D., Baudez, J.-C., and Slatter, P. (2013b). Rheological characterisation of municipal sludge: a review. *Water research*, 47(15):5493–5510.

Estellé, P., Lanos, C., and Perrot, A. (2008). Processing the Couette viscometry data using a Bingham approximation in shear rate calculation. *Journal of Non-Newtonian Fluid Mechanics*, 154(1):31–38.

Ferriman, A. (2007). BMJ readers choose the" sanitary revolution" as greatest medical advance since 1840. *BMJ: British Medical Journal*, 334(7585):111.

Ferziger, J. H. and Peric, M. (2012). *Computational methods for fluid dynamics*. Springer Science & Business Media.

Freidler, E., Butler, D., and Alfiya, Y. (2013). Wastewater composition. In Larsen, T. A., Udert, K. M., and Lienert, J., editors, *Source Separation and decentralization for wastewater management*, chapter 17. IWA Publishing.

Froishteter, G. B. and Vinogradov, G. V. (1980). The laminar flow of plastic disperse systems in circular tubes. *Rheologica Acta*, 19(2):239–250.

Gurung, A., Haverkort, J. W., Drost, S., Norder, B., Westerweel, J., and Poelma, C. (2016). Ultrasound image velocimetry for rheological measurements. *Measurement Science and Technology*, 27(9):94008.

Güzel, B., Burghelea, T., Frigaard, I. A., and Martinez, D. M. (2009a). Observation of laminarturbulent transition of a yield stress fluid in HagenPoiseuille flow. *Journal of Fluid Mechanics*, 627:97–128.

Güzel, B., Frigaard, I., and Martinez, D. M. (2009b). Predicting laminarturbulent transition in Poiseuille pipe flow for non-Newtonian fluids. *Chemical Engineering Science*, 64(2):254–264.

Hager, W. H. (2010). *Wastewater hydraulics: Theory and practice*. Springer Science & Business Media.

Hanks, R. W. (1963). The laminarturbulent transition for fluids with a yield stress. *AIChE Journal*, 9(3):306–309.

Hanks, R. W. (1969). A theory of laminar flow stability. *AIChE Journal*, 15(1):25–28.

Hanks, R. W. and Dadia, B. H. (1971). Theoretical analysis of the turbulent flow of non-Newtonian slurries in pipes. *AIChE Journal*, 17(3):554–557.

Hanks, R. W. and Ricks, B. L. (1974). Laminar-turbulent transition in flow of pseudoplastic fluids with yield stresses. *Journal of Hydronautics*, 8(4):163–166.

Harder, R. (2012). *Source-separation in the urban water infrastructure*. STOWA.

Hedstrom, B. O. A. (1952). Flow of plastic materials in pipes. *Industrial & Engineering Chemistry*, 44(3):651–656.

Herschel, W. H. and Bulkley, R. (1926). Konsistenzmessungen von gummi-benzollösungen. *Colloid & Polymer Science*, 39(4):291–300.

Heywood, N. I. (1991). Rheological characterisation of non-settling sluries. In *Slurry Handling Design of Solid-Liquid Systems*, pages 53–87. Elsevier Amsterdam, The Netherlands.

Heywood, N. I. and Cheng, D.-H. (1984). Comparison of methods for predicting head loss in turbulent pipe flow of non-Newtonian fluids. *Transactions of the Institute of Measurement and Control*, 6(1):33–45.

Hogendoorn, W. and Poelma, C. (2018). Particle-laden pipe flows at high volume fractions show transition without puffs. *Physical review letters*, 121(19):194501.

Hoornweg, D. and Bhada-Tata, P. (2012). *What a waste: a global review of solid waste management*. World Bank, Washington, DC.

Iacovidou, E., Ohandja, D.-G., Gronow, J., and Voulvoulis, N. (2012a). The household use of food waste disposal units as a waste management option: a review. *Critical reviews in environmental science and technology*, 42(14):1485–1508.

Iacovidou, E., Ohandja, D.-G., and Voulvoulis, N. (2012b). Food waste co-digestion with sewage sludgerealising its potential in the UK. *Journal of environmental management*, 112:267–274.

Kelessidis, V. C., Maglione, R., Tsamantaki, C., and Aspirtakis, Y. (2006). Optimal determination of rheological parameters for HerschelBulkley drilling fluids and impact on pressure drop, velocity profiles and penetration rates during drilling. *Journal of Petroleum Science and Engineering*, 53(3):203–224.

Koseoglu, H., Yigit, N. O., Civelekoglu, G., Harman, B. I., and Kitis, M. (2012). Effects of chemical additives on filtration and rheological characteristics of MBR sludge. *Bioresource technology*, 117:48–54.

Krieger, I. M. and Elrod, H. (1953). Direct determination of the flow curves of nonNewtonian fluids. II. Shearing rate in the concentric cylinder viscometer. *Journal of applied physics*, 24(2):134–136.

Kujawa-Roeleveld, K. and Zeeman, G. (2006). Anaerobic treatment in decentralised and source-separation-based sanitation concepts. *Reviews in Environmental Science and Bio/Technology*, 5(1):115–139.

Larsen, T. A., Alder, A. C., Eggen, R. I. L., Maurer, M., Lienert, J., Larsen*, T. A., Alder, A. C., Eggen, R. I. L., Maurer, M., and Lienert, J. (2009). Source Separation: Will We See a Paradigm Shift in Wastewater Handling? *Environmental science & technology*, 43(16):6121–6125.

Larsen, T. A. and Gujer, W. (1997). The concept of sustainable urban water management. *Water Science and Technology*, 35(9):3–10.

Larsen, T. A., Udert, K. M., and Lienert, J. (2013). *Source separation and decentralization for wastewater management*. Iwa Publishing.

Launder, B. E., Reece, G. J., and Rodi, W. (1975). Progress in the development of a Reynolds-stress turbulence closure. *Journal of fluid mechanics*, 68(3):537–566.

Launder, B. E. and Spalding, D. B. (1983). The numerical computation of turbulent flows. In *Numerical prediction of flow, heat transfer, turbulence and combustion*, pages 96–116. Elsevier.

Leong, Y. K. and Yeow, Y. L. (2003). Obtaining the shear stress shear rate relationship and yield stress of liquid foods from Couette viscometry data. *Rheologica Acta*, 42(4):365–371.

Lindgren, E. R. (1969). Propagation velocity of turbulent slugs and streaks in transition pipe flow. *The Physics of Fluids*, 12(2):418–425.

Longo, S., Di Federico, V., Archetti, R., Chiapponi, L., Ciriello, V., and Ungarish, M. (2013). On the axisymmetric spreading of non-Newtonian power-law gravity currents of time-dependent volume: an experimental and theoretical investigation focused on the inference of rheological parameters. *Journal of Non-Newtonian Fluid Mechanics*, 201:69–79.

Lundie, S. and Peters, G. M. (2005). Life cycle assessment of food waste management options. *Journal of Cleaner Production*, 13(3):275–286.

Malin, M. R. (1997). The turbulent flow of Bingham plastic fluids in smooth circular tubes. *International communications in heat and mass transfer*, 24(6):793–804.

Malin, M. R. (1998). Turbulent pipe flow of Herschel-Bulkley fluids. *International communications in heat and mass transfer*, 25(3):321–330.

Markis, F., Baudez, J.-C., Parthasarathy, R., Slatter, P., and Eshtiaghi, N. (2014). Rheological characterisation of primary and secondary sludge: Impact of solids concentration. *Chemical Engineering Journal*, 253:526–537.

Mehta, D., Thota Radhakrishnan, A., van Lier, J., and Clemens, F. (2018). A wall boundary condition for the simulation of a turbulent non-Newtonian domestic slurry in pipes. *Water*, 10(2):124.

Mehta, D., Thota Radhakrishnan, A., van Lier, J., and Clemens, F. (2019). Sensitivity Analysis of a Wall Boundary Condition for the Turbulent Pipe Flow of HerschelBulkley Fluids. *Water*, 11(1):19.

Metzner, A. B. and Reed, J. C. (1955). Flow of nonnewtonian fluidscorrelation of the laminar, transition, and turbulentflow regions. *AIChE Journal*, 1(4):434–440.

Mishra, P. and Tripathi, G. (1971). Transition from laminar to turbulent flow of purely viscous non-Newtonian fluids in tubes. *Chemical Engineering Science*, 26(6):915–921.

Mitsoulis, E. (2007). Flows of viscoplastic materials: models and computations. *Rheology reviews*, 2007:135–178.

Mofjeld, H. O. (1988). Formulas for velocity, sediment concentration and suspended sediment flux for steady uni-directional pressure-driven flow.

Mooney, M. (1931). Explicit formulas for slip and fluidity. *Journal of Rheology (1929-1932)*, 2(2):210–222.

Mori, M., Seyssiecq, I., and Roche, N. (2006). Rheological measurements of sewage sludge for various solids concentrations and geometry. *Process Biochemistry*, 41(7):1656–1662.

Nakakubo, T., Tokai, A., and Ohno, K. (2012). Comparative assessment of technological systems for recycling sludge and food waste aimed at greenhouse gas emissions reduction and phosphorus recovery. *Journal of Cleaner Production*, 32:157–172.

Nikuradse, J. (1933). *Strömungsgesetze in rauhen Rohren*. VDI-Verlag.

Nishi, M., Ünsal, B., Durst, F., and Biswas, G. (2008). Laminar-to-turbulent transition of pipe flows through puffs and slugs. *Journal of Fluid Mechanics*, 614:425–446.

Ohen, H. A. and Blick, E. F. (1990). Golden section search method for determining parameters in Robertson-Stiff non-Newtonian fluid model. *Journal of Petroleum Science and Engineering*, 4(4):309–316.

Otterpohl, R., Braun, U., and Oldenburg, M. (2002). Innovative technologies for decentralised wastewater management in urban and peri-urban areas. *Berichte-Wassergute Und Abfallwirtschaft Technische Universitat Munchen Berichtsheft*, 173:109–126.

Palsma, B., Swart, B., and STOWA (2010). Koepelgroep ONSS: Stand van zaken tot 2010, Ontwikkelingen 2011. Technical report, Amersfoort.

Peixinho, J., Nouar, C., Desaubry, C., and Théron, B. (2005). Laminar transitional and turbulent flow of yield stress fluid in a pipe. *Journal of Non-Newtonian Fluid Mechanics*, 128(2-3):172–184.

Pevere, A., Guibaud, G., Goin, E., Van Hullebusch, E., and Lens, P. (2009). Effects of physico-chemical factors on the viscosity evolution of anaerobic granular sludge. *Biochemical Engineering Journal*, 43(3):231–238.

Poelma, C. (2017). Ultrasound imaging velocimetry: a review. *Experiments in Fluids*, 58(1):3.

Poelma, C., Van der Mijle, R. M. E., Mari, J. M., Tang, M.-X., Weinberg, P. D., and Westerweel, J. (2012). Ultrasound imaging velocimetry: Toward reliable wall shear stress measurements. *European Journal of Mechanics-B/Fluids*, 35:70–75.

Poole, R. J. and Ridley, B. S. (2007). Development-length requirements for fully developed laminar pipe flow of inelastic non-Newtonian liquids. *Journal of Fluids Engineering*, 129(10):1281–1287.

Pope, S. B. and Pope, S. B. (2000). *Turbulent flows*. Cambridge university press.

Pothof, I. and Clemens, F. (2010). On elongated air pockets in downward sloping pipes. *Journal of Hydraulic Research*, 48(4):499–503.

Pothof, I. W. M. and Clemens, F. (2011). Experimental study of airwater flow in downward sloping pipes. *International journal of multiphase flow*, 37(3):278–292.

Prandtl, L. (1925). Zur turbulenten Strömung in glatten Röhren. *Zeitschrift für Angewandte Mathematik und Mechanik*, 5:136–139.

Prandtl, L. (1933). Neuere ergebnisse der turbulenzforschung. *VDI-Ztschr*, 77(5):105.

Quemada, D. (1998). Rheological modelling of complex fluids. I. The concept of effective volume fraction revisited. *The European Physical Journal-Applied Physics*, 1(1):119–127.

Rabinowitsch, B. (1929). Über die viskosität und elastizität von solen. *Zeitschrift für physikalische Chemie*, 145(1):1–26.

Ratkovich, N., Horn, W., Helmus, F. P., Rosenberger, S., Naessens, W., Nopens, I., and Bentzen, T. R. (2013). Activated sludge rheology: a critical review on data collection and modelling. *Water research*, 47(2):463–482.

Rooki, R., Ardejani, F. D., Moradzadeh, A., Mirzaei, H., Kelessidis, V., Maglione, R., and Norouzi, M. (2012). Optimal determination of rheological parameters for herschel-bulkley drilling fluids using genetic algorithms (GAs). *Korea-Australia Rheology Journal*, 24(3):163–170.

Rouse, H. (1937). Modern conceptions of the mechanics of fluid turbulence. *Trans ASCE*, 102:463–505.

Rouse, H. (1939). Experiments on the mechanics of sediment suspension.

Rouse, H. (1961). Fluid mechanics for hydraulic engineers. Technical report.

Ryan, N. W. and Johnson, M. M. (1959). Transistion from laminar to turbulent flow in pipes. *AIChE Journal*, 5(4):433–435.

Sanin, D. F. (2002). Effect of solution physical chemistry on the rheological properties of activated sludge. *Water Sa*, 28(2):207–212.

Schlichting, H. (1960). *Boundary layer theory*, volume 960. Springer.

Seyssiecq, I., Ferrasse, J.-H., and Roche, N. (2003). State-of-the-art: rheological characterisation of wastewater treatment sludge. *Biochemical Engineering Journal*, 16(1):41–56.

Skelland, A. H. P. (1967). Non-Newtonian flow and heat transfer(Book on quantitative relationships for non- Newtonian systems, considering classification and fluid behavior of materials with anomalous flow properties). *NEW YORK, JOHN WILEY AND SONS, INC., 1967. 469 P.*

Slatter, P. T. (1995). *Transitional and turbulent flow of non-Newtonian slurries in pipes (Doctoral dissertation)*. (doctoral dissertation, university of cape town), University of Cape Town.

Slatter, P. T. (1997). The rheological characterisation of sludges. *Water Science and Technology*, 36(11):9–18.

Soto, R. J. and Shah, V. L. (1976). Entrance flow of a yield-power law fluid. *Applied Scientific Research*, 32(1):73–85.

Tanner, R. I. and Milthorpe, J. F. (1983). Numerical simulation of the flow of fluids with yield stress. *Numer Meth Lami Turb Flow Seattle*, pages 680–690.

Taylor, J. (1997). *Introduction to error analysis, the study of uncertainties in physical measurements*.

Tervahauta, T., Hoang, T., Hernández, L., Zeeman, G., and Buisman, C. (2013). Prospects of Source-Separation-Based sanitation concepts: A model-based study. *Water*, 5(3):1006–1035.

Thomas, A. D. and Wilson, K. C. (1987). New analysis of non-newtonian turbulent flowndashyield-power-law fluids. *The Canadian Journal of Chemical Engineering*, 65(2):335–338.

Thota Radhakrishnan, A., Alidai, A., Pothof, I., van Lier, J., and Clemens, F. (2015). Predicting the onset of secondary flows in the rheological measurement of domestic slurry. In *10th International Conference on Urban Drainage Modelling*.

Thota Radhakrishnan, A., van Lier, J., and Clemens, F. (2018a). Rheological characterisation of concentrated domestic slurry. *Water research*, 141:235–250.

Thota Radhakrishnan, A. K., Langeveld, J., van Lier, J. B., and Clemens, F. (2018b). Challenge of Transport: Exploring the Limit of Gravity Sewers to Transport Concentrated Domestic Slurries. In *11th Urban Drainage Modelling Conference*.

TOMITA, Y. (1959). A study on non-Newtonian flow in pipe lines. *Bulletin of JSME*, 2(5):10–16.

Torrance, B. (1963). Friction factors for turbulent non-Newtonian fluid flow in circular pipes. *S. Afr. Mech. Eng*, 13:89–91.

Van Doorne, C. W. H. and Westerweel, J. (2007). Measurement of laminar, transitional and turbulent pipe flow using stereoscopic-PIV. *Experiments in Fluids*, 42(2):259–279.

Van Wazer, J. R. (1963). *Viscosity and flow measurement: a laboratory handbook of rheology*. Interscience Publishers.

Wasp, E. J., Kenny, J. P., and Gandhi, R. L. (1977). Solid–liquid flow: slurry pipeline transportation.[Pumps, valves, mechanical equipment, economics]. *Ser. Bulk Mater. Handl.;(United States)*, 1(4).

Wilcox, D. C. (1998). *Turbulence modeling for CFD*, volume 2. DCW industries La Canada, CA.

Wilson, K. C. and Thomas, A. D. (1985). A new analysis of the turbulent flow of nonnewtonian fluids. *The Canadian Journal of Chemical Engineering*, 63(4):539–546.

Woolley, S. M., Cottingham, R. S., Pocock, J., and Buckley, C. A. (2014). Shear rheological properties of fresh human faeces with different moisture content. *Water Sa*, 40(2):273–276.

Wygnanski, I., Sokolov, M., and Friedman, D. (1975). On transition in a pipe. Part 2. The equilibrium puff. *Journal of Fluid Mechanics*, 69(2):283–304.

Wygnanski, I. J. and Champagne, F. H. (1973). On transition in a pipe. Part 1. The origin of puffs and slugs and the flow in a turbulent slug. *Journal of Fluid Mechanics*, 59(2):281–335.

Yang, F., Bick, A., Shandalov, S., Brenner, A., and Oron, G. (2009). Yield stress and rheological characteristics of activated sludge in an airlift membrane bioreactor. *Journal of Membrane Science*, 334(1-2):83–90.

Yeow, Y. L., Ko, W. C., and Tang, P. P. P. (2000). Solving the inverse problem of Couette viscometry by Tikhonov regularization. *Journal of Rheology.*, 44(6):1335–1351.

Appendices

APPENDIX A

Rheology

Table A.1: RMSE for the model fit of slurry 1 rheograms at 20°C

Concentration	$RMSE$				
% TSS (wt./wt.)	HB	CHB	Power	Linear	Bingham
11.2	1.25E-2	6.93E-3	3.19E-2	6.16E0	2.61E-1
10	5.17E-3	2.63E-3	1.77E-2	1.56E0	6.49E-2
7.2	7.76E-4	5.52E-4	4.78E-3	2.15E-1	9.37E-3
5	4.93E-5	3.47E-5	6.16E-4	2.95E-2	1.74E-3
3.9	9.30E-5	1.44E-5	1.91E-4	7.15E-3	4.42E-4
3.2	1.26E-4	2.70E-5	1.40E-4	3.74E-3	2.74E-4
2.6	1.05E-4	4.28E-5	7.35E-5	8.40E-4	3.36E-5
1.8	1.72E-4	1.92E-5	2.12E-5	5.83E-5	4.38E-6
1.4	3.01E-4	2.18E-5	1.33E-4	8.95E-6	6.59E-6
0.7	8.40E-5	1.15E-5	1.32E-5	1.21E-5	1.16E-5
0.4	2.48E-4	1.83E-5	1.30E-5	1.47E-5	1.46E-5

Table A.2: RMSE for the model fit of slurry 2 rheograms at 20°C

Concentration	$RMSE$				
% TSS (wt./wt.)	HB	CHB	Power	Linear	Bingham
3	2.00E-4	1.49E-4	2.69E-4	6.25E-3	3.98E-4
2.6	2.14E-4	2.32E-4	1.25E-4	2.89E-3	2.04E-4
2.1	1.06E-4	8.72E-5	1.04E-4	1.56E-3	8.70E-5
1.8	1.62E-4	2.05E-5	7.67E-5	8.48E-4	3.16E-5
1.2	1.45E-4	4.08E-5	7.31E-5	4.02E-4	2.11E-5
1	2.80E-4	5.80E-5	6.01E-5	2.33E-4	1.44E-5
0.8	5.24E-5	9.07E-6	1.23E-5	1.89E-5	7.08E-6

Table A.3: Summary of the parameters estimated for the models representing the rheograms (rheometric) data of slurry 1

Concentration	Temperature	Model	τ_y	K	n	$RMSE$
% TSS (wt./wt.)	°C	-	Pa	$mPa.s^n$	-	Pa
11.2	10	HB	1.529	849.89	0.52	1.13E-2
	20	HB	1.398	820.11	0.49	1.25E-2
	30	HB	1.070	946.20	0.45	5.66E-3
	40	HB	0.855	1381.14	0.38	1.27E-2
10	10	HB	0.935	459.95	0.55	1.45E-3
	20	HB	1.101	232.14	0.62	5.17E-3
	30	HB	0.803	286.66	0.56	3.76E-3
	40	HB	0.701	317.36	0.53	2.59E-3

7.2	10	HB	0.307	194.44	0.60	1.77E-3
	20	HB	0.444	68.44	0.72	7.76E-4
	30	HB	0.325	87.41	0.65	7.41E-4
	40	HB	0.372	63.17	0.69	6.75E-4
5	10	HB	0.127	58.64	0.69	1.01E-4
	20	HB	0.145	27.10	0.77	4.93E-5
	30	HB	0.135	21.23	0.78	2.25E-4
	40	HB	0.119	20.21	0.77	2.07E-4
3.9	10	HB	0.081	26.47	0.76	1.30E-4
	20	HB	0.076	13.17	0.83	9.30E-5
	30	HB	0.073	11.87	0.82	1.81E-4
	40	HB	0.020	23.81	0.68	4.35E-4
3.2	10	HB	0.054	18.43	0.79	1.21E-4
	20	HB	0.045	10.57	0.85	1.26E-4
	30	HB	0.053	7.64	0.87	1.20E-4
	40	HB	0.020	13.30	0.75	2.68E-4
2.6	10	Bingham	0.069	4.49	1	1.12E-4
	20	Bingham	0.053	3.52	1	3.36E-5
	30	Bingham	0.052	2.93	1	2.14E-5
	40	Bingham	0.047	2.51	1	1.89E-5
1.8	10	Bingham	0.026	3.43	1	1.33E-5
	20	Bingham	0.018	2.70	1	4.38E-6
	30	Bingham	0.011	2.23	1	2.49E-6
	40	Bingham	0.011	1.86	1	3.43E-6
1.4	10	Linear	0	3.17	1	3.61E-5
	20	Linear	0	2.48	1	8.95E-6
	30	Linear	0	2.04	1	1.50E-5
	40	Linear	0	1.75	1	7.52E-6
0.7	10	Linear	0	2.31	1	9.85E-6
	20	Linear	0	1.82	1	1.21E-5
	30	Linear	0	1.52	1	6.87E-6
	40	Linear	0	1.29	1	5.80E-6
0.4	10	Linear	0	1.95	1	3.47E-5
	20	Linear	0	1.50	1	1.47E-5
	30	Linear	0	1.25	1	6.73E-6
	40	Linear	0	1.03	1	5.19E-6

Table A.4: Summary of the parameters estimated for the models representing the rheograms (rheometric) data of slurry 2

Concentration	Temperature	Model	τ_y	K	n	$RMSE$
% TSS (wt./wt.)	$^{\circ}C$	-	Pa	$mPa.s^n$	-	Pa

3	10	HB	0.043	32.25	0.74	1.08E-4
	20	HB	0.069	12.90	0.84	2.00E-4
	30	HB	0.054	10.21	0.85	1.91E-4
	40	HB	0.040	10.38	0.81	3.23E-4
2.6	10	HB	0.048	18.30	0.80	5.49E-4
	20	HB	0.043	9.35	0.86	2.14E-4
	30	Bingham	0.074	3.43	1	9.15E-5
	40	Bingham	0.057	2.92	1	7.37E-5
2.1	10	Bingham	0.123	5.01	1	5.73E-4
	20	Bingham	0.068	3.78	1	8.70E-5
	30	Bingham	0.061	3.03	1	3.19E-5
	40	Bingham	0.047	2.67	1	1.77E-5
1.8	10	Bingham	0.076	4.39	1	1.44E-4
	20	Bingham	0.059	3.28	1	3.16E-5
	30	Bingham	0.044	2.78	1	2.77E-5
	40	Bingham	0.035	2.35	1	3.14E-5
1.2	10	Bingham	0.051	3.75	1	6.44E-5
	20	Bingham	0.040	2.94	1	2.11E-5
	30	Bingham	0.035	2.44	1	7.43E-6
	40	Bingham	0.029	2.06	1	9.06E-6
1	10	Bingham	0.042	3.39	1	2.53E-5
	20	Bingham	0.030	2.71	1	1.44E-5
	30	Bingham	0.023	2.27	1	4.43E-6
	40	Bingham	0.021	1.87	1	6.17E-6
0.8	10	Linear	0	2.41	1	2.44E-5
	20	Linear	0	1.90	1	1.89E-5
	30	Linear	0	1.59	1	6.98E-6
	40	Linear	0	1.36	1	4.92E-6

APPENDIX B

Ultrasound Imaging Velocimetry

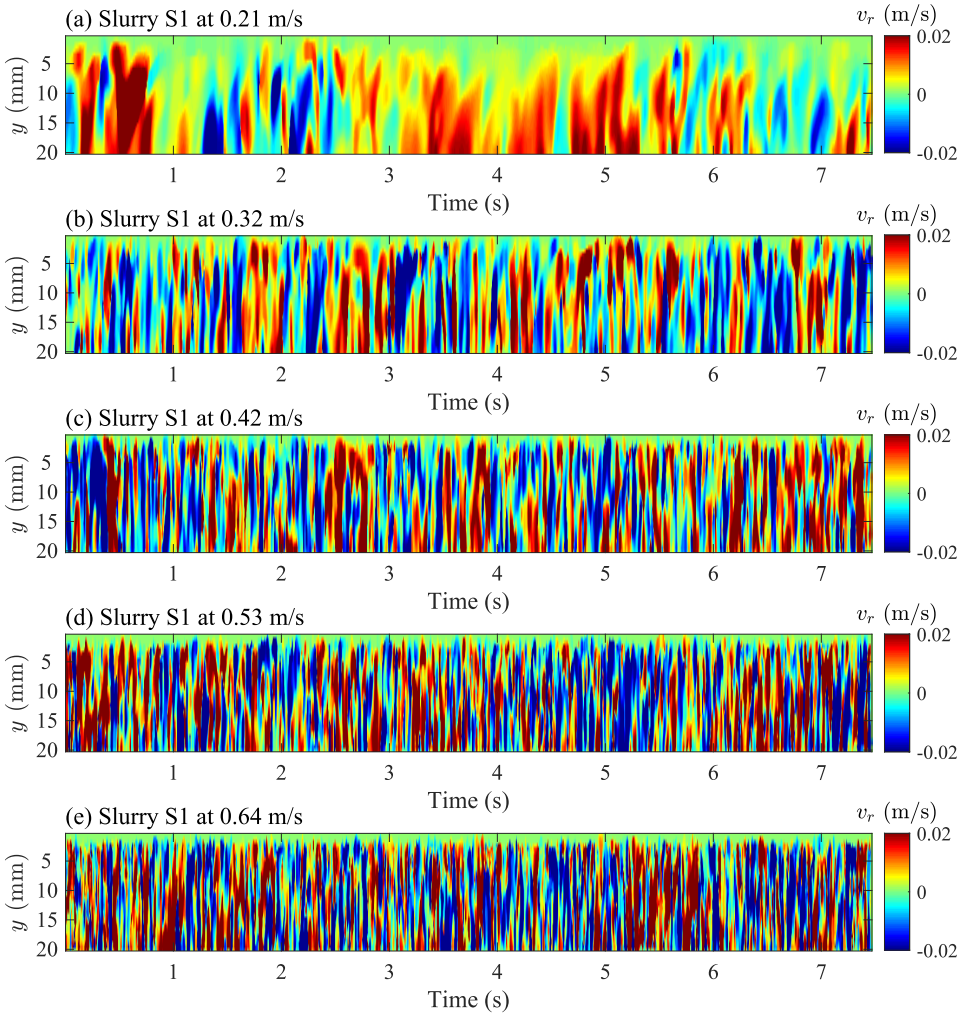

Figure B.1: Observing transition through the ultrasound velocimetry data. Plot of the radial component of the velocity vector against time as an estimate for the cross sectional plane for slurry 1.

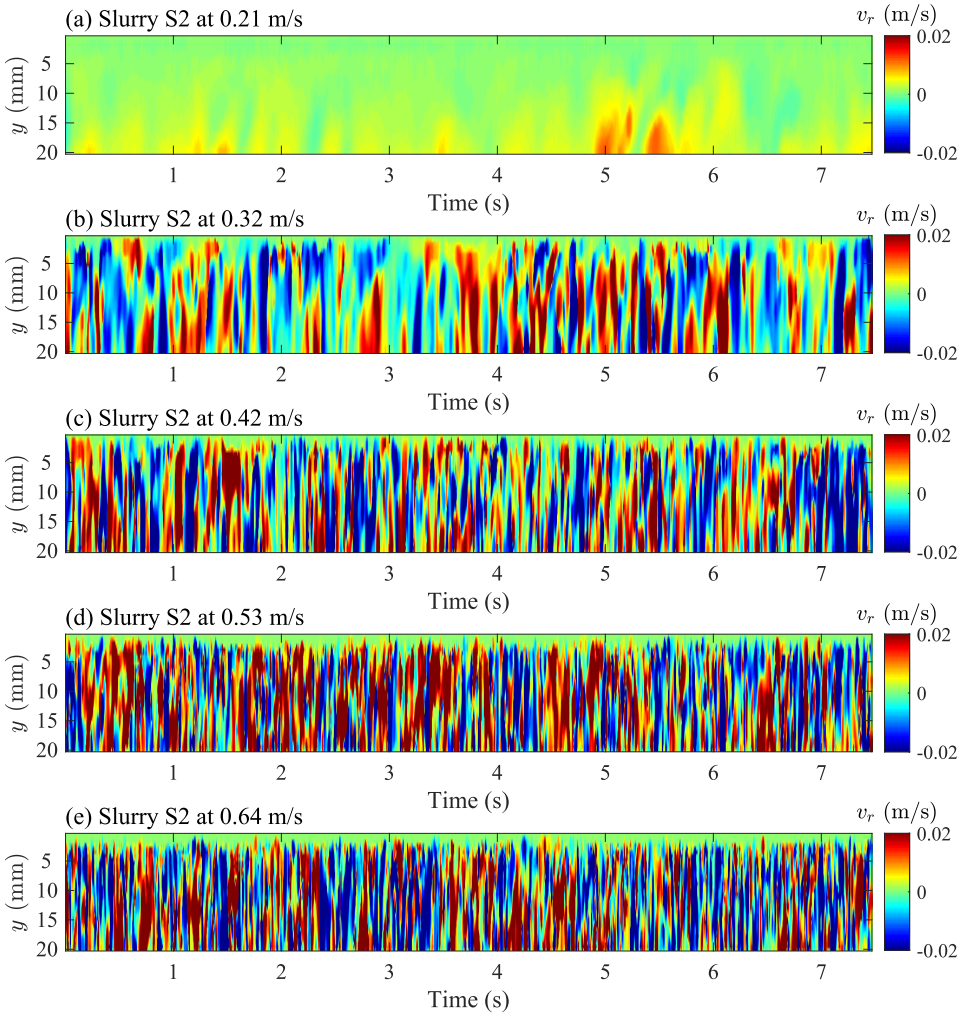

Figure B.2: Observing transition through the ultrasound velocimetry data. Plot of the radial component of the velocity vector against time as an estimate for the cross sectional plane for slurry 2.

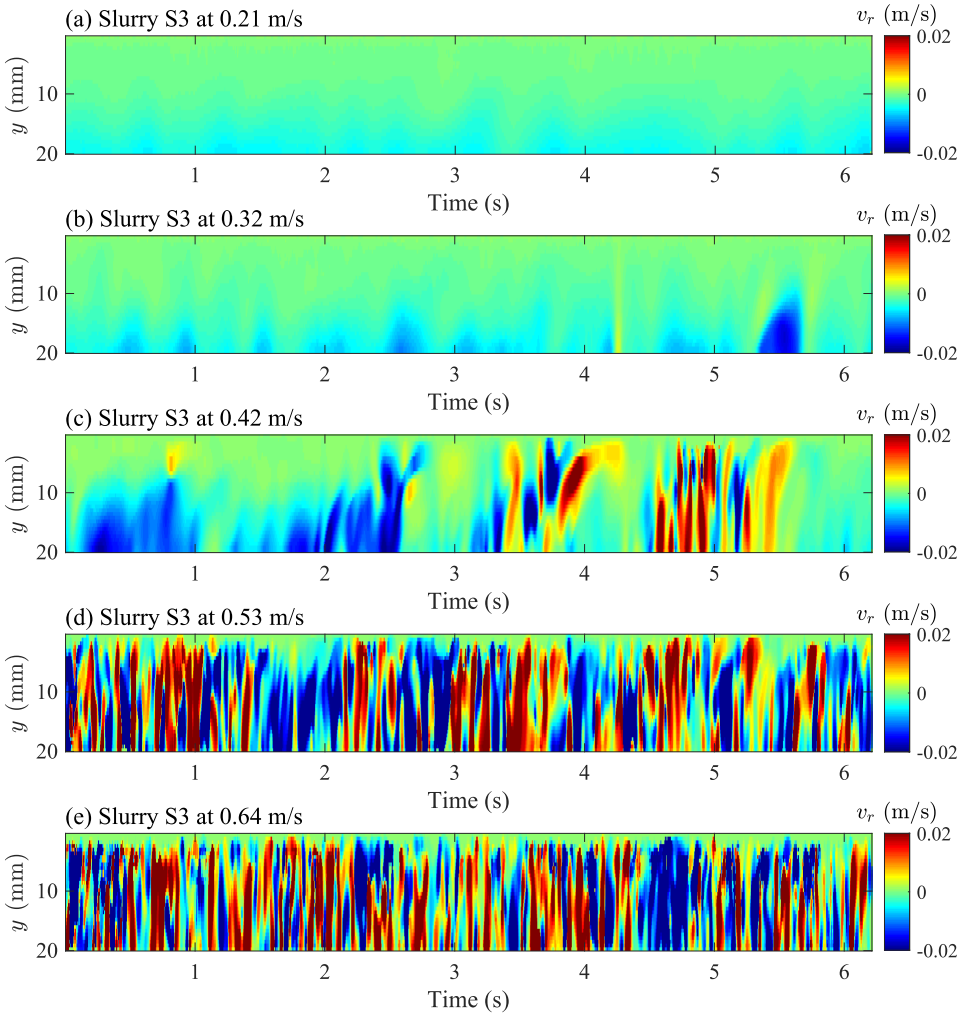

Figure B.3: Observing transition through the ultrasound velocimetry data. Plot of the radial component of the velocity vector against time as an estimate for the cross sectional plane for slurry 3.

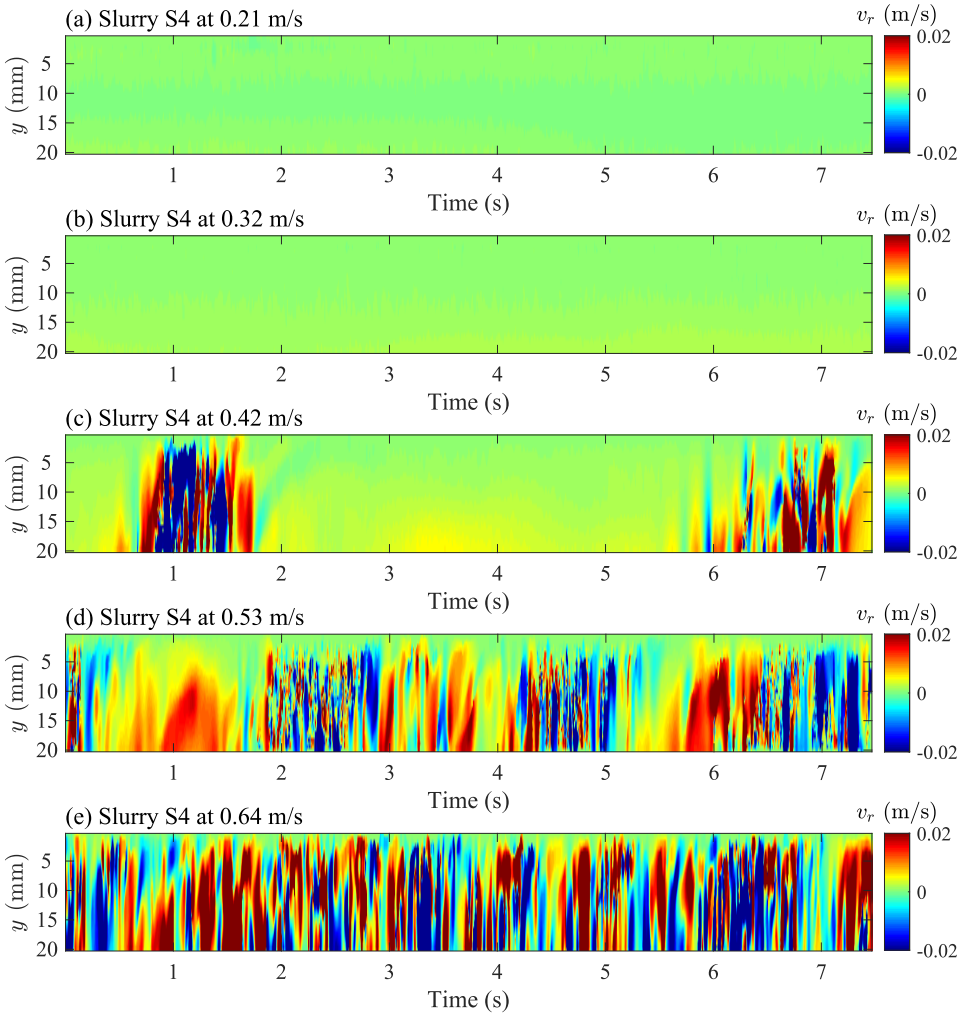

Figure B.4: Observing transition through the ultrasound velocimetry data. Plot of the radial component of the velocity vector against time as an estimate for the cross sectional plane for slurry 4.

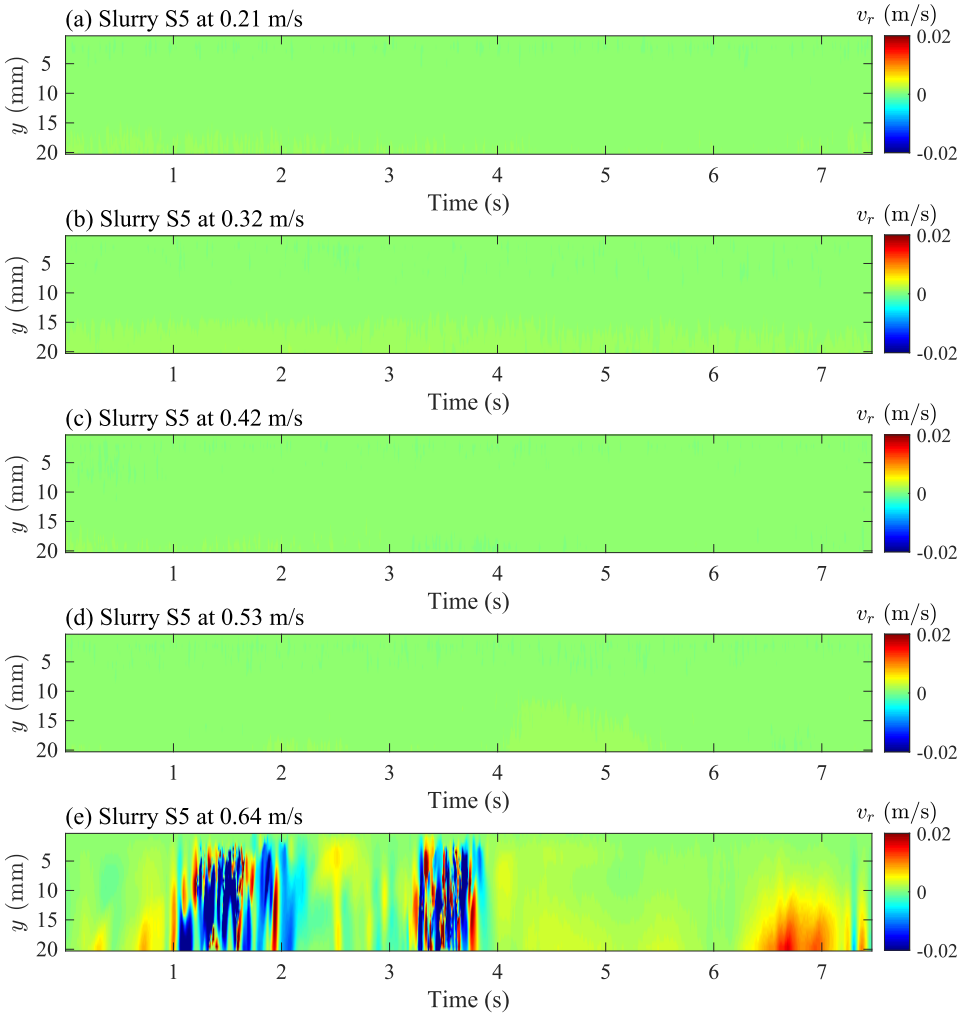

Figure B.5: Observing transition through the ultrasound velocimetry data. Plot of the radial component of the velocity vector against time as an estimate for the cross sectional plane for slurry 5.

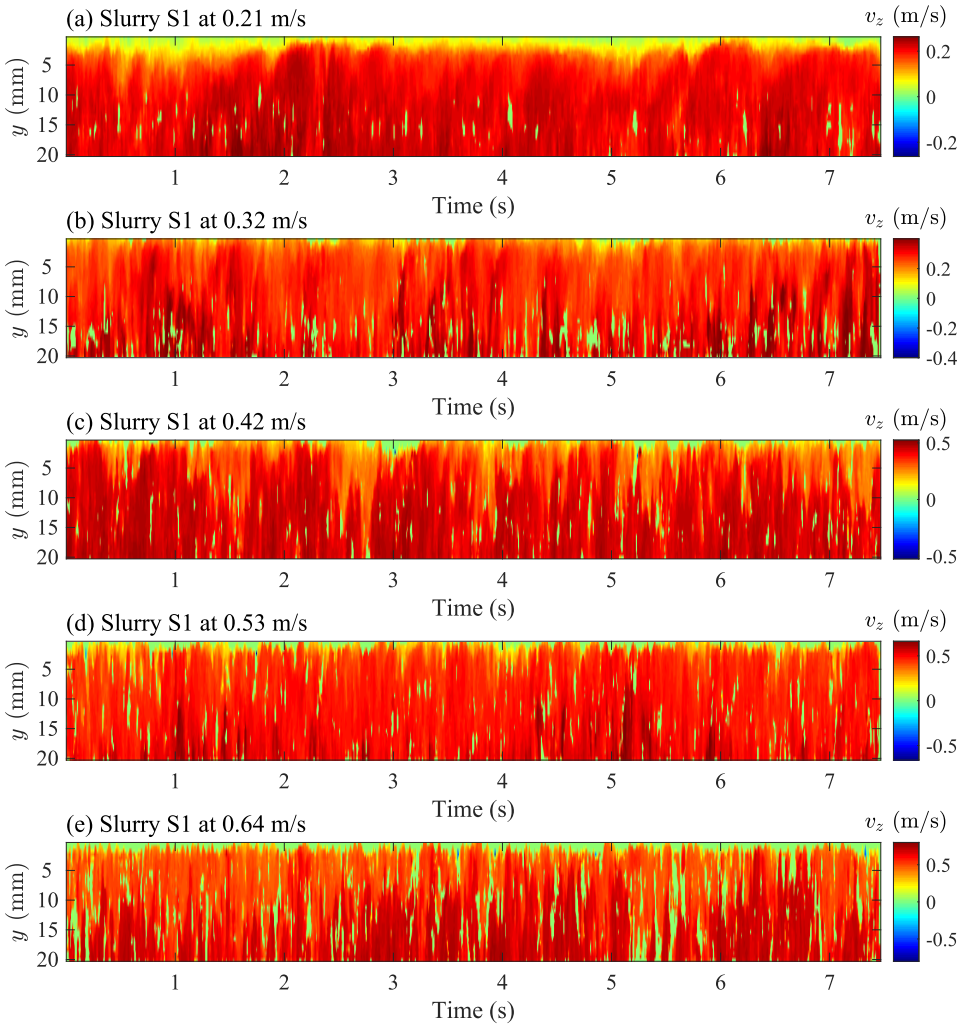

Figure B.6: Observing transition through the ultrasound velocimetry data. Plot of the axial component of the velocity vector against time as an estimate for the cross sectional plane for slurry 1.

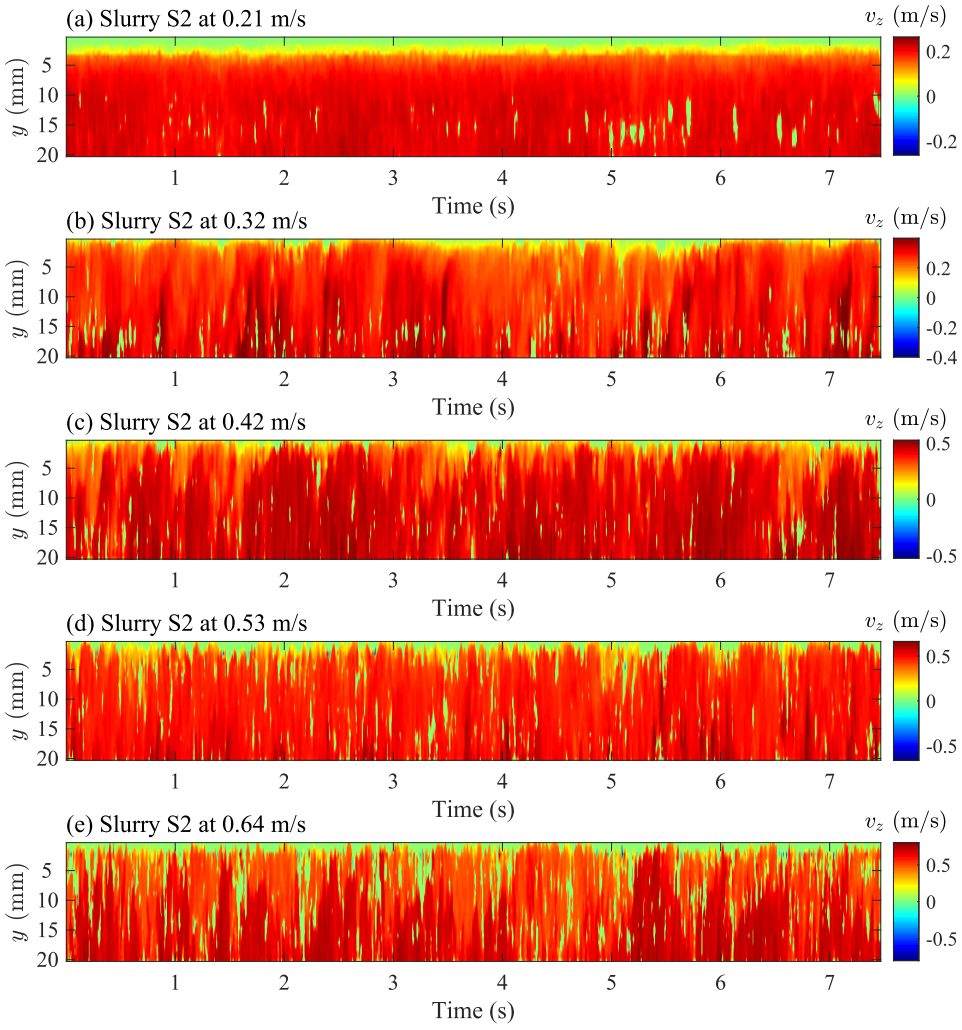

Figure B.7: Observing transition through the ultrasound velocimetry data. Plot of the axial component of the velocity vector against time as an estimate for the cross sectional plane for slurry 2.

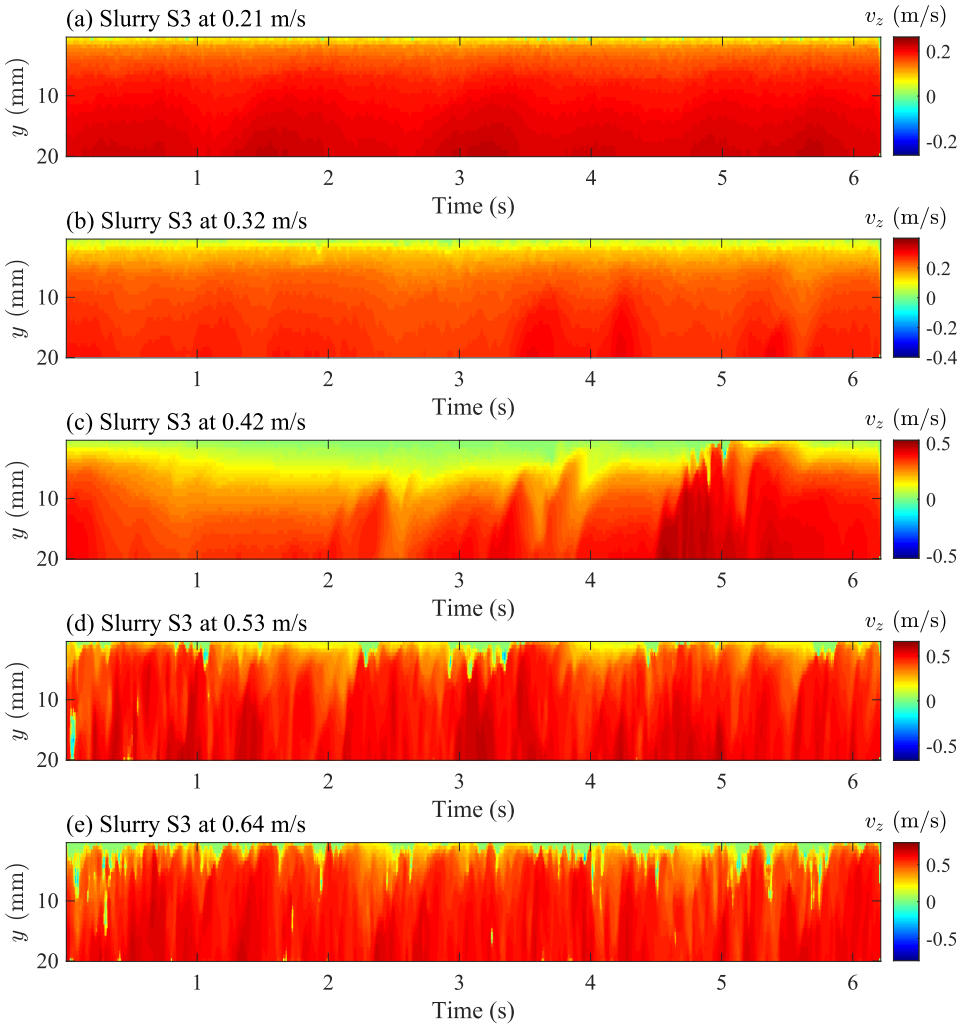

Figure B.8: Observing transition through the ultrasound velocimetry data. Plot of the axial component of the velocity vector against time as an estimate for the cross sectional plane for slurry 3.

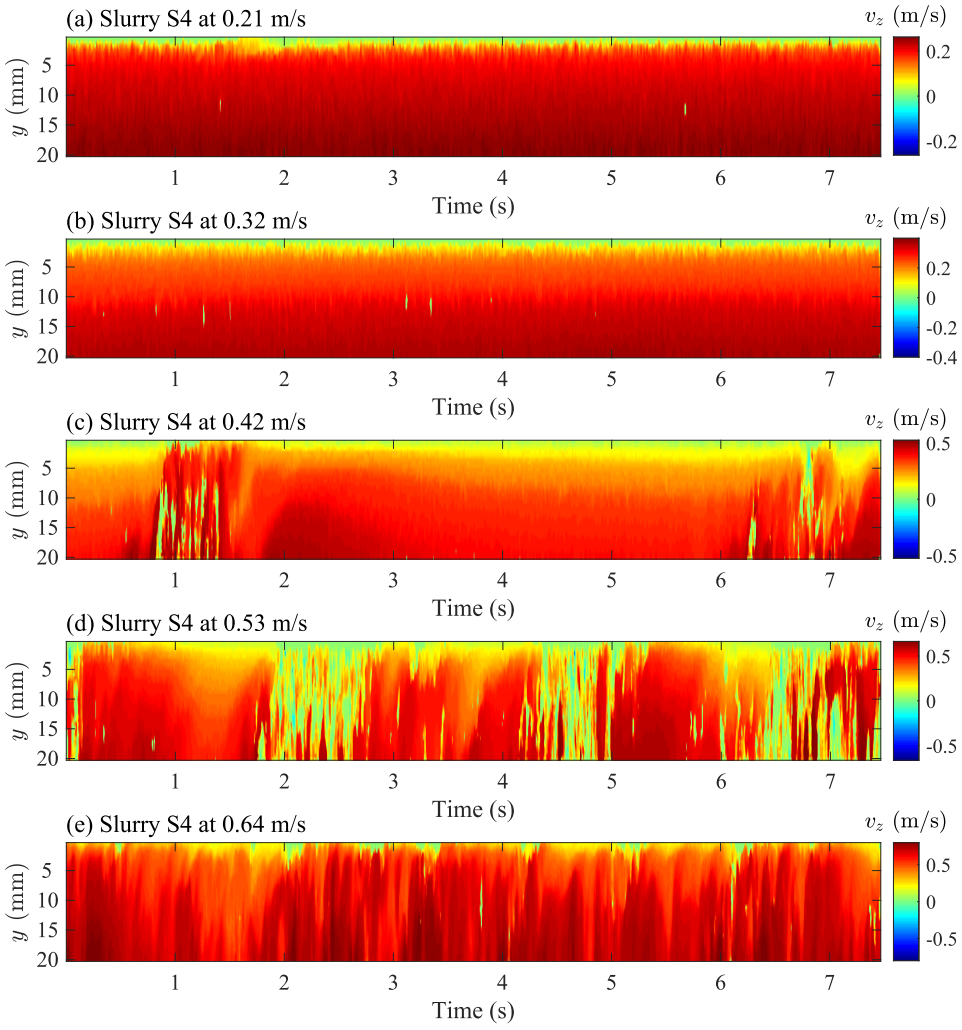

Figure B.9: Observing transition through the ultrasound velocimetry data. Plot of the axial component of the velocity vector against time as an estimate for the cross sectional plane for slurry 4.

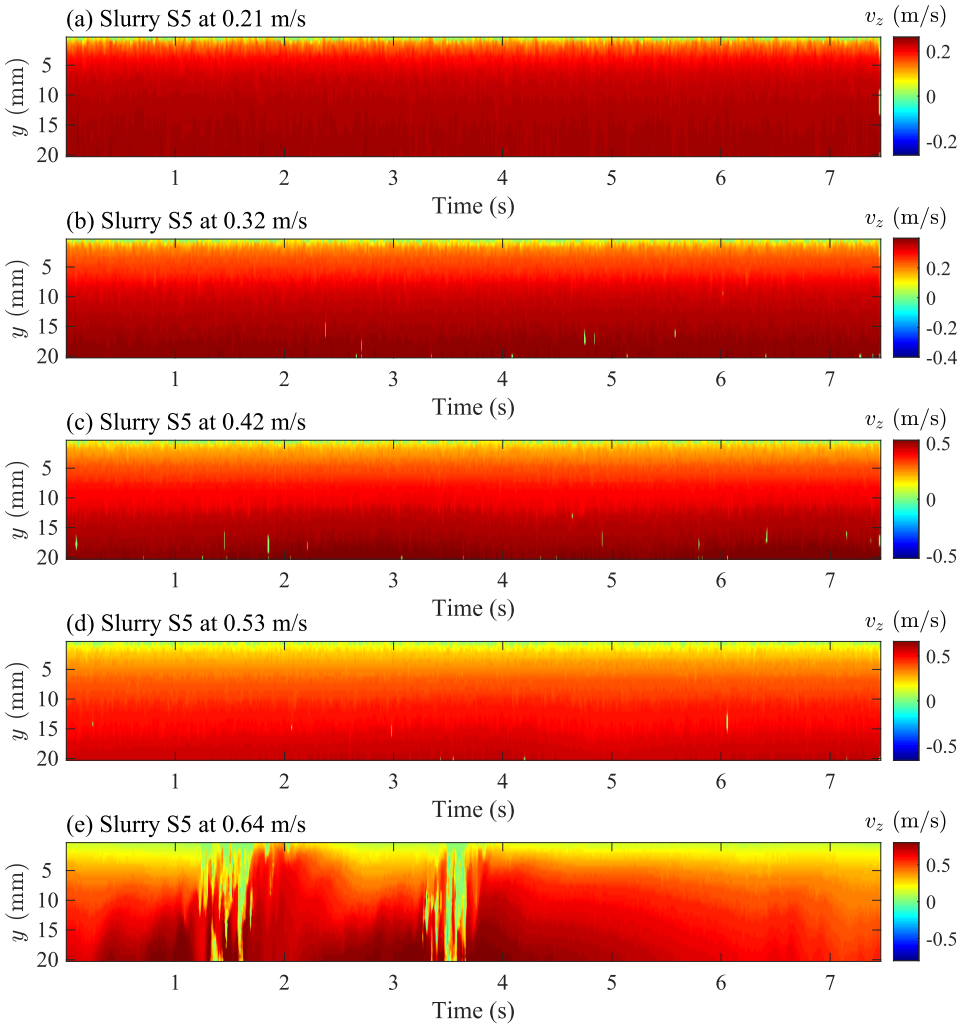

Figure B.10: Observing transition through the ultrasound velocimetry data. Plot of the axial component of the velocity vector against time as an estimate for the cross sectional plane for slurry 5.

APPENDIX C

Semi-Empirical Models

C.1 Tomita

Tomita's approach begins with the laminar equations to find a relationship between the average flow velocity V and the rheological properties of the fluid in question (PL and BP, in this case). For a BP fluid,

$$V = \frac{R\tau_y}{K} \underbrace{\left(\frac{\zeta^4 - 4\zeta + 3}{12\zeta}\right)}_{\alpha} \tag{C.1}$$

Further, the velocity of the plug or V_p , in the region $0 \leq r \leq r_p$ is,

$$V_p = \frac{R\tau_y}{K} \frac{(1-\zeta)^2}{2\zeta} \tag{C.2}$$

whereas the velocity at a radial distance r in the region $r_p \leq r \leq R$ is,

$$v(r) = \frac{\tau_y}{2r_p K}(R^2 - 2R_p + 2rr_p - r^2) \tag{C.3}$$

Next, the total shear stress at a distance r, which must equal the pressure gradient, is expressed as the sum of the laminar and turbulent contributions, in keeping with Prandtl's theory (Prandtl, 1933). For a BP fluid,

$$\tau_y + K\dot{\gamma} + \overline{\rho u'v'} = \left(\frac{\Delta p}{L}\right)\frac{r}{2} \tag{C.4}$$

where ρ is the density of the fluid and $\overline{\rho u'v'}$ is the Reynolds stress. When integrated for a laminar flow, eq. C.4 leads to the following relationship for pressure loss (see (Assefa and Kaushal, 2015) for details),

$$\left(\frac{\Delta p}{L}\right)_B = \frac{2VK}{R^2\zeta\alpha} \tag{C.5}$$

After non-dimensionalising eq. C.5, two non-dimensional numbers were obtained, which for the laminar flow of BP fluids are related through,

$$\frac{\rho V^2}{\tau_y} = \frac{\rho V R}{K}\alpha \tag{C.6}$$

The right-hand side of eq. C.6 is similar to the Reynolds number. Tomita used this similarity to analyse the turbulent flow of a BP fluid as an imaginary laminar flow with an average flow velocity V equal to that of a turbulent flow. This led to the deduction of a suitable friction factor for BP fluids. For completeness, the analysis is described here in brief.

The pressure gradient in case of a Newtonian fluid can be related to V, D and through,

$$\frac{1}{\rho}\frac{\Delta p}{L} = \frac{4f_N}{2D}V^2 \tag{C.7}$$

where f_N is the Fanning friction factor for a Newtonian fluid. Tomita further proposed that the dissipation for a BP, as opposed to a Newtonian fluid, is only due to the viscosity acting outside the plug region therefore, V^2 in eq. C.7 should represent the average velocity outside the plug. As a result, eq. C.7 is modified as,

$$\frac{1}{\rho}\frac{\Delta p}{L} = \frac{4f_*}{2D}V_*^2 \tag{C.8}$$

V_*^2 is obtained by integrating the square of eq. C.3 in the region $rp \leq r \leq R$ as,

$$V_*^2 = \frac{2}{R^2}\int_{r_p}^{R} rv(r)^2 dr = \frac{\tau_w^2 R^2}{60K^2}(1-\zeta)^4(5+6\zeta-11\zeta^2) \tag{C.9}$$

Further, using $\zeta = \tau_y/\tau_w$ in eq. C.1, one can relate V_*^2 and V^2 through,

$$V_*^2 = \frac{4}{3}.\underbrace{\frac{9}{5}\frac{(5+6\zeta-11\zeta^2)}{(3+2\zeta+\zeta^2)^2}}_{F(\zeta)}V^2 \tag{C.10}$$

Therefore, the friction factor can now be defined on the basis of similarity as

$$\frac{1}{\rho}\frac{\Delta p}{L} = \frac{4f_B}{2D}V^2F(\zeta) \tag{C.11}$$

where f_B is the friction factor for a BP fluid. Tomita considered simplifying $F(\zeta)$ as $(1-\zeta)$. Further, Fanning's relationship for a Newtonian fluids implies

$$f_N Re = 16 \tag{C.12}$$

which Tomita proposed must also be satisfied by BP fluids described using an appropriate friction factor and Reynolds number. Therefore, using eq. C.5 and eq. (C.10-C.12), Tomita obtained the following,

$$f_B = \frac{\tau_w}{\frac{1}{2}\rho V^2 F(\zeta)} \tag{C.13}$$

$$Re_B = \frac{\rho DV}{K}4\zeta\alpha F(\zeta) = \frac{\rho DV}{K}F(\zeta)\frac{(\zeta^4-4\zeta+3)}{3} \tag{C.14}$$

As mentioned earlier, $F(\zeta)$ in eq. (C.13-C.14) was simplified as $(1-\ zeta)$. Tomita also carried out the above procedure for a PL fluid to obtain f_{PL} and Re_{PL} such that,

$$f_{PL} = \frac{\tau_w}{\frac{1}{2}\rho V^2} \underbrace{\frac{4}{3}\frac{(2n+1)}{(3n+1)}}_{\frac{1}{G(n)}} \tag{C.15}$$

$$Re_{PL} = 6\frac{\rho D^n V^{2-n}}{K}(\frac{3n+1}{n})^{1-n}(\frac{n}{2n+1})\frac{1}{2n} = \frac{1}{8^{n-1}}\frac{\rho D^n V^{2-n}}{K}G(n)(4-\frac{3}{G(n)})^n \tag{C.16}$$

$$(\frac{\Delta p}{L})_{PL} = 2^{n+2}K(\frac{3n+1}{n})^n\frac{V^n}{D^{n+1}} \tag{C.17}$$

$$f_{PL}Re_{PL} = 16 \tag{C.18}$$

The final step involves finding a relation between the mean flow velocity and the wall shear-stress. This is done using eq. C.4 in which, the turbulent stress is rewritten in terms of the mixing length introduced by Prandtl (1933). Eq. C.4 then reads,

$$\tau_y + K\dot{\gamma} + \rho\kappa^2 y^2(\frac{\partial v}{\partial y})^2 = (\frac{\Delta p}{L})\frac{(R-y)}{2} \tag{C.19}$$

For a BP fluid, $K\dot{\gamma}$ is neglected and the right-hand side is rewritten in terms of the wall shear stress leading to,

$$\tau_y + \rho\kappa^2 y^2(\frac{\partial v}{\partial y})^2 = \tau_w(1-\frac{y}{R}) \tag{C.20}$$

Eq. 6.11 can be used to modify τ_y and rewrite it in terms of τ_w. Another modification needed here for the term $(1y/R)$. Near the wall, this term is close to unity, so eq. C.20 could be written as,

$$\rho\kappa^2 y^2(\frac{\partial v}{\partial y})^2 = \tau_w(1-\zeta) \tag{C.21}$$

Although the above should ideally hold only when $y << R$, eq. C.21 correlates well with experimental data in turbulent regions away from the wall, at least for Newtonian fluids. Tomita made the same assumption for BP fluids and upon integrating eq. C.21 obtained,

$$\frac{v_p - v}{v_*} = \frac{\sqrt{1-\zeta}}{\kappa}ln(\frac{R(1-\zeta)}{y}) \tag{C.22}$$

For succinctness, the steps that follow are not detailed but can be found in TOMITA (1959). On integrating eq. C.22, one finds a relation between v_p and V. Using this, eq. C.22 is modified as follows,

$$\frac{v}{v_*} = A\sqrt{1-\zeta} + B\sqrt{1-\zeta}ln(Re_B\frac{y}{R(1-\zeta)}\frac{\sqrt{2}u^*}{V\sqrt{F(\zeta)}}) \tag{C.23}$$

which when rewritten using the relationship between v_p and V reads,

$$\frac{1}{\sqrt{f_B}} = (A - \frac{(1-\zeta)(\zeta+3)}{2\kappa})\sqrt{\frac{F(\zeta)(1-\zeta)}{2}} + B\sqrt{\frac{F(\zeta)(1-\zeta)}{2}}ln(Re_B\sqrt{f_B}) \tag{C.24}$$

The contants A and B in eq. C.23 and C.24 are different from the ones in TOMITA (1959), wherein they were obtain from the integration and modified to incorporate $\sqrt{2}$. However, here, these are adjusted to accommodate an equation that is consistent for the three

types of non-Newotnian fluids considered.

Finally, with the assumption that for a turbulent flow and a reasonably high V, the wall shear-stress would be high enough for $<< 1$, implying that the $\sqrt{F(\zeta)(1-\zeta)}$ becomes close to 1, eq. C.24 was regressed against experimental data points to obtain,

$$\frac{1}{\sqrt{f_B}} = 4log(Re_B\sqrt{f_B}) - 0.38 \tag{C.25}$$

which when $_y = 0$, coincides with the relationship for a Newtonian fluid that was proposed by Nikuradse (1933). Similarly, beginning with Prandtl's equation for a PL fluid,

$$K\dot{\gamma}^n + \rho\kappa^2 y^2(\frac{\partial v}{\partial y})^2 = \tau_w(1 - \frac{y}{R}) \tag{C.26}$$

while making the assumptions made for BP fluids earlier, Tomita obtained,

$$\frac{v_p - v}{v_*} = \frac{1}{\kappa}ln(\frac{R}{y}) \tag{C.27}$$

Integration eq. C.27 for a relationship between v_p and V, and following the steps for eq. (C.23-C.24), Tomita proposed the PL equivalent for eq. C.24 as,

$$\frac{1}{\sqrt{f_{PL}}} = (A - \frac{3}{2\kappa})\sqrt{\frac{G(n)}{2}} + B\sqrt{\frac{G(n)}{2}}ln(Re_{PL}\sqrt{f_{PL}}) \tag{C.28}$$

which upon regression against experimental data was presented by Tomita as,

$$\frac{1}{\sqrt{f_{PL}}} = 4log(Re_{PL}\sqrt{f_{PL}}) - 0.38 \tag{C.29}$$

In either case (BP or PL), the friction factor, Reynolds number and the parameter ζ (for BP only) is obtain through the laminar relations detailed at the beginning of this section.

Tomita assumed that these laminar relations also hold for turbulent flows. In this study, the authors followed Tomita's procedure to derive an equivalent expression for HB fluids. The process is not detailed here for brevity, but is similar to the ones derived for PL and BP fluids mentioned earlier. The foremost assumption is that the equivalent friction factor and Reynolds numbers (also ζ in this case), derived for the laminar flow of HB fluids, also hold for turbulent flows. These expressions are as follows (see Section 6.1 for details),

$$v(r) = \frac{nR}{n+1}(\frac{\tau_w}{K})^{\frac{1}{n}}\{(1-\zeta)^{\frac{n+1}{n}} - (\frac{r}{R} - \zeta)^{\frac{n+1}{n}}\} \tag{C.30}$$

$$V = \frac{nR}{n+1}(\frac{\tau_w}{K})^{\frac{1}{n}}(1-\zeta)^{1+\frac{1}{n}}\underbrace{\{\frac{n+1}{3n+1}(1-\zeta)^2 + \frac{n+1}{2n+1}2\zeta(1-\zeta) + \frac{1}{n+1}\zeta^2\}}_{\alpha_{HB}} \tag{C.31}$$

$$v_p = \frac{nR}{n+1}(\frac{\tau_w}{K})^{\frac{1}{n}}(1-\zeta)^{1+\frac{1}{n}} \tag{C.32}$$

$$\tau_y + K\dot{\gamma}^n + \rho\kappa^2 y^2(\frac{\partial v}{\partial y})^2 = (\frac{\Delta p}{L})\frac{r}{2} \tag{C.33}$$

On removing the turbulent term from eq. C.33, replacing $\dot{\gamma}$ as $\partial v/\partial r$ and integrating the equation, one obtains an expression for the pressure gradient, similar to eq. C.5 derived by Tomita.

$$(\frac{\Delta p}{L})_{HB} = \frac{2KV^n}{\alpha_{HB}^n R^{n+1}} \frac{1}{(1-\zeta)^{n+1}} (\frac{n+1}{n})^n \tag{C.34}$$

Checking for consistency, eq. C.34 reduces to eq. C.5 for n=1. As per Tomita's argument, the pressure drop should be related to a friction factor such that, the value of the velocity used in eq. C.8, should in a way be obtained as an average of the flow outside the plug, which is directly responsible for frictional losses. Therefore, for an HB fluid, integrating the square of eq. C.30 in the region $r_p \leq r \leq R$ as done in eq. C.9, to obtain a suitable V_*^2, which can be related to eq. C.31 as,

$$V_*^2 = \frac{4}{3} \underbrace{\{\frac{3}{4} \frac{(2n+1)(3n+1)}{(3n+2)} \frac{(n+1)^2(3n+2+6n\zeta-(9n+2)\zeta^2)}{((2n+1)(n+1)+2n(n+1)\zeta+2n^2\zeta^2)^2}\}}_{H(\zeta,n)} V^2 \tag{C.35}$$

In eq. C.35, the term $H(\zeta, n)$ is a function of both the ratio of the yield stress to the wall shear-stress and the behaviour index for an HB fluid. By setting $n = 1$, one obtains eq. C.10 for a BP fluid and for $\zeta = 0$, one obtains the following for a PL fluid, indicating that eq. C.35 is a consistent extension of Tomitas concept,

$$V_*^2 = \frac{4}{3} \underbrace{\{\frac{3}{4} \frac{(3n+1)}{(2n+1)}\}}_{G(n)} V^2 \tag{C.36}$$

Extending Tomitas proposal that the equation $f_N Re = 16$ should also hold for HB fluids with the relevant friction factor and Reynolds number, one obtains the following set of relations for HB fluids,

$$f_{HB} = \frac{\tau_w}{\frac{1}{2}\rho V^2} \frac{1}{H(\zeta, n)} \tag{C.37}$$

$$Re_{HB} 8 \frac{\rho V^{2-n}}{K} h(\zeta, n) (\frac{n}{n+1} \alpha_{HB} R (1-\zeta)^{1+\frac{1}{n}})^n \tag{C.38}$$

Next, the steps illustrated through eq. (C.20-C.25) are repeated using eq. C.33. For a turbulent flow, the laminar contribution through $K\dot{\gamma}$ can be ignored while retaining τ_y, leading to the set of equations Tomita derived for BP fluids. However, the modification done in eq. C.23, can be adjusted for HB fluids leading to,

$$\frac{1}{\sqrt{f_{HB}}} = (A - \frac{(1-\zeta)(\zeta+3)}{2\kappa}) \sqrt{\frac{H(\zeta,n)(1-\zeta)}{2}} + B \sqrt{\frac{H(\zeta,n)(1-\zeta)}{2}} ln(Re_{HB}\sqrt{f_{HB}}) \tag{C.39}$$

One can verify that eq. C.38 reduces to that for a PL fluid by setting $\zeta = 0$ and to that for a BP fluid by setting $n = 1$. Further, for $\zeta = 0$ and $n = 1$, one must obtain the Nikuradse expression for Newtonian fluids, as Tomita's expression consistently did. This helps one set the values of A and B. The final expression reads,

$$\frac{1}{\sqrt{f_x}} = (3.31 - \frac{(1-\zeta)(\zeta+3)}{2\kappa}) \sqrt{\frac{H(\zeta,n)(1-\zeta)}{2}} + 2.49 \sqrt{\frac{H(\zeta,n)(1-\zeta)}{2}} ln(Re_x\sqrt{f_x}) \tag{C.40}$$

where x can be either types of non-Newtonian fluids considered so far (and even a Newtonian fluid with $H(\zeta, n) = 1$ and $\zeta = 1$). Eq. C.40 is solved iteratively to evaluate the wall shear-stress for a given non-Newtonian fluid and flow conditions.

C.2 Dodge & Metzner

C.2.1 DM approach extended to HB fluids

Skelland (1967) explains the approach followed by DM in a simple manner. First, DM used the Buckingham π (Buckingham, 1914) theorem (dimensional analysis) to establish a relation between $v(r)$ at any radial location (see Figure 6.1) and the radius of the pipe R, the wall shear-stress and the rheological parameters. Next, a similar relation was derived between v_* near the wall and the maximum velocity in the core v_p, and the rheological parameters.

This is followed by a relationship between the velocity defect or $v_p - V$ and the relevant parameters. Ultimately, the equations obtained by using the Buckingham π theorem are combined to relate a suitable friction factor and the flow conditions. For brevity, only the relevant final equations for an HB fluid are described here. The original equations for a PL fluid by DM, are described in Skelland (1967).

A major difference between the analysis of PL fluids by DM and the HB extension here, is the presence of a plug. As per Tomita, it is important to consider the region outside the plug as it is in this region that frictional losses actually occur, contributing to the eventual wall shear-stress. Therefore, instead of relating the velocities mentioned in the previous paragraphs to the wall shear-stress, the velocities will be related to $_w - _y$. The final equations with the symbols used by DM are

$$\frac{v}{v_{\tau_{HB}}} = \overbrace{h_1}^{0\leq r\leq R}\left(\underbrace{v_{\tau_{HB}}^{2-n}\frac{R^n\rho}{K}}_{Z}, \underbrace{\frac{R-r}{R}}_{\xi}, n\right) \tag{C.41}$$

$$\frac{v}{v_{\tau_{HB}}} = \overbrace{h_2}^{r\to R}(Z\xi^n, n) \tag{C.42}$$

$$\frac{v_p - v}{v_{\tau_{HB}}} = \overbrace{h_3}^{0\leq r\leq r_p}(\xi, n) \tag{C.43}$$

In the above equations, $v_{_{HB}}$ is a special case of the friction velocity (v_τ) for HB fluids. It is defined as,

$$v_{\tau_{HB}} = \underbrace{v_\tau}_{\sqrt{\frac{\tau_w}{\rho}}}\sqrt{1-\zeta} \tag{C.44}$$

Further, h_1, h_2 and h_3 are arbitrary functions of the non-dimensional terms contained within the functions brackets and deduced using the Buckingham π theorem. Eq. (C.41-C.43) are combined to obtain the velocity deficit, as done by DM, leading to,

$$\frac{v_p - V}{v_{\tau_{HB}}} = D_n \tag{C.45}$$

where D_n is a dimensionless function of n. With all these equations, one obtains a relationship between the friction factor of an HB fluid and the flow parameters (similar to DM) as,

$$\sqrt{\frac{2}{f_{HB}}} = H_1(Z,n) - D_n \tag{C.46}$$

In eq. C.46, $H_1(Z,n)$ is the value of $h_1(Z,\xi,n)$ at the centreline (or $\xi = 1$). f_{HB} is the friction factor for HB fluids, defined in this case as,

$$f_{HB} = \underbrace{\frac{\tau_w}{\frac{1}{2}\rho V^2}}_{f_N}(1-\zeta) \tag{C.47}$$

Although f_N is the same as previously in eq. C.7, f_{HB} derived here is different from the one derived using Tomita's procedure through eq. C.37. Further analysis as defined in Skelland (1967) for PL fluids, when done for HB fluids, leads to the following equation, similar to what DM derived but with parameters defined for HB fluids instead of PL fluids.

$$\frac{1}{\sqrt{f_{HB}}} = \underbrace{1.63A_n}_{A_{1n}} log(\underbrace{\frac{\rho D^n V^{2-n}}{K}}_{N^0_{Re}} . f_{HB}^{1-\frac{n}{2}}) - \underbrace{0.49A_n(1+\frac{n}{2}) + \frac{B_n - D_n}{\sqrt{2}}}_{C_n} \tag{C.48}$$

where A_n is also a function of n. For a PL fluid, the above equation as proposed by DM contains f_n instead of f_{HB}, as the friction factor for a fluid with zero yield stress is effectively f_N, as per eq. C.47.

N^0_{Re} as a modified Reynolds number, produces a family of curves depending on the value of n, instead of a unique relationship between the Reynolds number and the friction factor for a laminar flow (Metzner and Reed, 1955). Instead, the protocol put forth by Rabinowitsch (1929) and Mooney (1931) was extended to PL fluids to find a suitable Reynolds number to be used in eq. C.48 (Dodge and Metzner, 1959; Metzner and Reed, 1955).

C.2.2 A Reynolds number for HB fluids

The Rabinowitsch-Mooney (RM) criterion establishes that for a laminar flow through a circular tube, the relationship between the pseudo shear rate $8V/D$ and the wall shear-stress is unique as long as the shear-stress is a function of the shear-rate (for time-independent fluids). Just as one uses the Newtonian viscosity determined under laminar conditions for turbulent flows, DM proposed that the unique relationship established for non-Newtonian fluids with the RM criterion, could be extended to turbulent flows too. As per RM, the wall shear-stress can be related to $8V/D$ as,

$$\tau_w = \frac{D\Delta p}{4L} = K'(\frac{8V}{D})^{n'} \tag{C.49}$$

where n' is obtained using

$$n' = \frac{dln(\frac{D\Delta p}{4L})}{dln(\frac{8V}{D})} \tag{C.50}$$

Metzner and Reed (1955) extended the RM criterion to define the generalised Reynolds number as,

$$N_{Re-Gen} = \frac{\rho D^{n'} V^{2-n'}}{K' 8^{n'-1}} \tag{C.51}$$

Further, the RM criterion also states that the shear-rate at the wall $\dot{\gamma}_w$ is,

$$\dot{\gamma}_w = \frac{3n'+1}{4n'}\frac{8V}{D} \tag{C.52}$$

DM used the above criteria to propose the following Reynolds number for PL fluids to be used in eq. C.48,

$$N_{Re-Gen_{PL}} = \frac{\rho D^n V^{2-n}}{8^{n-1}K(\frac{3n+1}{4n})^n} = 8N^0_{Re}(\frac{n}{6n+2})^n \tag{C.53}$$

N^0_{Re} is defined in eq. C.48. Further, to prevent the loss of generality, the n is replaced with n'. For a PL fluid $n' = n$. Eq. C.48 when written for PL fluid (as proposed by DM) finally reads,

$$\frac{1}{\sqrt{f_{PL}}} = A_{1n}log(N_{Re-Gen_{PL}} f_{PL}^{1-\frac{n'}{2}}) + \underbrace{A_{1n}log(\frac{1}{8}(\frac{6n'+2}{n'})^{n'}) + C_n}_{C_{n'}} \tag{C.54}$$

DM determined the constants A_{1n} and $C_{n'}$ as follows,

$$A_{1n} = \frac{4}{(n')^{0.75}} \qquad\qquad C_{n'} = \frac{-0.4}{(n')^{1.2}} \tag{C.55}$$

In terms of consistency, eq. C.54 reduces to the Nikuradse equation for $n' = n = 1$. DM did not extend their results to HB fluids as they demonstrated in the article from Dodge and Metzner (1959) that eq. C.54 also works well for fluids with a non-zero yield stress.

Using the RM criterion, n' is derived for an HB fluid and $N_{Re-Gen_{HB}}$, a procedure that is also followed in the work from Chilton and Stainsby (1998). n' for an HB fluid is,

$$n' = \frac{n\theta}{1-3n\theta} \tag{C.56}$$

where θ is defined as follows (symbols are the ones used by Chilton and Stainsby (1998) for consistency),

$$\theta = \frac{1}{3n+1}(1 - \underbrace{\frac{1}{2n+1}}_{a}\zeta - \underbrace{\frac{2n}{(2n+1)(n+1)}}_{b}\zeta^2 - \underbrace{\frac{2n^2}{(2n+1)(n+1)}}_{c}\zeta^3) \tag{C.57}$$

For brevity, the procedure used to obtain $8V/D$ (for laminar flows as per RM) and K' for a general fluid is not detailed here. For an HB fluid these are,

$$(\frac{8v}{D})_{HB} = \frac{4}{K^{\frac{1}{n}}}\frac{1}{\tau_w^3}\phi \tag{C.58}$$

$$K'_{HB} = \frac{\tau_w^{3n'+1}}{4^{n'}}\frac{1}{\phi^{n'}}K^{\frac{n'}{n}} \tag{C.59}$$

where ϕ is,

$$\phi = n\tau_w^{3+\frac{1}{n}}(1-\zeta)^{\frac{1}{n}}\theta \tag{C.60}$$

Combining the above, $N_{RE-Gen_{HB}}$ is obtained as defined by eq. C.51,

$$N_{Re-Gen_{HB}} = \frac{\rho D^{n'} V^{2-n'}}{8^{n'1}}\frac{4^{n'}}{\tau_w^{3n'+1}}\frac{\phi}{K^{\frac{n'}{n}}} \tag{C.61}$$

CS suggested a simplified version of eq. C.61, which does not contain the parameters K' and n'. Further, eq. C.61 can also be expressed in terms of N_{Re}^{0} as proposed by DM.

$$N_{Re-Gen_{HB}} = \frac{\rho V D}{K} \frac{1}{(\frac{8V}{D})^{n-1}} (44\theta)^{n} (1-\zeta) = N_{Re}^{0} \frac{(4n\theta)^{n}(1-\zeta)}{8^{n-1}} \tag{C.62}$$

It can be verified that eq. C.62 is same as eq. C.53 should $\zeta = 0$ (PL fluid). It is fair to mention at this point that CS deemed this Reynolds number to not be physically realistic for turbulent flows as the entire derivation was based on a laminar velocity profile. Instead, they proposed a new Reynolds number based on the wall-effective viscosity defined as the ratio of the wall shear-stress to the shear-rate at the wall,

$$\eta_w = \frac{\tau_w}{\dot{\gamma}_w} \tag{C.63}$$

$\dot{\gamma}_w$ can be calculated from eq. 6.5 by setting the shear-stress equal to the wall shear-stress, which ultimately provides the means to calculate η_w,

$$\eta_w = \frac{K^{\frac{1}{n}} \tau_w}{(\tau_w - \tau_y)^{\frac{1}{n}}} \tag{C.64}$$

The procedure for deriving the Reynolds number based on the wall-effective viscosity is illustrated by Chilton and Stainsby (1998); the Reynolds number so obtained is,

$$Re_{CS} = \frac{\rho V D}{\eta_w} 4n\theta \tag{C.65}$$

For extending eq. C.54 to HB fluids, the Reynolds number defined by eq. C.62 can be used or the one defined by CS through eq. C.65.

C.2.3 Dodge-Metzner equation for HB fluids

To achieve this, eq. C.54 could be extended to HB fluids by carefully combining eq. C.48, C.54 and C.62. However, the replacement of $n = n'$ which is convenient for PL fluids may not always be consistent. DM did not provide a clear explanation as to why every n is replaced with n' and if every replacement is justified. DM however asserted that eq. C.54 should ideally be suitable for non-PL fluids based on a calculation that proves that shear-rates that are less than 80% of τ_w account for no more than 7% of the mean velocity that results from frictional losses. Therefore, regions away from the wall have significantly lower (perhaps ignorable) contributions to the mean velocity. An experimental verification of this hypothesis along with more details can be found in the work of Skelland (1967).

Further, as a the flow of an HB fluid gets more turbulent, the value ζ gets smaller due to increasing wall shear-stress. As a result, θ becomes nearly $1/(3n+1)$, reducing n' to n and effectively making eq. C.54 suitable for further analyses. Bearing this and DMs assertion in mind, it is perhaps futile to extend eq. C.54 to HB fluids and more so, for highly turbulent flows. Nonetheless, for less turbulent HB flows where ζ is such that it may not be ignored, an extension of eq. C.54 is warranted.

Assuming that every n can be replaced with n', a consistent extension of eq. C.54 to HB fluids must read,

$$\frac{1}{\sqrt{f_{HB}}} = \frac{4}{(n')^{0.75}} \sqrt{1-\zeta} log(N_{Re-Gen_{HB}} f_{HB}^{1-\frac{n'}{2}}) - \frac{0.4}{(n')^{1.2}} \sqrt{1-\zeta} \tag{C.66}$$

Eq. C.66 shall be referred to as DM-HB. Further, CS suggested a similar equation based on eq. C.65 as

$$\frac{1}{\sqrt{f_{HB}}} = 4log(Re_{CS}\frac{1}{n^2}\frac{1}{(1-\zeta)^4}\sqrt{f_{HB}}) - 0.4 \tag{C.67}$$

which shall be called CS-HB from hereafter.

APPENDIX D

Computational Fluid Dynamics

This appendix section provides details on the NS solver used for the CFD analysis presented in this study, ANSYS FLUENT (Ansys, 2011), how the wall functions ψ_1 and ψ_2 are implemented in the solver and how are they solved. Details on the computational mesh are also provided.

D.1 Solver and Numerics

ANSYS FLUENT (Ansys, 2011) that is based on a finite volume method is used to solve the RANS equations. The spatial discretisation is done with a second order upwind scheme to ensure numerical stability. The pressure is resolved with second order accuracy, but is decoupled from the velocity field with the Semi-Implicit Method for Pressure-Linked Equations (SIMPLE). The standard $k-\epsilon$ and the Reynolds Stress Model (RSM) are used to resolve the turbulence. These models are chosen because the flow near the wall boundaries is not resolved as a solution of the RANS equations, but modelled indirectly through a wall function. As a result, the transition of the turbulent flow into a laminar regime near the wall is not directly a part of the solution, in effect, implying a fully turbulent flow, with which both the standard $k-\epsilon$ and RSM are compatible.

Furthermore, these models are used with their standard model constants, which were experimentally-determined for Newtonian fluids (Ansys, 2011). The choice of these constants stems from the fact that any difference in their values for HerschelBulkley fluids will require detailed experimental investigation on the nature of turbulence within such fluids. This is currently missing in literature, at least for the relatively high Reynolds numbers considered in this article. Given the turbulent nature of the pipe flow, the effect of molecular viscosity (by extension, the Newtonian or non-Newtonian nature of the fluid) would be small as opposed to the effect of turbulent viscosity. Therefore, the modification of the model constants for HerschelBulkley fluids may not be completely necessary for strongly turbulent flows. Another motivation to use the standard model constants were studies by Malin (1998,

1997) and Bartosik (2006, 2010), which showed promising results with the standard model constants but with modified wall functions to incorporate the non-Newtonian behaviour of the fluid under consideration.

To implement the constitutive rheological relation, FLUENT uses a bi-viscosity model similar to the one proposed by Tanner and Milthorpe (1983) (see Mitsoulis (2007) for a summary of similar approaches and ANSYS (Ansys, 2011) for the implementation in FLUENT). This approach prevents numerical instability arising from the yield stress at zero strain. Lastly, both ψ_1 and ψ_2 are implicit in terms of τ_w for a given value of v in the first cell near a wall boundary. Thus, unlike the original wall function, ψ_1 and ψ_2 must be implemented as a specified shear boundary conditions as described in Mehta et al. (2018). Once a flow field is initialised, τ_w is calculated from the initial velocity field, following which the RANS equations are solved to obtain a new velocity field. This process is repeated until a converged solution is obtained. A solution is considered as converged once the iterative (absolute, not normalised) residuals for continuity, velocity, k and ϵ are below 10^{-6}.

D.2 Mesh

The computational grid for simulating fluids in horizontal pipes is shown in Figure D.1. Instead of simulating the entire circular cross-section, two symmetry boundaries are used to simulate a quarter-pipe. The boundaries mathematically reduce the gradient across them to zero and allow no flux to leave or enter the quarter-pipe. The inlet has a specified velocity and turbulence intensity, whereas the outlet has a simple outflow condition with a diffusion gradient and a mass flow balance.

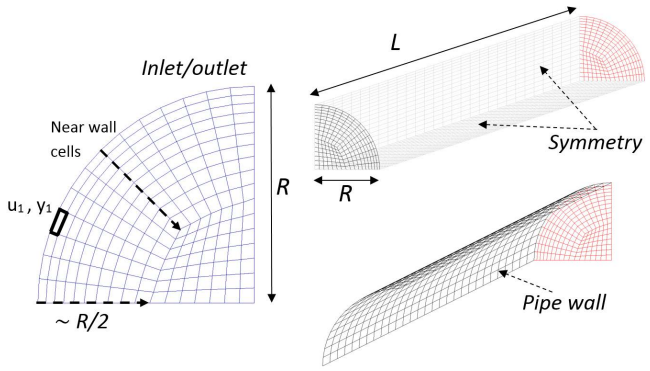

Figure D.1: The computational grid.

The pipe walls are modelled with the specified spear approach, that is, ψ_1 or ψ_2. I can be seen from Figure D.1, the cells along the pipe increase in height from the pipe's wall towards the centre. This pattern is a part of the standard treatment used with wall functions while simulating turbulent boundary layers (Wilcox, 1998; Ansys, 2011). In every case, the grid follows the same pattern from the wall until half the radius, following which the cells are more uniformly arranged into an O-grid. The height of the first cell, $2y_1$ (y_1 was used as the first grid point, which is located at half the height of the first cell) must be set as per guidelines similar to those for Newtonian fluids (for wall bounded flows).

The η_w and Re_w values were calculated for each test case, following which, the distance for the first grid point or y_1 was obtained by setting y^+ to values from 20 to 120. Once the first grid cell's height was known, cells were added with an expansion ratio of between 1.05 and 1.1 until the cells reached the central O-grid, following which the O-grid was created. In either case, the cells along the pipe were sized to maintain an aspect ratio below 40. There is no specific literature on aspect ratios. However, on the basis of multiple guidelines available freely, the maximum aspect ratio was restricted to 40.

To ascertain the grid convergence, the height of the first grid point was varied between $y^+ = 20$ and $y^+ = 200$ (higher values of y^+ were possible only with higher Reynolds numbers, Re_w). It is noted that for $Re_w < 2x10^4$, y^+ for a converged value of the wall shear-stress was closer to 20, whereas for $Re_w > 10^5$, y^+ was at least 60 (as high as 200). Thus, the first grid point was placed progressively further from the wall (in terms of y^+) as the Re_w value increased.

For the standard Newtonian wall function, one should be aware that the first cell must be placed between $30 < y^+ < 300$ (Newtonian definition of y^+) to avoid being completely within the fully laminar or turbulent regimes Davidson (2015); Pope and Pope (2000). This has been corroborated through various studies. As a result of a lack of experimental or numerical evidence, it is impossible to conclude the same for a non-Newtonian fluid, and hence we refrain from discussing any trends in the relation between y^+, u^+ and τ_w. Therefore, the data reported here is that obtained with values of y^+ (HerschelBulkley definition), beyond which the τ_w did not change (as mentioned previously, this y^+ increased with Re_w).

Summary

Domestic wastewater streams from households implemented with source separation, vacuum toilets, and food waste disposers are highly concentrated with respect to the total suspended solids. The concentrated domestic slurries (CDS), which generally consist of faecal matter, urine, ground kitchen waste (GKW) and water, need to be transported from the point of collection to its treatment. In order to design a transportation systems to convey CDS, its flow characteristics must be known. The objective of this thesis is to establish the flow characteristics of CDS that supports the design of its transportation system with pressurised pipelines.

CDS is characterised as a non-Newtonian fluid with respect to its rheology. It has a shear-thinning property with a yield stress. However, at low concentrations it behaves as a Newtonian fluid, its non-Newtonian properties are only physically meaningful above a concentration of 2.0 % TSS (wt./wt.). The rheology of CDS is represented using a Herschel-Bulkley model, the parameters of which are a function of TSS concentration which describes the influence of concentration changes. The yield-stress (τ_y) follows a power law function with concentration and is significant only above a concentration of 2.0 % TSS (wt./wt.). The consistency index (K) follows an exponential behaviour with the concentration, which tends towards the viscosity of water at low TSS concentration. The behaviour index (n) follows an inverse logarithmic function decreasing from 1, and this change is significant only above a TSS concentration of 2.6 % (wt./wt.). The temperature of the slurry also influence the rheology of CDS. The influence of temperature is represented using an Arrhenius type equation with respect to the apparent viscosity. On the other hand, the influence of installing food waste disposers is reflected on the change in the overall particle size distribution (PSD) of the slurry, where an increase in the effective diameter of the particle shows an increase in the viscosity of the slurry.

The pressure losses incurred in the transport of non-Newtonian slurries, including CDS, in pressurised pipelines are well represented using the Slatter transport model. The pressure losses are very much impacted by the rheological characteristics of the fluid. The pressure losses incurred increase with the increase in TSS concentration, but with the onset of non-Newtonian behaviour, the yield-stress and shear-thinning behaviour, provide some damping to the pressure losses particularly in the turbulent flow regime. The transition from laminar to turbulent flow occurs as a multi-stage process starting with the occurrence of puffs, and then to slugs and both together. The Slatter Reynolds number, provides good prediction of the transition to turbulence compared to the other available models.

To conclude, a functional design of a pressurised pipeline transport system for CDS would have to meet the pressure losses estimated using the rheology of CDS at a certain concentration of TSS and temperature of the slurry.

List of publications

Peer reviewed journal papers

Thota Radhakrishnan, A.K., Poelma, C., van Lier, J.B., Clemens, F.H.L.R. (2019). Laminar-turbulent transition of a non-Newtonian fluid flow. *Journal of Hydraulic research*, submitted.

Mehta, D., **Thota Radhakrishnan A.K.**, van Lier, J.B., Clemens, F.H.L.R. (2019). Assessment of semi-empirical models for estimating frictional losses incurred in the turbulent flow of non-Newtonian slurries through closed circular pipes. *Journal of Hydraulic research*, submitted.

Mehta, D., **Thota Radhakrishnan A.K.**, van Lier, J.B., Clemens, F.H.L.R. (2019). Sensitivity Analysis of a Wall Boundary Condition for the Turbulent Pipe Flow of Herschel-Bulkley Fluids. *Water*, 11(1), 19.

Thota Radhakrishnan, A.K., van Lier, J.B., Clemens, F.H.L.R. (2018). Rheology of Un-Sieved Concentrated Domestic Slurry: A Wide Gap Approach. *Water*, 10(10), 1287.

Thota Radhakrishnan, A.K., van Lier, J.B., Clemens, F.H.L.R. (2018). Rheological characterisation of concentrated domestic slurry. *Water research*, 141 (2018): 235-250.

Mehta, D., **Thota Radhakrishnan A.K**., van Lier, J.B., Clemens, F.H.L.R. (2018). A Wall Boundary Condition for the Simulation of a Turbulent Non-Newtonian Domestic Slurry in Pipe. *Water*, 10(2), 124.

Conference papers

Thota Radhakrishnan, A.K., Langeveld, J., van Lier, J.B., Clemens, F.H.L.R. (2018). Challenge of Transport: Exploring the Limit of Gravity Sewers to Transport Concentrated Domestic Slurries. Presented at the *11^{th} Urban Drainage Modelling Conference*, Palermo, Italy, 23 - 26 September 2018.

Mehta, D., **Thota Radhakrishnan, A.K.**, van Lier, J.B., Clemens, F.H.L.R. (2018). Numerical and CFD-based modelling of concentrated domestic slurry in turbulent flow through circular pipes. Presented at the *11^{th} Urban Drainage Modelling Conference*,

Palermo, Italy, 23 - 26 September 2018.

Thota Radhakrishnan, A.K., van Lier, J.B., Clemens, F.H.L.R. (2017). Effect of temperature on the transport of concentrated domestic slurry. Presented at the *4th Water Research Conference*, Waterloo, Canada, 10 - 13 September 2017.

Mehta, D., **Thota Radhakrishnan, A.K.**, van Lier, J.B., Clemens, F.H.L.R. (2017). Concentrated domestic slurry in pipes: a computational analysis. Presented at the *14th International Conference on Urban Drainage*, Prague, Czech Republic, 10 - 15 September 2017.

Thota Radhakrishnan, A.K., van Lier, J.B., Clemens, F.H.L.R. (2016). Experimental design to study concentrated domestic slurry transport hydraulics. Presented at the *8th Sewer Processes Network conference*, Rotterdam, the Netherlands, 31 August - 2 September 2016.

Thota Radhakrishnan, A.K., Alidai, A., Pothof, I.W.M., Clemens, F.H.L.R. (2015). Transport aspect of domestic slurry: a step ahead forward towards new sanitation systems. Presented at the *10th Urban Drainage Modelling Conference*, Mont-Saint-Anne, Qubec, Canada, 20 - 23 September 2015.

Thota Radhakrishnan, A.K., Alidai, A., Pothof, I.W.M., Clemens, F.H.L.R. (2015). Predicting The Onset Of Secondary Flows In The Rheological Measurement Of Domestic Slurry. Presented at the *10th Urban Drainage Modelling Conference*, Mont-Saint-Anne, Qubec, Canada, 20 - 23 September 2015.

Pothof, I.W.M., Alidai, A., **Thota Radhakrishnan, A.K.**, Clemens, F.H.L.R. (2015). The missing link in future sanitation. Presented at *Environmental Technology for Impact (ETEI2015)*, Wageningen, Netherlands, 29 - 30 April 2015.

About the author

Adithya Krishnan Thota Radhakrishnan was born in Chennai, India on April 16th 1990. He did his general schooling in P.S. Senior Secondary School in Chennai. His passion for science and engineering led him to take up a Chemical Engineering program in SSN College of Engineering in Chennai, where he obtained his Bachelor of Engineering degree in 2012. Following which, he started his masters study in Chemical Engineering and obtained a Master in Science - Chemical Engineering diploma from TU Eindhoven, the Netherlands in 2014. During his masters study he specialised in "Process Engineering" and with interest for both experimental and numerical work, he did his master thesis on designing a process to extract polyphenols from tea. Following his interest in process systems, and particularly complex fluids he started his PhD on the transport of concentrated domestic wastewater slurries. The research focussed on characterising the rheology and pressure losses for concentrated domestic wastewater slurries which are non-Newtonian in nature. At every stage, extra-curricular activities have played an important role. He has been the president of PromooD (PhD representative body) at TU Delft, board member (communications) of the international association at TU Eindhoven, president of the Entrepreneur Development Cell at SSN College of Engineering, and has been an integral part of many others. In the recent years, following his love for mountains, he has started rock climbing and mountaineering, which has become an integral part of his life.